MOLTEN METAL ANODES FOR

DIRECT CARBON-SOLID OXIDE FUEL CELLS

Abhimanyu Jayakumar

A DISSERTATION

in

Chemical and Biomolecular Engineering

Presented to the Faculties of the University of Pennsylvania

in Partial Fulfillment of the Requirements for the

Degree of Doctor of Philosophy

2012

Supervisor of Dissertation

_____

Raymond J. Gorte, Professor, CBE

Co-Supervisor of Dissertation

_____

John M. Vohs, Professor, CBE

Graduate Group Chairperson

_____

Raymond J. Gorte, Professor, Chemical and Biomolecular Engineering

Dissertation Committee

Warren D. Seider, Professor, Chemical and Biomolecular Engineering

Donald H. Berry, Professor, Chemistry

To my parents, for their unconditional support

Acknowledgements

I am very grateful to my advisor, Prof. Ray Gorte, for his guidance and encouragement at every step of my thesis research. His hands on approach and vigilant inputs were very effective in instilling the qualities of a research engineer into me. I would also like to thank my co-advisor, Prof. John Vohs, for his helpful insights and discussions.

I would also like to thank all my colleagues in the Gorte – Vohs laboratory for all their help and for making my graduate learning experience a very enjoyable one. In particular, I want to thank Ashay and Rainer for always being there for discussions and Jesse for his help and for making sure that there was never a dull moment in the lab. I am also very grateful to Shiwoo Lee for teaching me all the techniques in the lab that I have used throughout my research.

My student life at Penn could not have been a great experience without the support of my friends in Philadelphia, Sameer, Hridey, Siddharth and Zain.

Additionally, I am very thankful to the Catalysis Center for Energy Innovation, an Energy Frontier Research Center at the University of Delaware, for funding my thesis research and giving me the opportunity to learn from some of the brightest minds in the business.

Finally and most importantly, I want to thank my parents for always having faith in me and teaching me that with hard work you can achieve anything.

ABSTRACT

MOLTEN METAL ANODES FOR DIRECT CARBON - SOLID OXIDE FUEL CELLS

Abhimanyu Jayakumar

Raymond J. Gorte

John M. Vohs

The aim of this thesis was to enable the direct utilization of solid carbonaceous fuels like coal and biomass, in solid oxide fuel cells (SOFC). Since SOFCs are based on ceramic oxygen-ion conducting electrolytes, it is possible, in principle, to generate electricity by the direct oxidation of solid fuels in these fuel cells. The electrochemical conversion of these fuels can realize high efficiencies in power generation and decrease environmental impact by allowing easy CO_2 capture and minimizing NO_x and SO_x emissions. The main challenge in this technology involves finding an anode system to enable the facile transfer of oxygen from the SOFC electrolyte to the solid fuel. In this study, several molten-metal/metal-oxide systems were examined as anodes for such direct carbon fuel cells (DCFC). The molten metal candidates tested were, Tin(Sn), Bismuth(Bi), Indium(In), Lead(Pb) and Antimony(Sb). The oxygen transport properties of these molten metal systems were studied by placing them in direct contact with the SOFC electrolyte. The open circuit voltage (OCV) related to the anode oxidation reaction and its contribution to the cell resistance were the two major considerations for anode viability. Characterization of the electrochemical oxidation of the metal at the electrolyte

interface showed that, metals like Sn and In had high OCVs but exhibited a time-dependent increase in non-ohmic resistance due to formation of solid oxide layers of their high-melting oxides, which blocked further ion transfer. Bi had low resistances because of its ionically conductive oxide, but had a low OCV. The key anode characteristic for low resistance was observed to be a low melting oxide from the study of Pb and Sb. Sb was the most intriguing because it had a reasonable OCV and oxidized most types of solid fuels below 973 K.

High power DCFCs based on molten Sb anodes were demonstrated using various types of solid fuels at stable power levels for over 250 h at 973 K. These long-term stability tests revealed thinning of scandia-stabilized zirconia electrolytes, but no thinning was observed using yttria-stabilized zirconia. Hence, efficient and long-term stable DCFCs using molten Sb are possible with the correct choice of electrolyte material.

Table of Contents

List of Tables:

List of Figures:

Chapter 1: Introduction

1.1 Motivation

Coal is a non-renewable fossil-fuel resource and is widely used in traditional combustion-based energy generation technologies. Thermal power plants based on coal produce electricity by converting the heat generated by combustion into mechanical energy, which is then converted into electrical energy. However, the efficiency of this process is limited thermodynamically by the Carnot cycle. In a typical power plant, almost 66% of the heating value of the fuel remains unused and is lost as waste heat. The overall efficiency of these power plants is only around 34% in their most modern form, despite the efforts to improve them for decades [1].

Biomass is the biological material obtained from living organisms and is an abundant renewable energy resource. Most biomass consists of complex organic compounds and also contains many trace impurities like sulfur and nitrogen, along with alkali and other metal compounds. Unfortunately, biomass is not easily converted into more usable fuels [2] and the direct combustion of biomass in thermal power plants leads to increased levels of air pollution in the form of CO, NO_x, SO_x, volatile organic compounds (VOCs), and particulates [3].

Looking at this present scenario, the development of a technology that allows the utilization of non-renewable coal and effectively enables the eco-friendly conversion of biomass to generate useful forms of energy at high efficiencies would be extremely helpful in addressing increasing global energy needs. One promising approach to more efficient utilization of coal and biomass involves oxidizing these fuels electrochemically

in fuel cells. Fuel cells are electrochemical devices that convert the chemical energy stored in the fuel directly into electrical energy. Therefore, their process efficiencies are not limited by the Carnot cycle as in the case of thermal power plants. Because of this, the efficiencies of fuel cells are generally significantly higher than those of traditional combustion based processes, by up to 20%. For high temperature fuel cells, operating at temperatures above 973 K, the overall efficiency can be further increased by using the hot exhaust gases to recover more of the heating value of the fuel in a combined heat and power cycle (CHP) [4]. Furthermore, fuel cells can utilize solid carbonaceous fuels like coal and biomass, without directly contacting them with air, thereby resulting in lower and more concentrated emissions of CO_2 with decreased amounts of NO_x, SO_x and particulates, allowing CO_2 to be easily captured and sequestered [5, 6].

Attempts to utilize solid carbon electrochemically date back to the late 1890's, using fuel cells based on molten hydroxide electrolytes [7]. However, these systems were found to be impractical due to carbonate formation [8] and demonstrated very low performance efficiencies [7]. As a result, work on their development was soon discontinued. In the past 20 years, research into enabling the electrochemical utilization of solid carbon has seen a revival using technologies based on molten carbonate and ceramic solid oxide electrolytes [5, 9].

In the following sections of this chapter, the working principles of fuel cells based on solid oxide and molten carbonate electrolytes will be presented, followed later by a discussion of the various approaches being developed for carbon utilization using these two fuel cell types. Since this thesis focused on the use of molten metals as anodes to enable the utilization of carbon in fuel cells, the use of a molten carbonate electrolyte was

not feasible because molten alkali carbonates are highly reactive with most types of metals at the high temperatures required for cell operation. Therefore, all of the work performed in this study has been based on solid oxide fuel cells with inert ceramic solid oxide electrolytes.

1.2 Operating principles of solid oxide fuel cells and molten carbonate fuel cells

The three main components of any fuel cell are the cathode, the electrolyte, and the anode. The cathode catalyzes the electrochemical reduction of an oxidizing species (typically oxygen from air), while the anode facilitates the electrochemical oxidation of the fuel. The electrolyte membrane serves as a selectively permeable barrier between the two electrodes, preventing the mixing of their contents and blocking electron transfer, while only allowing the transport of a particular ionic species from one electrode to the other.

Many different types of fuel cells have been developed and they are distinguished by the electrolyte material that is used. Proton exchange membrane fuel cells (PEMFC), alkaline fuel cells (AFC), phosphoric acid fuel cells (PAFC), molten carbonate fuel cells (MCFC) and solid oxide fuel cells (SOFC) are some of the existing types of fuel cells that are being commercialized [4, 10, 11]. Only MCFC and SOFC are practical for direct-carbon applications due to the fact that the electrolytes are anion conductors and do not require the presence of hydrogen.

1.2.1 Solid oxide fuel cells

SOFCs are based on ceramic membrane electrolytes, which conduct oxygen anions at high temperatures. The solid oxide electrolyte material is most commonly ZrO_2

which is aliovalently doped with oxides like, Y_2O_3 or Sc_2O_3. The operating temperature for these fuel cells is dictated by the ionic conductivity of the electrolyte and ranges from 873 K to over 1273 K [12]. The solid oxide membrane separates the air (oxidant) on the cathode side from the fuel (reductant) on the anode side as shown in Fig. 1.1. These fuel cells generate electricity by electrochemically combining the oxygen from air on the cathode side with the fuel on the anode side through the ionically conductive electrolyte as follows:

- Oxygen from air reacts with the conductive cathode to produce oxygen anions by gaining electrons from the external circuit as shown by Equation 1.1,

$$O_2\,(g) + 4e^- \rightarrow 2O^{2-} \qquad \text{Equation 1.1}$$

- Oxygen anions formed at the cathode migrate through the ionically conductive, solid oxide electrolyte membrane to the anode side as shown by Equation 1.2,

$$O^{2-}_{cathode} \text{—electrolyte}\rightarrow O^{2-}_{anode} \qquad \text{Equation 1.2}$$

- Oxygen anions react with the fuel (e.g. H_2, CH_4, C_xH_y etc) fed to the conductive anode and release electrons into the external circuit as shown by Equations 1.3, 1.4 and 1.5,

$$H_2 + O^{2-} \rightarrow H_2O + 2e^- \qquad \text{Equation 1.3}$$

$$CH_4 + 4O^{2-} \rightarrow CO_2 + 2H_2O + 8e^- \qquad \text{Equation 1.4}$$

$$C_xH_y + (x + y/2)\,O^{2-} \rightarrow x\,CO_2 + (y/2)\,H_2O + (2x + y)\,e^- \qquad \text{Equation 1.5}$$

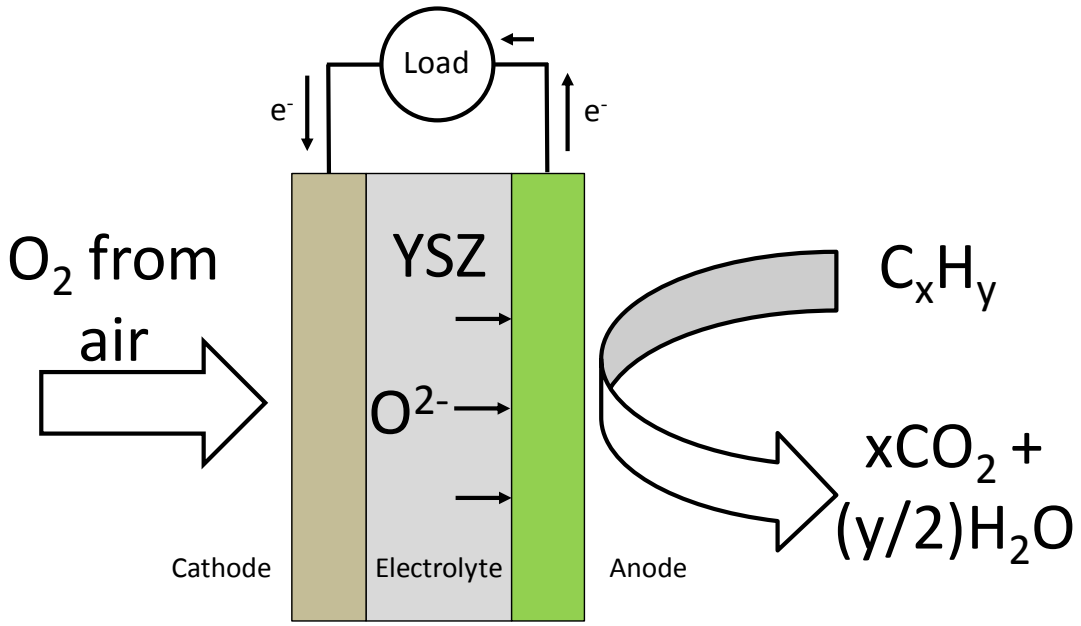

Figure 1.1: Operating schematic of a solid oxide fuel cell.

Therefore, if a continuous supply of reactants is maintained at the electrodes, i.e. air at the cathode and fuel at the anode, an SOFC can continuously generate a direct electronic current from the anode to the cathode in the external circuit. This direct current can be used to power an external load connected in circuit.

It is important to note that reactions at fuel cell electrodes can only occur at interfaces or lines of contact where the reactant, electronic conductor and ionically conductive phase all meet. These interfaces are known as three phase boundaries (TPB) [13]. To this end, typical gas-fuelled SOFC electrodes are usually porous composites of the electrolyte material with an active and electronically conductive phase, such as a metal or a conductive mixed-metal oxide. For the cathode reaction to occur, oxygen from air needs to be present at the line of contact between the suspended electronically conductive phase and its containing porous electrolytic scaffold (which serves as an extension of the

electrolyte) in order to gain electrons from the external circuit and be transported into the dense electrolyte. For the anode fuel oxidation reaction to occur, the fuel needs to be present at the interface between the electronically and ionically conductive phases where it can react with the oxygen anions from the dense electrolyte and simultaneously release electrons. The anode reaction mechanism for a SOFC fuelled with H_2 is shown in Fig. 1.2.

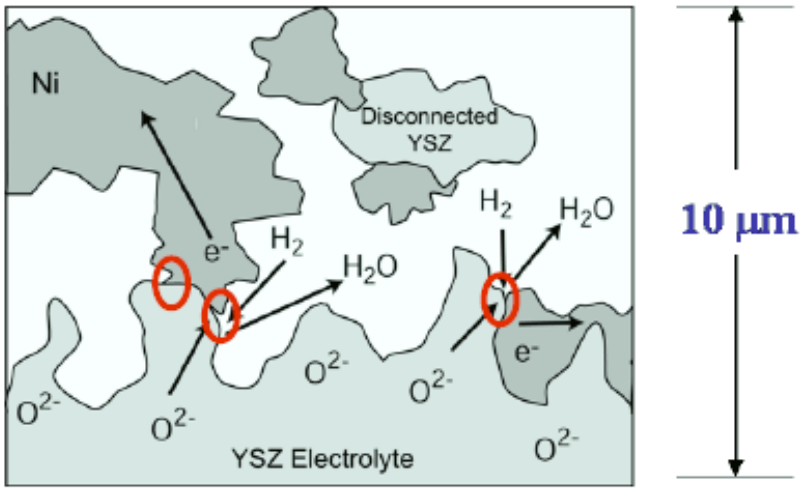

Figure 1.2: Anode reaction mechanism for a H_2-fuelled SOFC (Three Phase Boundary concept) [14].

Since O^{2-} ions are the charge carriers, SOFCs have the inherent advantage of better fuel flexibility than most other types of fuel cells, because they can utilize any combustible fuel. This encompasses a wide variety of fuels like H_2, CO, gaseous and liquid hydrocarbons and, in principle, SOFCs can even operate on solid carbonaceous fuels such as, coal and renewable biomass [4, 11, 14-21]. SOFCs also have a higher tolerance for fuel impurities than other types of fuel cells like, PEMFCs and AFCs [4, 11, 15].

1.2.2 Molten carbonate fuel cells

Molten carbonate fuel cells (MCFC) are based on molten carbonate salt mixtures as electrolytes, which conduct carbonate anions at high temperatures. The molten salts are usually held in an inert solid ceramic porous matrix, such as beta-alumina or zirconia, via surface tension. The electrolytes are typically composed of a mixture of Li_2CO_3, K_2CO_3 and Na_2CO_3 salts and can be either binary eutectic mixtures containing (Li, $K)_2CO_3$ or (Li, $Na)_2CO_3$ or ternary eutectic mixtures of (Li, K, $Na)_2CO_3$. Based on the need to maintain the carbonate mixture in molten form, the operating temperatures for these fuel cells range from 873 K to 1073 K. The molten electrolyte separates the air (oxidant) and recycled CO_2 on the cathode side from the fuel (reductant) on the anode side as shown in Fig. 1.3. These fuel cells generate electricity by electrochemically combining the oxygen from air on the cathode side with the fuel on the anode side through the ionically conductive electrolyte as follows:

- Oxygen from air and recycled CO_2 from the anode chamber react with the conductive cathode to produce carbonate anions by gaining electrons from the external circuit as shown by Equation 1.6,

$$2CO_2 + O_2 + 4e^- \rightarrow 2CO_3^{2-} \qquad \text{Equation 1.6}$$

- Carbonate anions formed at the cathode migrate through the ionically conductive, molten electrolyte-containing ceramic matrix to the anode side as shown by Equation 1.7,

$$CO_3^{2-}{}_{cathode} \text{—electrolyte}\rightarrow CO_3^{2-}{}_{anode} \qquad \text{Equation 1.7}$$

- Carbonate anions react with the fuel (e.g. H_2, CH_4, C_xH_y etc) fed to the conductive anode and release electrons into the external circuit as shown by Equations 1.8, 1.9 and 1.10. CO_2 from the reaction products is then recycled back to the cathode.

$$H_2 + CO_3^{2-} \rightarrow CO_2 + H_2O + 2e^- \quad \text{Equation 1.8}$$

$$CH_4 + 2CO_3^{2-} \rightarrow 3CO_2 + 2H_2O + 4e^- \quad \text{Equation 1.9}$$

$$C_xH_y + (x + y/2)\, CO_3^{2-} \rightarrow (x + y/2)\, CO_2 + (y/2)\, H_2O + (2x + y)\, e^- \quad \text{Equation 1.10}$$

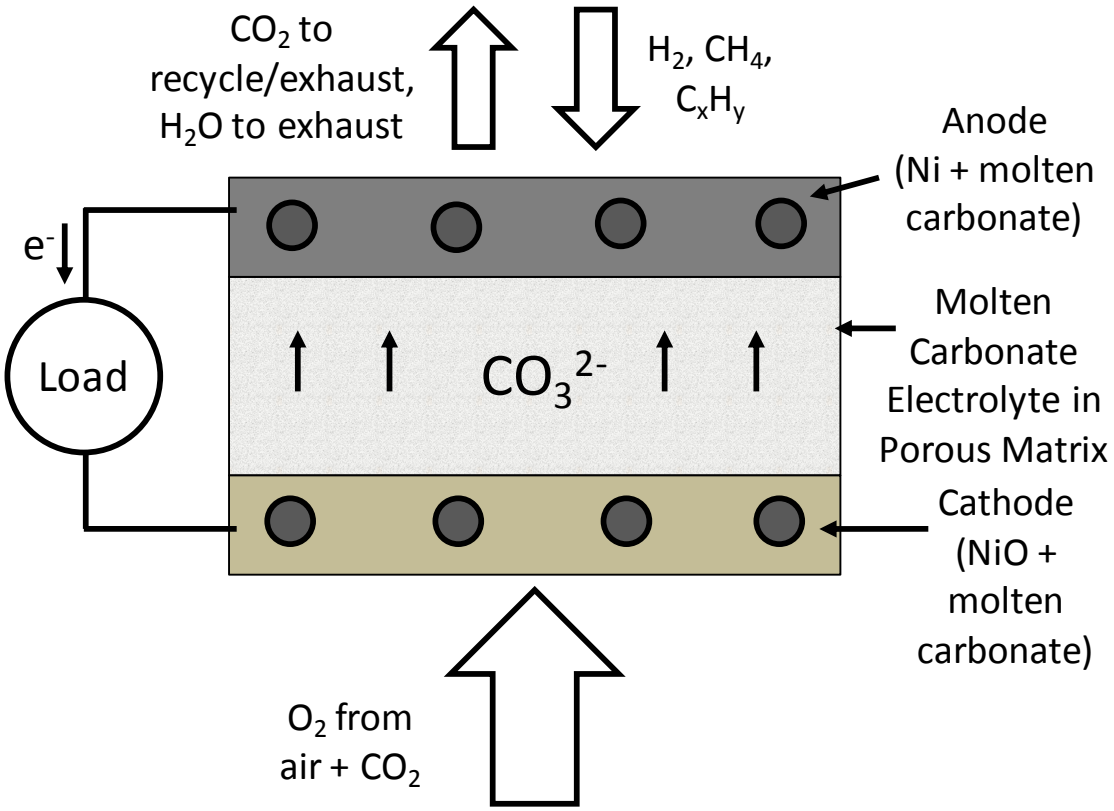

Figure 1.3: Operating schematic of a molten carbonate fuel cell.

In MCFCs, three phase boundaries are achieved by the use of electrodes that consist of a porous conductive or metallic scaffold with the molten carbonate maintained in it by surface tension [22]. The electrode reactions occur when the gaseous reactants come

into contact with the interfacial regions between the metallic scaffold and the ionically conductive molten carbonate phase.

The key aspect of MCFCs is that they essentially operate by the transfer of O^{2-} ions as charge carriers, in the form of carbonates. Therefore, like SOFCs, MCFCs also have the fuel flexibility for being able to utilize any type of combustible fuel and, in principle, can also operate on solid carbonaceous fuels like coal and biomass.

1.3 Performance characterization techniques for fuel cells

The operating properties of a fuel cell and the factors governing its performance output can be characterized through V-i polarization curves and impedance spectroscopy. These techniques are useful in determining the cell characteristics that limit performance and can provide clues for improving the design of cell components.

1.3.1 V-i polarization curves

V-i polarization curves are basically voltage-current response plots for fuel cells. These curves are generated by ramping through the applied voltages across the cell and plotting them against the corresponding currents drawn from the fuel cell. A sample V-i curve is shown in Fig. 1.4. The voltage at which the current drawn is zero is called the Open Circuit Voltage (OCV). For electrolytes that are pure ion conductors, this voltage is the potential associated with the anode oxidation reaction and is directly related to its free energy (ΔG) by the Nernst Equation (Equation 1.11),

$$E = -\Delta G(T)/nF \qquad \text{Equation 1.11}$$

where T is the cell operating temperature, ‘n’ is the number of moles of electrons released in the oxidation reaction, and ‘F’ is the Faraday constant.

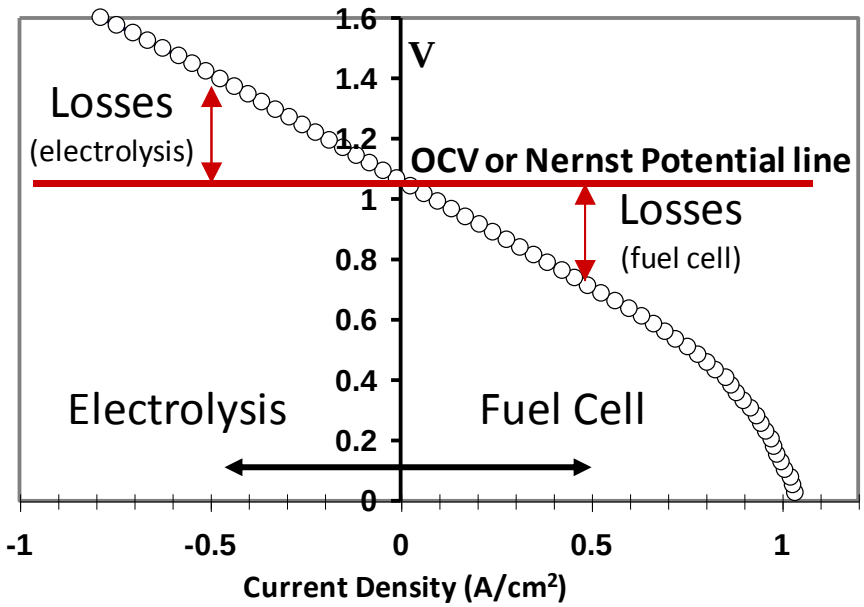

Figure 1.4: Sample V-i polarization curve.

Since a real fuel cell has resistance losses, varying the voltage will cause the V-i curve to deviate from the Nernst Potential. For positive currents, the cell is said to be in "fuel cell mode" and the cell potential is below the Nernst Potential. The spontaneous anode oxidation reaction is then used to drive electrons in the external circuit, to cause oxygen dissociation at the cathode, and to transport oxygen anions to the anode for further fuel oxidation. At negative currents, the cell operation is in "electrolysis mode". In this mode, the excess countervoltage (above OCV) is used to dissociate the oxidized fuel, for example H_2O, forming the fuel (H_2), while the oxygen anions are then transported through the electrolyte to produce oxygen gas at the electrode exposed to air.

The slope of the V-i curve gives the overall cell resistance at each point,

$$V = i.R_{total} \qquad \text{Equation 1.12}$$

R_{total} consists of the losses from the electrolyte and each of the electrodes. The electrolyte loss is simply the resistance associated with the transfer of O^{2-} ions through the electrolyte and depends on the thickness and conductivity of the electrolyte material used. The electrode losses are the kinetic losses associated with the ease of the reactions occurring at the cathode and the anode. However, it is not possible to separate R_{total} into each of its constituent losses only by using V-i curves. Impedance spectroscopy is a technique used for this purpose, as described in the next sub-section.

A corresponding power density curve can also be plotted for a V-i curve by calculating the product of the voltage and the corresponding current at each point of the V-i curve (Equation 1.13). As a practice, current values are always normalized to the effective or working area of the electrolyte to give area specific values.

$$P = V.i \qquad \text{Equation 1.13}$$

1.3.2 Electrochemical impedance spectroscopy

The contributions of each of the cell components towards the overall cell resistance (R_{total}) are obtained by impedance spectroscopy. This technique is used to measure the impedance of the fuel cell over a range of frequencies, and therefore its frequency response. A Nyquist impedance plot is one way to represent the data obtained by impedance spectroscopy. A sample Nyquist plot for a fuel cell is shown in Fig. 1.9. These are plots of the imaginary parts of the cell impedance against its real parts at each of the frequencies. These plots are obtained galvanostatically (at a fixed current) by performing a frequency sweep (from ∞ to 0 Hz) on an applied a.c. perturbation to the fuel cell current.

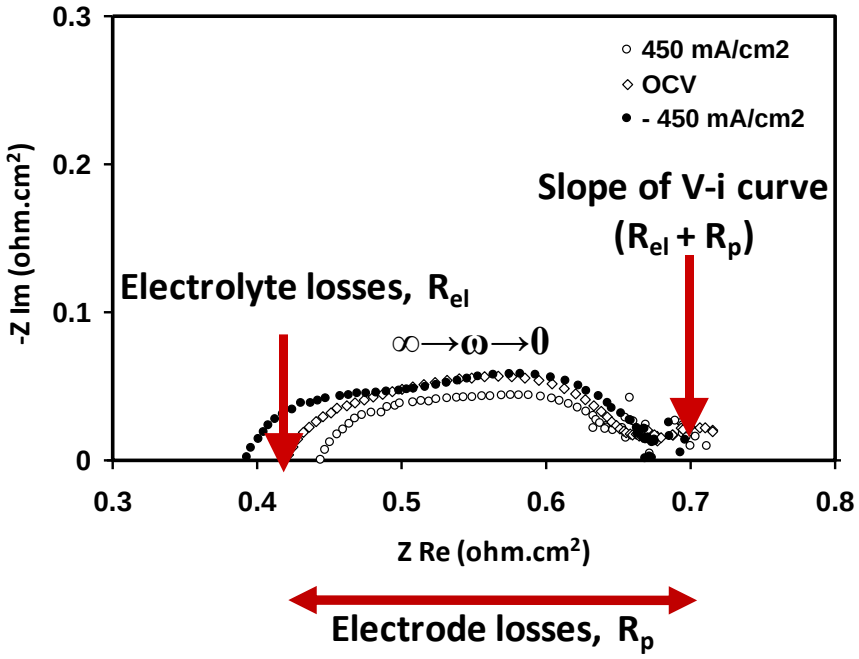

Figure 1.5: Sample Nyquist plot.

At high frequencies, the capacitive components (terms related to the ease of electrode reactions) go to zero, so that the high frequency intercept of the Nyquist plot with the abscissa gives the purely resistive component, or the ohmic resistance, of the cell impedance. This term is mostly due to the resistance offered by the electrolyte to oxygen ion transfer (R_{el}). At very low frequencies, the capacitive components also start behaving like resistors. The length of the line segment underneath the Nyquist curve, between the high and low frequency intercepts with the abscissa, gives the polarization resistance (R_p) or the non-ohmic resistance.

Together, R_{el} and R_p give the total resistance associated with the flow of a d.c. current (zero frequency) through the fuel cell. That is,

$$R_{tot} = R_{el} + R_p \qquad \text{Equation 1.14}$$

$$R_p = R_{cathode} + R_{anode} \qquad \text{Equation 1.15}$$

R_{el} is related to the conductivity and the thickness of the electrolyte used, while R_p is the sum of the non-ohmic resistances due to the cathode and anode reactions (Equation 1.15). In this thesis, the ohmic contributions of the electrolytes and the non-ohmic contributions of the composite cathodes were known from previous studies [23]. Therefore, the impedance contributions of the various molten-metal anode systems could be determined by difference from the Nyquist plots.

1.4 Direct carbon fuel cells

A direct carbon fuel cell (DCFC) is a fuel cell that uses a solid, carbon-rich material as the fuel. The cell produces energy by electrochemically combining carbon and oxygen, releasing carbon dioxide as a by-product. The overall reaction of a DCFC is shown in Equation 1.17,

$$C + O_2 \rightarrow CO_2 \qquad \text{Equation 1.17}$$

This reaction proceeds via mechanisms that vary with cell design and the type of electrolyte used. The majority of the DCFC technologies being developed at present are based on MCFC or SOFC. In a direct-carbon MCFC, the carbon oxidation reaction at the anode side proceeds by reaction of the solid fuel with carbonate anions (Equation 1.18). Carbonates are good oxidizing agents but electronic insulators, so that the performance of these cells is usually limited by electron transfer to the external circuit.

$$C + 2CO_3^{2-} \rightarrow 3CO_2 + 4e^- \qquad \text{Equation 1.18}$$

In the case of direct-carbon SOFCs, the overall anode reaction is that of the carbon being oxidized by oxygen anions from the solid oxide electrolyte (Equation 1.19). However, direct contact between the solid fuel and the solid electrolyte is inefficient.

Various anode designs have been employed in order to make contact between the fuel and the oxygen ions from the solid electrolyte. Typically, this occurs through intermediate steps, making the anode reaction mechanisms more involved, as will be discussed in the next section.

$$C + 2O^{2-} \rightarrow CO_2 + 4e^- \qquad \text{Equation 1.19}$$

The total efficiency of a DCFC is a product of several factors. Three of the most important are the thermodynamic (theoretical) efficiency of the overall process, the fuel utilization fraction (the fraction of the fuel that is converted electrochemically), and the operating efficiency of the cell. The thermodynamic efficiency, for any fuel cell, including DCFC, is given by the ratio between the free energy (ΔG) and the enthalpy (ΔH) of the carbon oxidation reaction (Equation 1.17). The thermodynamic efficiency is basically the fraction of the total chemical energy stored in the carbon fuel that can be effectively converted into electrical work. It can be written as,

$$\text{Theoretical Efficiency} = (\Delta G/\Delta H) \qquad \text{Equation 1.20}$$

Since, $\Delta G = \Delta H - T\Delta S$, where T = absolute temperature (K) and ΔS = Entropy change,

$$\text{Theoretical Efficiency} = 1 - (T\Delta S/\Delta H) \qquad \text{Equation 1.21}$$

The entropy change for the carbon oxidation is a small decrease ($\Delta S > 0$), while $\Delta H < 0$. This gives a ($\Delta G/\Delta H$) ratio greater than 1. Therefore, for a DCFC, it is possible to convert all of the chemical energy in the carbon fuel into electrical energy when an external source of heat is provided.

Fuel utilization efficiency is defined as the fraction of the fuel that converts to electrical energy once it enters the fuel cell. When pure hydrogen is used as a fuel in high temperature fuel cells, the presence of steam as a reaction product dilutes the remaining

hydrogen (decreases its chemical potential), thereby reducing its ability to produce electrical energy. A typical maximum fuel utilization is 90%, after which the fuel is too dilute to be useful in the fuel cell. In the case of DCFCs, it may be possible to convert all of the solid carbon fuel into electrical energy because the reaction product, CO_2, is in a separate gas phase and at a constant pressure. Therefore, the presence of CO_2 will not diminish the chemical potential of the solid carbon allowing the possibility of 100% fuel conversion. In practice, 100% fuel utilization may not be possible because, depending on cell design, there could be some energy penalties associated with ensuring that the carbon fuel remains in contact with the electrode interface. Moreover, at high temperatures (> 1123 K) some of the carbon may be converted mostly to CO.

The Nernst potential of carbon oxidation (Equation 1.17) is ~1 V. An ideal DCFC would be able to operate at this voltage no matter how much current is being drawn and operate at 100% voltage efficiency. In practical use, all fuel cells have kinetic and resistive losses and have to operate at a voltage which is a trade-off between fuel cell efficiency and cost. For example, if the voltage efficiency were to be increased by decreasing the current density, the active area would need to be increased to obtain the necessary power, which in turn would increase capital costs.

1.5 Approaches in DCFC technology based on SOFCs and MCFCs

With fuel cell electrolytes and their respective air-contacting cathodes being well-studied and considered as standard, the main challenge in making a practical DCFC involves the design of an anode system that efficiently contacts the carbon fuel with the oxidizing species from the electrolyte. This will help minimize cell performance losses

and make the high-level of efficiencies, theoretically achievable by DCFCs, possible. There are various approaches that are being developed for this purpose.

1.5.1 Direct carbon-molten carbonate fuel cell

This type of DCFC is based on a conventional MCFC with the CO_3^{2-} ions migrating from the cathode towards the anode. At MCFC operating temperatures, carbon can be oxidized to CO_2 via the cathode and anode reactions shown in Equations 1.6 and 1.18 respectively. Since molten carbonates are good oxidizers but poor electronic conductors, the main factor limiting performance in direct carbon-MCFCs is the slow anode kinetics associated with the limited TPB caused by the lack of contact of the fuel with an electronic conductor.

The operating schematic of a typical direct carbon-molten carbonate fuel cell is shown in Fig. 1.6 and is similar to that used by N. Cherepy et al [24]. In this system, the anode consists of a porous Ni scaffold containing the molten carbonate mixture. The fuel consists of a conductive form of carbon present at a high enough concentration in a slurry with the molten carbonate as the carrier. This configuration helps the electrochemical reaction also occur out of direct electrical contact with the metallic current collector, since the conductivity of the carbon also facilitates current collection.

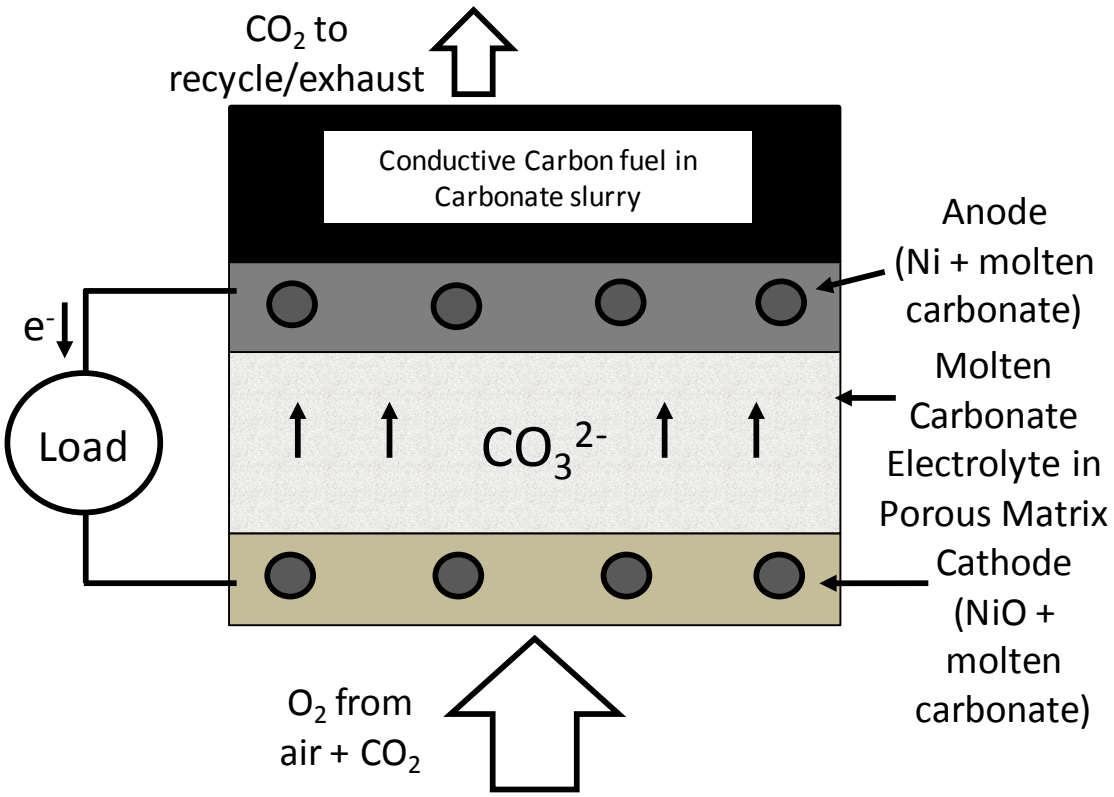

Figure 1.6: Operating schematic of a direct carbon-MCFC.

Since the carbon fuel is directly oxidized by the carbonate anions, the open circuit potential for these DCFCs is ~1 V, the same as that of the carbon oxidation reaction (Equation 1.17). The best possible performance levels in these DCFCs have been observed only when conductive carbons are used as fuels. However, not all forms of carbon are conductive and one of the main drawbacks of DCFCs based on MCFCs is their reduced fuel flexibility.

Moreover, it has been found that the reactivity of the carbon used, i.e. low crystallinity, presence of surface reactive sites, small particle size and high surface area, is also related to the performance of these DCFCs [24, 25]. Conductive carbons are not the most reactive forms of carbon and their poor reactivity will always contribute to the

anode polarization losses. Therefore, the ideal fuel required by these DCFCs is a form of carbon fuel with sufficient electronic conductivity and chemical reactivity to minimize performance losses due to the anode reaction [24].

Apart from the issues associated with sluggish anode kinetics and high costs associated with producing carbon in a suitable form, DCFCs based on molten carbonates also have problems due to ash build-up in the electrolyte and poor durability due to the highly corrosive nature of the molten carbonate mixture causing damage to other cell components [26]. Therefore, these DCFCs require a lot more development in order to be made practical.

1.5.2 Direct carbon-solid oxide fuel cells

Using conventional SOFC cathode and electrolyte materials, there are currently three major types of anode technologies being developed to enable the utilization of solid carbonaceous fuels in SOFCs.

1.5.2.1 Gasification-driven direct carbon-SOFCs

These DCFCs are similar to conventional gas-fuelled SOFCs. The cell components used in gasification-driven direct carbon SOFCs are the same as in conventional SOFCs and the composite anode consists of the porous ceramic scaffold containing an electronically conductive and catalytic material as shown in Fig 1.7. The conventional Ni-YSZ (yttria-stabilized zirconia) cermet is the common anode used in gasification-driven direct carbon-SOFCs.

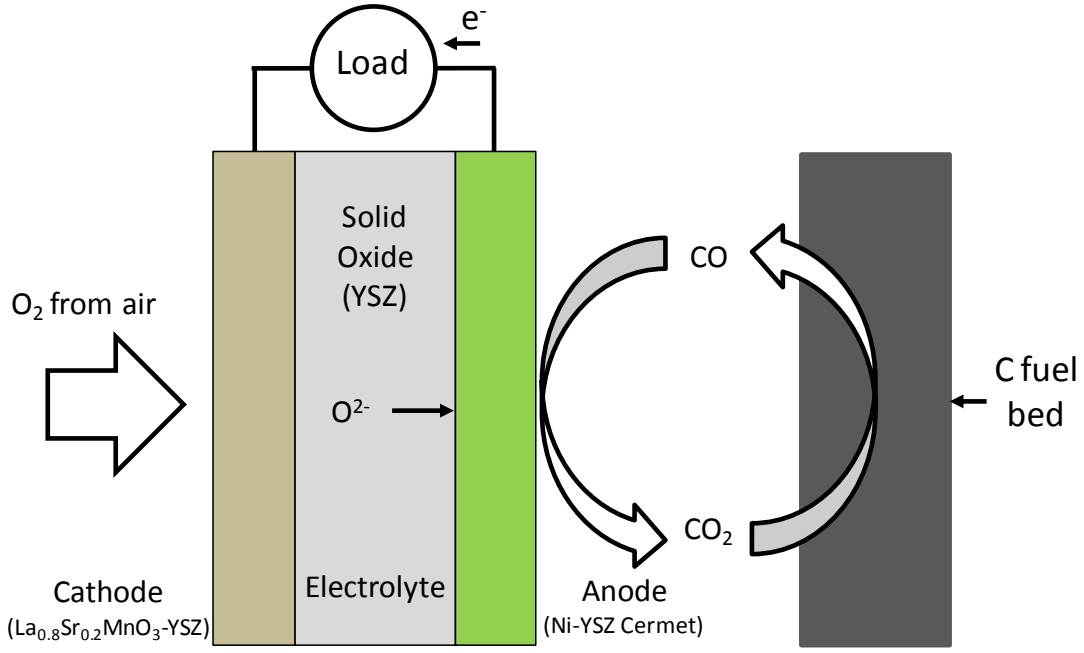

Figure 1.7: Operating schematic of a gasification-driven direct carbon-SOFC.

In these fuel cells being developed by Gur et al [27], oxygen anions from the electrolyte react with CO in the porous anode to form CO_2 and release electrons (Equation 1.22). A fraction of the CO_2 is then recycled and passed through a bed of carbon particles to form CO by the reverse Boudouard reaction (Equation 1.23). The CO produced from the Boudouard gasifier is then cycled to the anode for oxidation.

$$CO + O^{2-} \rightarrow CO_2 + 2e^- \qquad \text{Equation 1.22}$$

$$CO_2 + C \rightarrow 2CO \qquad \text{Equation 1.23}$$

The main issue with this $CO_2 \leftrightarrow CO$ shuttling mechanism is that the reverse Boudouard reaction is an endothermic reaction and is kinetically very slow. This reaction needs very high temperatures to occur and a considerable amount of heat is required to maintain the temperature of the gasifier [28]. Therefore, low fuel consumption along with high heat demands drastically brings down the efficiencies of these fuel cells.

1.5.2.2 Direct carbon-SOFCs with molten carbonate anodes

This technology is a "hybrid" of the key elements of both direct carbon-MCFC and direct carbon-SOFC designs. Essentially, both electrolytes from the MCFC and SOFC are used within one cell with the fuel dispersed within the molten carbonate electrolyte. The physical cell resembles a typical SOFC cell with the molten carbonate residing in the anode chamber as shown in Fig 1.8.

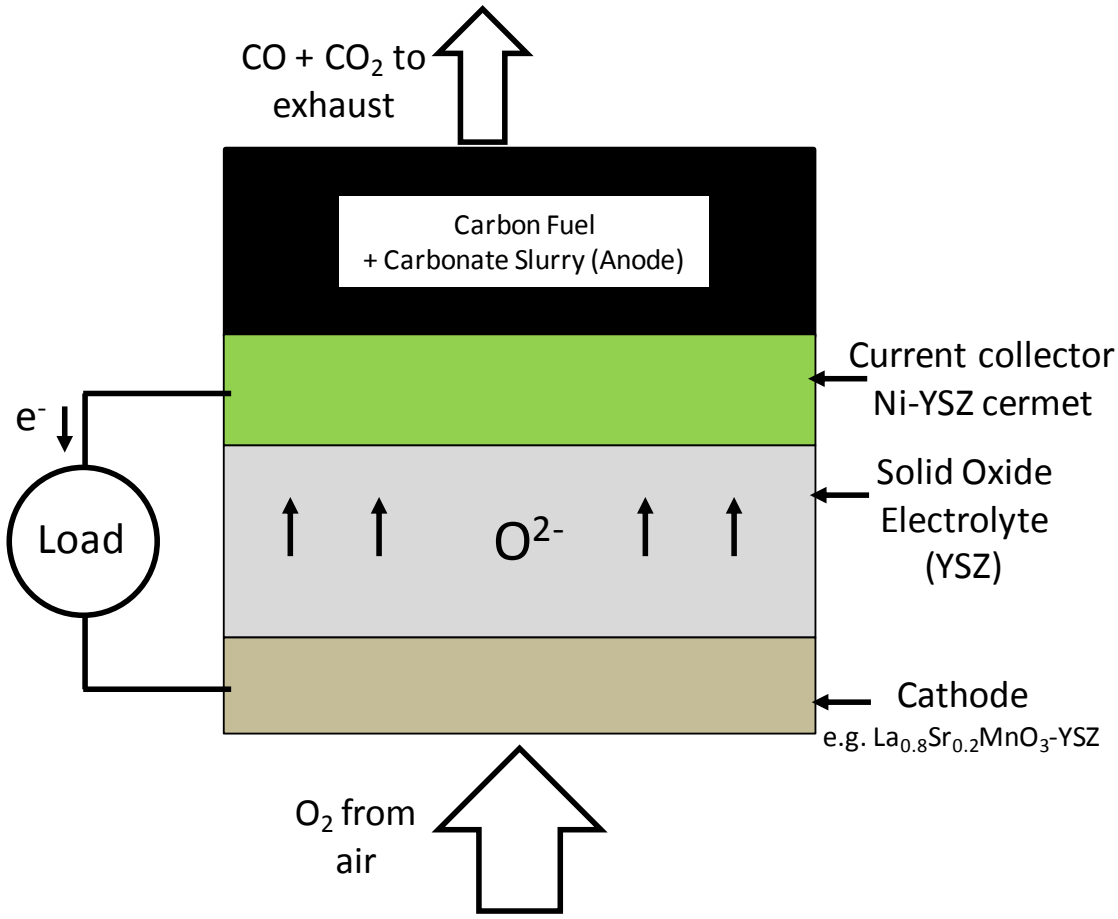

Figure 1.8: Operating schematic of a direct carbon-SOFC with a molten carbonate anode.

These DCFCs are also called Hybrid direct carbon fuel cells (HDCFC) and were conceived by the scientists at SRI International [29]. This "hybrid" concept helps alleviate some issues associated with the standalone versions of the direct carbon-MCFC and

SOFC. In the hybrid fuel cell, the cathode is separated from the molten carbonate by the SOFC electrolyte, thus reducing the possibility of cathode corrosion as observed in direct carbon MCFCs [30, 31]. It also negates the need to recycle CO_2 because the SOFC cathode can operate directly on air. However, the primary motivation for incorporating the molten carbonate in the SOFC anode chamber is for it to serve as an ionically conductive anode for the SOFC electrolyte. This will allow the oxygen to directly contact the carbon fuel and facilitate its oxidation. In HDCFCs, oxygen anions from the SOFC electrolyte contact the carbon particles via the molten carbonate anode to produce a mixture of CO and CO_2 in the manner similar to a direct carbon-MCFC [31].

Nevertheless, molten carbonates lack electronic conductivity and the performance of these cells still remains is limited due a lack of TPB as in the case of the direct carbon MCFC. Performances can be somewhat improved by introducing an electronically conductive, high surface area metallic mesh for current collection with a reactive form of carbon fuel [32] or by using a conductive form carbon fuel in the molten carbonate anode [33]. Optimal performance can only be achieved if the conductive fuel is always present in the anode at a high enough concentration and if it has a morphology that allows for intimate physical contact with the current collector. Therefore, the incorporation of an electronic conductor is always going to be a performance limiting factor for these fuel cells, requiring an optimal preparation of the fuel-carbonate mixture [20] and adversely affecting their fuel flexibility. Also, etching of the electrolyte [34] and corrosion of the current collectors on the anode side can be problems for cell durability.

1.5.2.3 Direct carbon-SOFCs with molten metal anodes

The use of a molten metal as an anode for SOFCs was pioneered by Tao et al. at CellTech Power [35]. A very clear advantage of this technology is that the entire anode will be electronically conductive. Moreover, metals are known to react with oxygen to form oxides and have certain amounts of oxygen solubility; therefore, metals could serve as oxygen-transport media as well. The appropriate choice of metal could be very promising in that the entire anode would be active for fuel oxidation, given the high electronic conductivity of all metals and the possibility for good oxygen transport in some.

In choosing a molten metal for operation at 1273 K, Tao et al. considered the following metals based on their melting temperatures: Al, Ga, Ge, In, Sn, Sb, Tl, Pb, Bi, Po, Ag, Hg and Cd. This group then considered the possibility that the metals could be reduced under typical anode conditions by examining the ΔG of reduction for the respective metal oxides. For example, Al and Ga were eliminated from consideration because they form very stable oxides that cannot be reduced by carbon. Ge and In were less desirable because their OCV was too close to that of carbon making them poor fuel oxidation catalysts. Cd, Sb, Pb, Po, Tl, Bi and Hg were ruled out because their volatility was too high at 1273 K. This left Sn and Ag as the two remaining anode choices. Based on the work done by CellTech Power, as discussed next, it is still unclear why Ag was eliminated as an anode choice despite its higher oxygen solubility. However, Ag has a positive ΔG for oxidation at 1273 K and will not form an oxide. The reason for choosing Sn is probably its higher OCV. This will allow oxygen transport to occur in the form of tin dioxide (SnO_2) at a higher potential when the metal is saturated with dissolved oxygen at high currents [36].

Most of the work done by CellTech Power using their molten Sn anode SOFC concept has been focused only on operation with H_2 and JP-8 (jet fuel) as the fuels at 1273 K [35, 37, 38]. In these experiments, a thin layer (300-500 μm) of molten Sn was held in contact with an SOFC electrolyte using a porous ceramic separator as shown in Fig 1.9. Surface tension prevents molten Sn from entering the porous ceramic, so that gaseous fuel (H_2 or gaseous pyrolysis products of JP-8) and gaseous oxidation products (H_2O and CO) can make contact with the Sn surface. The OCV for Sn oxidation (Equation 1.24) is 0.78 V, which is lower than the oxidation potentials for H_2 and other hydrocarbons at 1273 K [35]. Therefore SnO_2 formed can be readily reduced by H_2 (Equation 1.25) and other carbonaceous fuels.

$$Sn + 2O^{2-} \rightarrow SnO_2 + 4e^- \qquad \text{Equation 1.24}$$

$$SnO_2 + H_2 \rightarrow Sn(l) + H_2O \qquad \text{Equation 1.25}$$

The operation of this system was suggested to rely on the diffusivity of the dissolved oxygen from the electrolyte in the molten tin (Equation 1.26) and the diffusivity of the gaseous fuel into the molten tin for the fuel oxidation to occur (Equation 1.27) [21, 35].

$$Sn + xO^{2-} \rightarrow Sn\,[O^{2-}]_x \qquad \text{Equation 1.26}$$

$$Sn\,[O^{2-}]_x + xH_2 \rightarrow Sn(l) + xH_2O + 2xe^- \qquad \text{Equation 1.27}$$

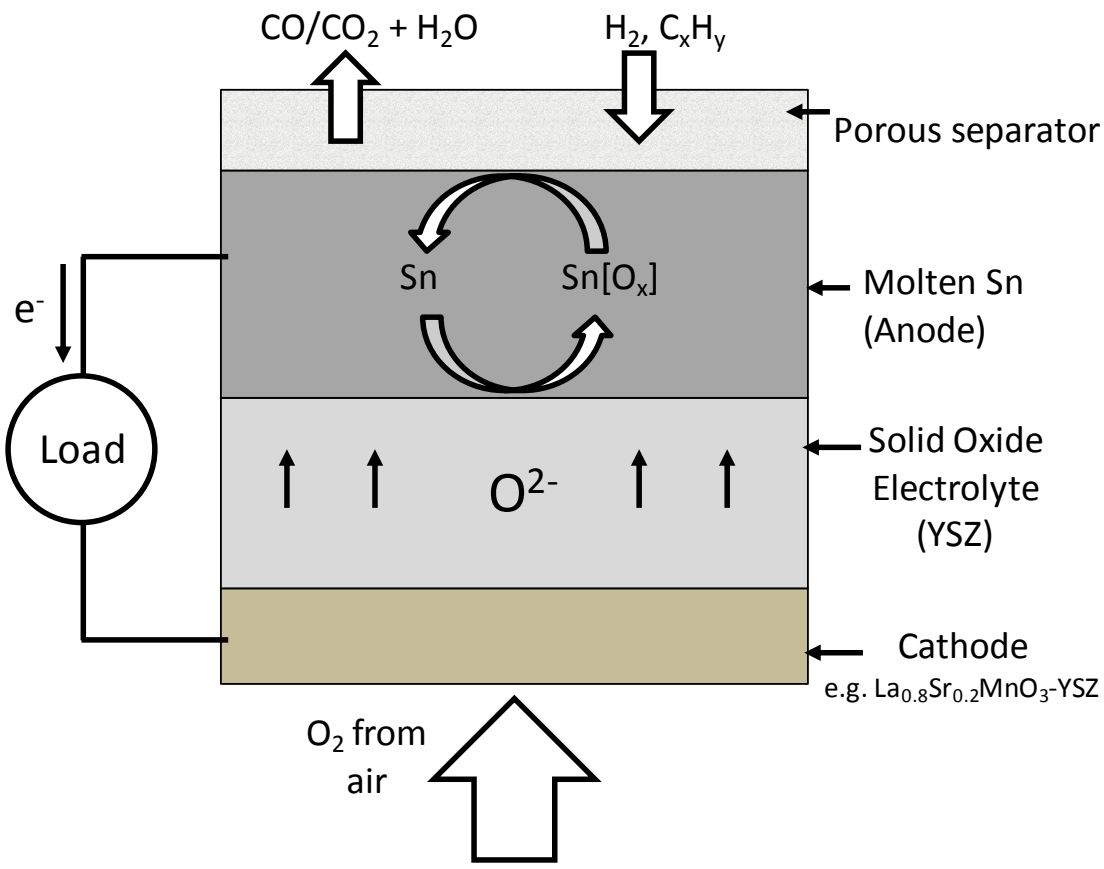

Figure 1.9: Operating schematic of CellTech Power's molten Sn anode-SOFC.

In these fuel cells, H_2 fuel from the feed stream diffuses through the porous separator into the molten tin where it is oxidized by the dissolved oxygen (Equation 1.27). The liquid JP-8 fuel was directly injected into the hot zone of the anode chamber and underwent pyrolysis. The pyrolysis products, consisting of a mixture of various gaseous hydrocarbon components, then diffuse through the porous separator and contact the molten tin to get oxidized by the dissolved oxygen. However, the effect of formation of pyrolysis soot which would clog the porous separator and cause cell failure was not clearly discussed. The performance levels observed with H_2 as the fuel were significantly

higher than those observed with JP-8. This was because a small molecule like H_2 would have a much higher diffusivity in the molten tin compared to the much larger hydrocarbon molecules formed in the case of JP-8. Therefore, for JP-8 the anode polarization losses would be much higher, resulting in lower power levels.

At high temperatures like 1273 K, the diffusivities of the fuel and oxygen in tin still might not have high enough values, even for H_2, and their contributions to the ohmic and anode polarization losses can be significant. Given that the electrolyte and cathode losses for an SOFC at 1273 K are nearly zero, the poor performances observed in these experiments prove that almost all of the losses are due to the sluggish oxygen transport in the molten Sn anode [39].

From the work done by CellTech Power, it was clear that molten Sn did not provide an efficient anode mechanism for fuel oxidation. However, the factors limiting the performance of these electrodes and the properties of SnO_2 to serve as the oxygen carrying medium to the fuel still needed to be studied. Moreover, the operating temperature used in this study was too high and could compromise cell component stability in conventional SOFCs. With the advancement in cell fabrication techniques, new catalytic materials for the cathode and the use of thin electrolytes, the typical operating temperature for a SOFC can be as low as 973 K [13]. Studying the practicality of Sn as an anode at these lower temperatures would actually determine if it could be a realistic solution.

Due to the inherent benefits of having a molten metal anode based direct carbon-SOFC, a further investigation of the oxygen transport properties of molten Sn and other molten metal anode candidates was warranted in order to understand their suitability for

oxidizing solid carbon and formed the basis of this thesis research. In the next sections, the SOFC materials and cell fabrication techniques used to setup the experiments carried out in this study will be discussed.

1.6 Materials used

1.6.1 Electrolyte: Y_2O_3-stablized ZrO_2 or Sc_2O_3-stabilized ZrO_2

Yttria-stabilized zirconia (YSZ) is a zirconium oxide based ceramic. Pure ZrO_2 is an insulator and exists in the monoclinic phase up to 1443 K. Between 1443 and 1973 K it transforms into a tetragonal phase and only at temperatures above 2613 K exists in the cubic phase [40]. The addition of a trivalent oxide, like Y_2O_3, to pure tetravalent ZrO_2, causes some of the Zr^{4+} ions in the lattice to be replaced by Y^{3+} ions. This creates oxygen vacancies in the lattice as three O^{2-} ions replace four O^{2-} ions. At high temperatures, the oxygen ions gain sufficient mobility and can hop from one lattice site to next, thus giving the material the property of O^{2-} ion conductivity.

SOFC operating temperatures range from 873-1273 K. For the doped ZrO_2, to be able to conduct ions at these temperatures, it is necessary that it exists in the cubic phase. At dopant levels of around 8 mol% Y_2O_3, this phase is stable from room temperature throughout the entire SOFC temperature range. It is also important to note that YSZ is not an electronic conductor, with an electronic transference number (number of electrons transported per ion transported) of around 10^{-4}, over a wide range of oxygen partial pressures [15, 41]. The maximum ionic conductivity for YSZ is also seen at the 8% Y_2O_3 dopant level (0.0188 S/cm at 973 K [15]). Therefore, most of the experiments carried out in this thesis research involve the use 8% doped YSZ electrolytes. At higher dopant levels,

defect concentrations in the YSZ increase causing electrostatic interactions in between the vacancies and the dopants, resulting in a lowering of the oxygen ion mobility [11, 15].

For the purpose of demonstrating high performances in the experiments discussed in chapters 4 and 5, the author used 10% Sc_2O_3-stabilized ZrO_2 (ScSZ) as the electrolyte. The reason for using ScSZ is that the Sc^{3+} dopant cations in the lattice are smaller than Y^{3+}, allowing for higher O^{2-} ion mobility. Therefore, these electrolytes have an ionic conductivity about 3 times that of YSZ at the operating temperature of 973 K (0.045 S/cm [23]). This allows for a thicker electrolyte made from a material with a higher mechanical strength than YSZ to be used in fuel cell conditions with heavy metal and fuel loadings.

1.6.2 Cathode: $La_{0.8}Sr_{0.2}FeO_{3-\delta}$ – porous YSZ or ScSZ composite

$LaFeO_3$ is an oxide material with a perovskite structure from the family of mixed oxides that have the general formula ABO_3. The A-site in this case contains lanthanum and the B-site contains iron. In this form the ionic and electronic conductivities of the oxide are relatively small and its electronic conductivity is low (0.4 S/cm in air at 973 K) [42]. But, the performance of an SOFC cathode is shown to be dependent on these properties [43].

In order to improve the ionic and electronic conductivities of $LaFeO_3$, the La^{3+} containing A-site is doped with 20 mol% of Sr^{2+} to form $La_{0.8}Sr_{0.2}FeO_{3-\delta}$ (LSF). This Sr-doped $LaFeO_3$ has an improved oxygen ion conductivity of (1.5×10^{-4} S/cm at 973 K in air) [44] due to oxygen vacancies created by substituting a divalent ion for a trivalent ion in the A-site. The electronic conductivity also increases significantly to ~80 S/cm in air at

973 K [45]. This is caused by the oxygen non-stoichiometry introduced by the oxidation of Fe^{3+} to Fe^{4+} [46]. LSF is known as a mixed ionic electronic conductor (MIEC) [11, 13, 47, 48].

LSF is chosen as the active phase for the composite cathode because it has a low impedance even at intermediate SOFC temperatures [49], unlike the popular choice of Sr-doped $LaMnO_3$ (LSM) which exhibits very high impedances at temperatures below 1073 K [50]. It also does not show any degradation in performance over long term testing at intermediate SOFC temperatures, as compared to Sr-doped $LaCoO_3$ which forms insulating phases like $La_2Zr_2O_7$ even at temperatures as low as 973 K [51]. The porous composite LSF-YSZ/ScSZ cathode was fabricated using the infiltration method, developed at the University of Pennsylvania, as discussed next in the cell fabrication methods section.

1.7 Cell fabrication methods

SOFC electrolyte-cathode bilayer wafers were fabricated by the techniques of tape-casting and infiltration as described below. These bilayer wafers consisted of a dense YSZ (or ScSZ) electrolyte layer attached with a porous composite cathode, LSF-YSZ (or LSF-ScSZ), on one side.

1.7.1 Tape-casting

In this fabrication process, a ball-milled slurry consisting of a mixture of the YSZ or ScSZ powder, a polymeric binder, dispersant, plasticizers and the solvent was cast on a silicone oil coated sheet on a conveyor by the help of a doctor-blade as shown in Fig 1.10. This formed the green dense electrolyte film. When a carbonaceous pore former like graphite (Sigma-Aldrich) was added to the slurry and cast, the green porous ceramic

film was formed [13, 18]. These green tapes were then punched out into circular disks 3/4 and 3/8 inches in diameter respectively. The green dense electrolyte disk was then laminated with the green porous ceramic disk on one side by hot pressing. The laminates were then sintered to 1773 K (to burn off the pore formers and densify the ceramic) to form the bilayer wafers consisting of the dense electrolyte layer and a porous ceramic scaffold layer. After sintering, the dense electrolyte layer was 1.4 cm in diameter and the porous layer was 0.67 cm in diameter.

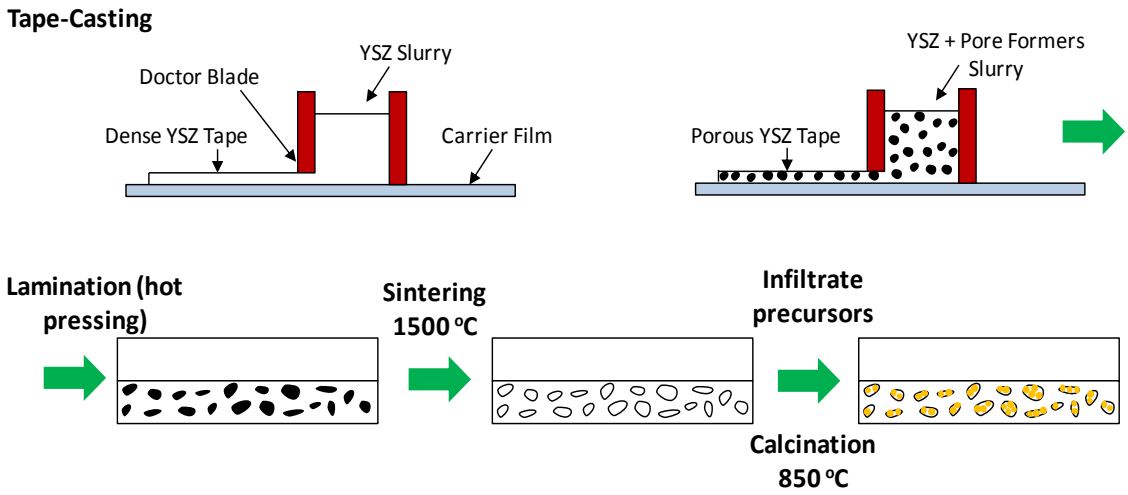

Figure 1.10: Tape-casting followed by Infiltration to form dense electrolyte (YSZ) porous composite cathode (LSF-YSZ) bilayer wafers.

1.7.2 Infiltration

The method of infiltration was used to add the active LSF ($La_{0.8}Sr_{0.2}FeO_3$) perovskite phase into the porous-ceramic scaffold to form the composite cathode. In this technique, an aqueous solution containing the nitrates of the components metals, $La(NO_3)_3.6H_2O$, $Sr(NO_3)_2$ and $Fe(NO_3)_3.9H_2O$ at a molar ratio of La : Sr : Fe = 0.8 : 0.2 : 1 was prepared. To this solution, a chelating agent like citric acid was added in a 1:1 molar ratio to the metal cations to aid in the formation of the perovskite phase at lower

temperatures. This solution was then infiltrated into the porous scaffold. Upon calcining to 1123 K, the nitrates decompose and the cations arrange to form the desired perovskite phase. The final LSF-YSZ or LSF-ScSZ composite cathode contained 35-40 wt% of LSF [52, 53].

The infiltration method made it possible to sinter the ceramic components and the perovskite component of the cell in two separate steps. This enabled much better control over the microstructure of the infiltrated perovskite and allowed the usage of more active cathode catalysts, resulting in the better performance of the cathode.

1.8 Experimental setup for cell tests

The electrolyte-cathode bilayer wafer with the infiltrated composite cathode was attached to the end of an alumina tube with a ceramic adhesive (Aremco Ceramabond 552). The wafer was attached such that the cathode side was outside and the blank dense electrolyte face was sealed inside the tube. Silver paste and silver wires were used to make electrical connections to the cathode. The metal to be tested was then added in powder form into the alumina tube, making contact with the anode side of the electrolyte surface by gravity. The anode current collectors or leads were then dipped into the metal in order to make electrical connections to the anode. The anode current collector materials and configurations used in the short term experiments (in chapters 2 and 3) and the long term molten Sb based DCFC tests (in chapters 4 and 5) were different.

The current collector materials used in the short term characterization experiments were the conductive perovskite materials of reduced-$La_{0.7}Sr_{0.3}TiO_3$ (LST) and $La_{0.8}Sr_{0.2}CrO_3$ (LSCr). These perovskite powders were fabricated from a stoichiometric

solution of their precursors using the Pechini method [54]. The powders were pelletized by mechanical pressing and sintering to 1773 K. The LST pellets were then reduced in H_2 at 1173 K for 12 hours to form reduced LST, which is electronically conductive.

The conductive perovskite pellets made of reduced-LST or LSCr were then attached to an alumina tube that allowed the metal to be "pressed" onto the electrolyte, as shown in Fig. 1.11a. Ag wires pasted on one side of the pellet were passed through the thin alumina tube for electrical contact with the perovskite pellets. The pellets served as the anode current collectors for the short term experiments. Pressing down with the pellets ensured that the metal was completely covering the effective area of the electrolyte. This was done because the metals showed the tendency to ball-up on the electrolyte surface when added in limited quantities, due to their high surface tension.

In the long term cell tests demonstrating DCFCs based on molten antimony, the LST and LSCr perovskites along with many other metal oxides and metal wires that were tested as anode current collectors, were found to react with the Sb-Sb_2O_3 anode and lose their conductivity, causing the cell performance to drop. Finally, long term stable cell performance was achieved by the use of Rhenium wires as the anode current collectors. This is because Re does not alloy with molten Sb [55] and also does not get oxidized by Sb_2O_3 at the operating temperature of 973 K, thereby maintaining a constantly low contact resistance with the anode throughout the duration of the experiment. Re wires were dipped into the molten Sb anode for current collection as shown in Fig 1.11b. In these experiments, the solid fuel was then added over the molten Sb pool. The bed of solid fuel was maintained in direct contact with the Sb anode below.

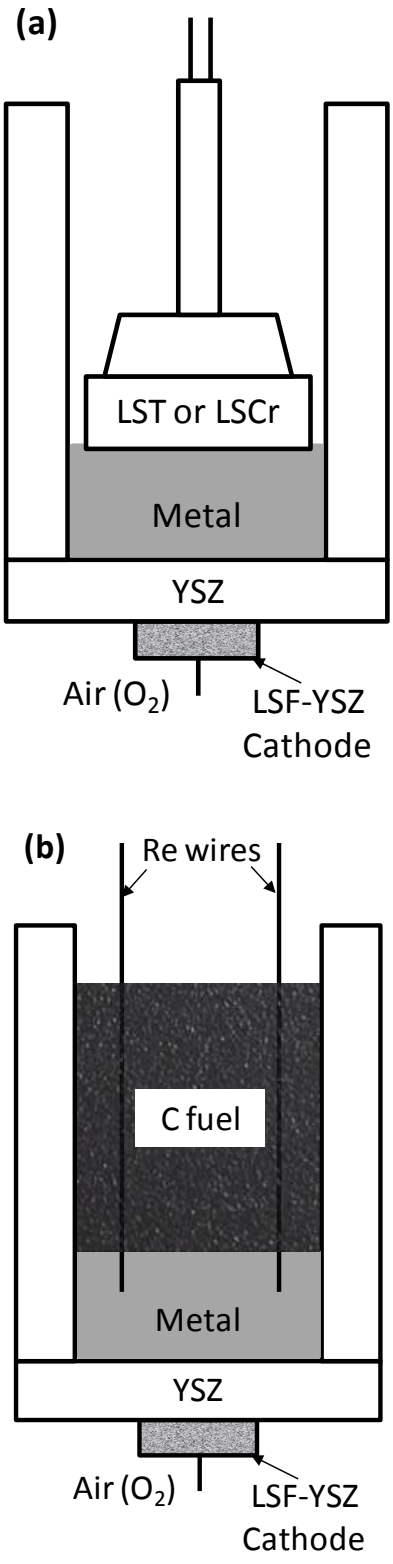

Figure 1.11a-b: (a) Perovskite pellet anode current collector setup (chapters 2 and 3). (b) Re wire anode current collector setup for long-term Sb anode tests (chapters 4 and 5).

After putting the anode current collectors in place, and adding fuel as the case may be, the alumina cell tube was then held vertically inside a tubular furnace and heated upto the cell operating temperature.

1.9 References

1. Energy Efficiency: A Recipe for Success. *World Energy Council, London* **2010**.
2. Ptasinski, K. J., Thermodynamic efficiency of biomass gasification and biofuels conversion. *Biofuels Bioproducts & Biorefining-Biofpr* **2008,** 2, (3), 239-253.
3. Levine, J. S.; Cofer, W. R.; Cahoon, D. R.; Winstead, E. L., Biomass Burning - a Driver for Global Change. *Environ. Sci. Tech.* **1995,** 29, (3), A120-A125.
4. Singhal, S. C., *High temperature Solid Oxide Fuel Cells: fundamentals, design and applications*. Elsevier, Oxford: 2003.
5. Cao, D. X.; Sun, Y.; Wang, G. L., Direct carbon fuel cell: Fundamentals and recent developments. *J. Power Sources* **2007,** 167, (2), 250-257.
6. *Program on Technology Innovation: Systems Assessment of Direct Carbon Fuel Cells Technology*; Electric Power Research Institute: Palo Alto, CA, 2008.
7. Kurzweil, P., *History – Fuel cells*. Elsevier: Amsterdam, 2009.
8. Goret, J.; Tremillion, B., Proprietes chimiques et electrochimiques en solution dans les hydroxydes alcalins fondus-IV. Comportement electrochimique de quelques metaux utilises comme electrodes indicatrices. *Electrochim. Acta* **1967,** 12, (8), 1065-1083.
9. Dicks, A. L., The role of carbon in fuel cells. *J. Power Sources* **2006,** 156, (2), 128-141.

10. Cropper, M. A. J.; Geiger, S.; Jollie, D. M., Fuel cells: a survey of current developments. *J. Power Sources* **2004,** 131, (1-2), 57-61.
11. O'Hayre, R. P.; Cha, S. W.; Collela, W.; Prinz, F. B., *Fuel cell fundamentals*. John Wiley & Sons: Hoboken, N.J., 2009; p xxii, 409 p.
12. Yamahara, K.; Jacobson, C. P.; Visco, S. J.; DeJonghe, L. C., Influence of powders on polycrystalline zirconias. *Proceedings of the Eighth Symposium on Solid Oxide Fuel Cells (SOFC-VIII)* **2003**, 187-195.
13. Vohs, J. M.; Gorte, R. J., High-Performance SOFC Cathodes Prepared by Infiltration. *Adv. Mater.* **2009,** 21, (9), 943-956.
14. McIntosh, S.; Gorte, R. J., Direct hydrocarbon solid oxide fuel cells. *Chem. Rev.* **2004,** 104, (10), 4845-4865.
15. Minh, N. G.; Takahashi, T., *Science and Technology of Ceramic Fuel Cells*. Elsevier: Amsterdam, 1995.
16. Bove, R.; Lunghi, P., Electric power generation from landfill gas using traditional and innovative technologies. *Energy Conv. Mgmt.* **2006,** 47, (11-12), 1391-1401.
17. Pusz, J.; Bove, R.; Sammes, N. M., Landfill gas energy recovery based on micro-tubular solid oxide fuel cells. *Proceedings of the Ninth Symposium on Solid Oxide Fuel Cells (SOFC-IX)* **2005**, 277.
18. Park, S. D.; Vohs, J. M.; Gorte, R. J., Direct oxidation of hydrocarbons in a solid-oxide fuel cell. *Nature* **2000,** 404, (6775), 265-267.
19. Kim, H.; Park, S.; Vohs, J. M.; Gorte, R. J., Direct oxidation of liquid fuels in a solid oxide fuel cell. *J. Electrochem. Soc.* **2001,** 148, (7), A693-A695.

20. Jain, S. L.; Lakeman, J. B.; Pointon, K. D.; Marshall, R.; Irvine, J. T. S., Electrochemical performance of a hybrid direct carbon fuel cell powered by pyrolysed MDF. *Energy Environ. Sci.* **2009,** 2, (6), 687-693.
21. Abernathy, H.; Gemmen, R.; Gerdes, K.; Koslowske, M.; Tao, T., Basic properties of a liquid tin anode solid oxide fuel cell. *J. Power Sources* **2011,** 196, (10), 4564-4572.
22. Dicks, A. L., Molten carbonate fuel cells. *Current Opinion in Solid State & Materials Science* **2004,** 8, (5), 379-383.
23. Kungas, R.; Vohs, J. M.; Gorte, R. J., Effect of the Ionic Conductivity of the Electrolyte in Composite SOFC Cathodes. *J. Electrochem. Soc.* **2011,** 158, (6), B743-B748.
24. Cherepy, N. J.; Krueger, R.; Fiet, K. J.; Jankowski, A. F.; Cooper, J. F., Direct conversion of carbon fuels in a molten carbonate fuel cell. *J. Electrochem. Soc.* **2005,** 152, (1), A80-A87.
25. Cooper, J. F. In *Direct conversion of coal and coal-derived carbon in fuel cells*, Second International Conference on Fuel Cell Science, Engineering and Technology, ASME, Rochester, NY, 2004; 2004.
26. Selman, J. R., Molten-salt fuel cells - Technical and economic challenges. *J. Power Sources* **2006,** 160, (2), 852-857.
27. Gur, T. M.; Huggins, R. A., Direct Electrochemical Conversion of Carbon to Electrical Energy in a High-Temperature Fuel-Cell. *J. Electrochem. Soc.* **1992,** 139, (10), L95-L97.
28. Gur, T. M.; Homel, M.; Virkar, A. V., High performance solid oxide fuel cell operating on dry gasified coal. *Journal of Power Sources* **2010,** 195, (4), 1085-1090.

29. Heydorn, B.; Crouch-Baker, S., Direct Carbon Conversion: Progressions of Power. *Fuel Cell Rev., IOP, New York* **2006**.
30. Nabae, Y.; Pointon, K. D.; Irvine, J. T. S., Electrochemical oxidation of solid carbon in hybrid DCFC with solid oxide and molten carbonate binary electrolyte. *Energy Environ. Sci.* **2008,** 1, (1), 148-155.
31. Jiang, C. R.; Irvine, J. T. S., Catalysis and oxidation of carbon in a hybrid direct carbon fuel cell. *J. Power Sources* **2011,** 196, (17), 7318-7322.
32. Nabae, Y.; Pointon, K. D.; Irvine, J. T. S., Ni/C Slurries Based on Molten Carbonates as a Fuel for Hybrid Direct Carbon Fuel Cells. *J. Electrochem. Soc.* **2009,** 156, (6), B716-B720.
33. Lipilin, A. S.; Balachov, I. I.; Dubois, L. H.; Sanjurjo, A.; McKubre, M. C. Liquid Anode Electrochemical Cell. U.S. Patent 2006/0019132, 2006.
34. Jiang, C. R.; Ma, J. J.; Bonaccorso, A. D.; Irvine, J. T. S., Demonstration of high power, direct conversion of waste-derived carbon in a hybrid direct carbon fuel cell. *Energy Environ. Sci.* **2012,** 5, (5), 6973-6980.
35. Tao, T.; Bateman, L.; Bentley, J.; Slaney, M., Liquid Tin Anode Solid Oxide Fuel Cell for Direct Carbonaceous Fuel Conversion. *ECS Trans.* **2007,** 5, (1), 463-472.
36. Tao, T.; White, R.; Klotz, S., Liquid Metal Anode for JP-8 Fuel Cell. In DTIC Document: 2009; pp 11-63.
37. Tao, T.; Slaney, M.; Bateman, L.; Bentley, J., Anode Polarization in Liquid Tin Anode Solid Oxide Fuel Cell. *ECS Trans.* **2007,** 7, (1), 1389-1397.
38. McPhee, W. A. G.; Bateman, L.; Koslowske, M.; Slaney, M.; Uzep, Z.; Bentley, J.; Tao, T., Direct JP-8 Conversion Using a Liquid Tin Anode Solid Oxide Fuel Cell

(LTA-SOFC) for Military Applications. *Journal of Fuel Cell Science and Technology* **2011,** 8, (4).

39. Koslowske, M. T.; McPhee, W. A.; Bateman, L. S.; Slaney, M. J.; Bentley, J.; Tao, T., Advanced Cell Development for Increased Direct JP-8 Performance in the Liquid Tin Anode SOFC. *Ceramic Engineering and Science Proceedings (American Ceramic Society)* **2009,** 30, (4), 27-35.
40. Scott, H. G., Phase relationships in the zirconia-yttria system. *J. Mater. Sci.* **1975,** 10, 1527.
41. Kingery, W. D.; Bowen, H. K.; Uhlmann, D. R., *Introduction to Ceramics* 2nd ed.; John Wiley and Sons: 1976.
42. Waernhus, I.; Grande, T.; Wiik, K., Electronic properties of polycrystalline LaFeO3. Part II: Defect modelling including Schottky defects. *Solid State Ionics* **2005,** 176, (35-36), 2609-2616.
43. Bidrawn, F.; Kungas, R.; Vohs, J. M.; Gorte, R. J., Modeling Impedance Response of SOFC Cathodes Prepared by Infiltration. *J. Electrochem. Soc.* **2011,** 158, (5), B514-B525.
44. Ren, Y. Y.; Kungas, R.; Gorte, R. J.; Deng, C. S., The effect of A-site cation (Ln = La, Pr, Sm) on the crystal structure, conductivity and oxygen reduction properties of Sr-doped ferrite perovskites. *Solid State Ionics* **2012,** 212, 47-54.
45. Sogaard, M.; Hendriksen, P. V.; Mogensen, M., Oxygen nonstoichiometry and transport properties of strontium substituted lanthanum ferrite. *J. Solid State Chem.* **2007,** 180, (4), 1489-1503.

46. Montini, T.; Bevilacqua, M.; Fonda, E.; Casula, M. F.; Lee, S.; Tavagnacco, C.; Gorte, R. J.; Fornasiero, P., Relationship between Electrical Behavior and Structural Characteristics in Sr-Doped LaNi0.6Fe0.4O3-delta Mixed Oxides. *Chem. Mater.* **2009,** 21, (8), 1768-1774.
47. Tanner, C. W.; Fung, K. Z.; Virkar, A. V., The effect of porous composite electrode structure on solid oxide fuel cell performance .1. Theoretical analysis. *J. Electrochem. Soc.* **1997,** 144, (1), 21-30.
48. Adler, S. B., Factors governing oxygen reduction in solid oxide fuel cell cathodes. *Chem. Rev.* **2004,** 104, (10), 4791-4843.
49. Bidrawn, F.; Lee, S.; Vohs, J. M.; Gorte, R. J., The effect of Ca, Sr, and Ba doping on the ionic conductivity and cathode performance of LaFeO(3). *J. Electrochem. Soc.* **2008,** 155, (7), B660-B665.
50. Barbucci, A.; Bozzo, R.; Cerisola, G.; Costamagna, P., Characterisation of composite SOFC cathodes using electrochemical impedance spectroscopy. Analysis of Pt/YSZ and LSM/YSZ electrodes. *Electrochim. Acta* **2002,** 47, (13-14), 2183-2188.
51. Sase, M.; Ueno, D.; Yashiro, K.; Kaimai, A.; Kawada, T.; Mizusaki, J., Interfacial reaction and electrochemical properties of dense (La,Sr) CoO3-delta cathode on YSZ(100). *J. Phys. Chem. Solids* **2005,** 66, (2-4), 343-348.
52. Huang, Y. Y.; Vohs, J. M.; Gorte, R. J., Fabrication of Sr-doped LaFeO3-YSZ composite cathodes. *J. Electrochem. Soc.* **2004,** 151, (4), A646-A651.
53. Wang, W. S.; Gross, M. D.; Vohs, J. M.; Gorte, R. J., The stability of LSF-YSZ electrodes prepared by infiltration. *J. Electrochem. Soc.* **2007,** 154, (5), B439-B445.

54. Mori, M.; Sammes, N. M., Sintering and thermal expansion characterization of Al-doped and Co-doped lanthanum strontium chromites synthesized by the Pechini method. *Solid State Ionics* **2002,** 146, (3-4), 301-312.

55. Moffatt, W. G., *Re-Sb (Rhenium-Antimony)*. Schenectady, NY, 1978.

Chapter 2. A Comparison of Molten Sn and Bi for Solid Oxide Fuel Cell Anodes

Summary

Molten Sn and Bi were examined at 973 and 1073 K for use as anodes in solid oxide fuel cells with yttria-stabilized zirconia (YSZ) electrolytes. Cells were operated under "battery" conditions (no fuel), with dry He flow in the anode compartment, to characterize the electrochemical oxidation of the metals at the YSZ interface. For both metals, the open circuit voltages (OCVs) were close to that expected based on their oxidation thermodynamics, ~0.93 V for Sn and ~0.48 V for Bi at 973 K. With Sn, the cell performance degraded rapidly after the transfer of approximately 0.5–1.5 C/cm^2 of charge due to the formation of a SnO_2 layer at the YSZ interface. At 973 K, the anode impedance at OCV for freshly reduced Sn was approximately 3 Ω.cm^2 but this increased to well over 250 Ω.cm^2 after the transfer of 1.6 C/cm^2 of charge. Following the transfer of 8.2 C/cm^2 at 1073 K, the formation of a 10 μm thick SnO_2 layer was confirmed by scanning electron microscopy. With Bi, the OCV anode impedance at 973 K was less than 0.25 Ω.cm^2 and remained constant until essentially all of the Bi had been oxidized to Bi_2O_3. Some implications of these results for direct carbon fuel cells are discussed.

2.1 Introduction

Previous studies of SOFCs operating with molten-Sn anodes showed very low power densities and overall poor performance, even at the high operating temperature of 1273 K [1]. Besides the suggestion for electrode limitations due to sluggish transport of dissolved oxygen in molten Sn, there was no explanation for what factors limit the

performance of these electrodes and no data available that would prove that oxygen diffusion is limiting. Therefore, the performance characteristics of the molten Sn anode and the properties of SnO_2 to serve as an oxygen-transport medium needed to be further evaluated. The typical intermediate SOFC temperature of 973 K was considered as the ideal operating temperature for this study of molten Sn. For comparison purposes, molten Bi, which has a low volatility at 973 K and forms O^{2-} ion-conductive Bi_2O_3, was also considered.

$$M + nO^{2-} \rightarrow MO_n + 2ne^- \qquad \text{Equation 2.1}$$

The work presented in this chapter set out to investigate metal oxidation (Equation 2.1) in a fuel cell with a YSZ electrolyte, using molten Sn or Bi as the anode. These experiments were carried out in "battery" mode (no fuel present) in order to study the characteristics of oxygen transfer at the electrolyte-anode interface. With Sn, a critical issue that limits performance at temperatures below 1073 K is the formation of a solid SnO_2 film at the electrolyte interface due to the very low solubility of oxygen in molten Sn [2]. The performance of the Sn-based electrodes appears to be limited by the low ionic conductance of this SnO_2 layer, at least for temperatures below 1073 K. With molten Bi, the electrochemical reaction is facile, probably because the oxide is a good ionic conductor [3]; however, the critical issue with Bi is its lower open-circuit potential.

2.2 Experimental

The electrolyte-cathode bilayer wafers for these experiments were fabricated as described in section 1.7. The dense YSZ electrolyte layers were 900 μm thick and the LSF-YSZ porous composite cathodes were 50 μm thick containing 40 wt% of LSF.

The cell was then setup as discussed in section 1.8. The ceramic current collector made of reduced-$La_{0.3}Sr_{0.7}TiO_3$ (LST) or $La_{0.8}Sr_{0.2}CrO_3$ (LSCr) in the form of a circular pellet was used to "press" the metal onto the electrolyte, as shown in Fig. 1.11a. The porous separator in the work by CellTech Power likely plays a similar role in maintaining contact between Sn and the electrolyte [4]. In this study, 800 mg of either Sn (Aldrich) or Bi (Aldrich) was added to the anode compartment. Based on the densities of the metals and the inner diameter of the tube used for the anode compartment, the thicknesses of the resulting metal layers were approximately 1.5 mm.

For electrochemical characterization, the cathode was held in air and a gas flow was maintained over the anode. Most experiments were conducted in battery mode (no fuel) since the metal oxidation reaction (Equation 2.1) was of interest. The anodes were first reduced in humidified (3% H_2O) H_2, but the electrochemical measurements were performed while flowing dry He into the anode compartment. Impedance spectra and voltage–current (V-i) polarization curves were measured using a Gamry Instruments potentiostat. After reduction of the metal in humidified H_2, the anode compartment was exposed to dry, flowing He and the V-i curves were measured by ramping the voltage from open circuit OCV to 0 V (short circuit) and back at 10 mV/s. Impedance spectra were measured galvanostatically at various currents in the frequency range of 300 kHz–0.1 Hz, with a 1 mA a.c. perturbation. The average of the anode and cathode diameters was used to calculate the effective electrode area, which was then used to normalize the current densities. Scanning electron microscopy (SEM) was performed using a JEOL 7500F HRSEM, together with energy-dispersive X-ray spectroscopy (EDX).

2.3 Results

2.3.1 Molten Sn anodes

Fig. 2.1 shows the V-i characteristics of the cell with the molten Sn anode at 973 K. In this experiment, the anode compartment was reduced in flowing, humidified (3% H_2O) H_2 while holding the cell at open circuit. After flushing the H_2 from the anode compartment with dry He, the initial open-circuit voltage (OCV) of the freshly reduced cell was approximately 0.93 V, very close to the expected potential for the oxidation of Sn (Equation 2.2), when it is referenced to air [5].

$$Sn + 2O^{2-} \rightarrow SnO_2 + 4e^- \qquad \text{Equation 2.2}$$

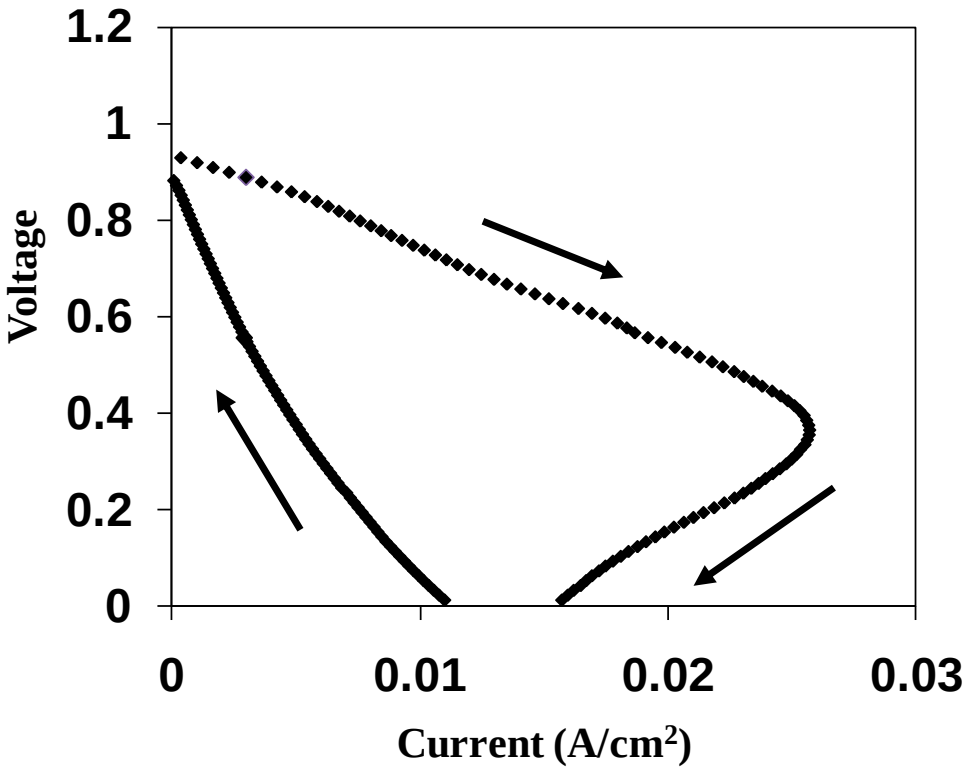

Figure 2.1: V-i polarization curve for the cell with the molten Sn anode at 973 K. After reduction of the Sn in humidified H_2, the anode compartment was exposed to dry, flowing He while ramping the voltage from open circuit to 0 V and back at 10 mV/s.

Next, the current generated by the cell was measured while decreasing the potential at 10 mV/s. After the cell potential reached zero, the potential was ramped up at 10 mV/s. The data shows that the current reached a maximum as the potential was lowered and then began to decrease. The decrease in current was not reversed by increasing the potential. In fact, the observed currents were much lower than before. Results obtained at 1073 K were qualitatively similar to those at 973 K as shown in Fig. 2.1. The impedance measurements in Fig. 2.2 demonstrate that the changes occurring in the cell are associated with the anode. Figure 2.2a is the Cole–Cole plot of the reduced cell at 973 K in dry He before applying any current. The high frequency intercept with the real axis, which corresponds to the ohmic resistance of the cell, occurs at 5.37 $\Omega.cm^2$ and is reasonably close to the expected value of 4.7 $\Omega.cm^2$ for the measured YSZ electrolyte thickness of this cell, 890 μm, based on tabulated conductivity of YSZ at 973 K, 0.0188 S/cm [6]. The non-ohmic impedance, determined from the difference between the low and high frequency intercepts, is approximately 3 $\Omega.cm^2$. Because the contribution from the LSF-YSZ cathode at this temperature is between 0.1 and 0.2 $\Omega.cm^2$ [7, 8], most of the non-ohmic contribution is from the Sn anode. Figure 2.2b shows the impedance data at OCV after completing a cycle like that shown in Fig. 2.1. The ohmic resistance has not changed significantly, demonstrating that the electrode retains high electronic conductivity. However, the non-ohmic losses in the cell are now enormous; approximately 250 $\Omega.cm^2$. Experiments performed at 1073 K gave results that were qualitatively similar.

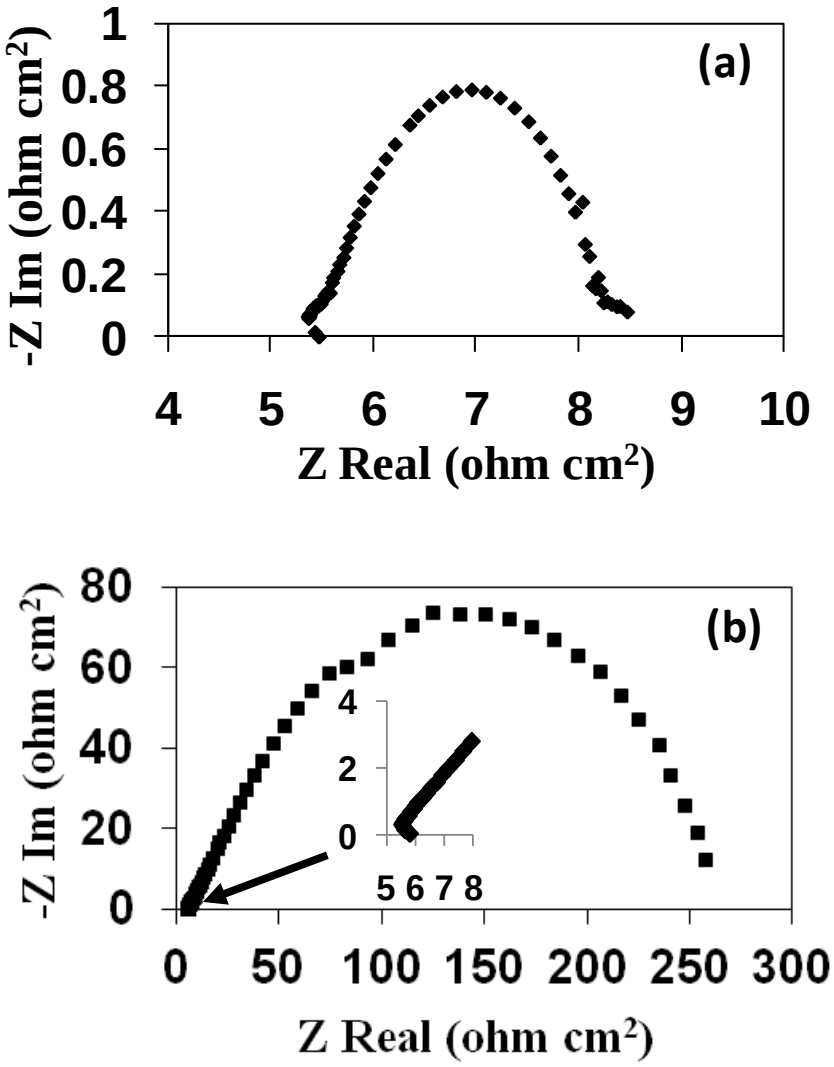

Figure 2.2a-b: Impedance data for the cell with the molten Sn anode at 973 K, corresponding to the V-i polarization data in Figure 2.1. (a) Cole-Cole plot obtained at open circuit immediately after reduction of the Sn. (b) Cole-Cole plot after completing the ramps from open circuit to 0 V and back.

The drop in current and increase in impedance are related to the amount of charge that had been drawn from the cell. When experiments like that shown in Fig. 2.1 were conducted at lower ramp rates, the maximum current occurred at lower values. Measurements at 1073 K with ramp rates between 1 and 10 mV/s indicated that the total amount of charge transferred across the electrolyte was nearly constant, between 4 and 6

C/cm^2, before the impedance became very large. Furthermore, once this charge had been transferred, the only way to restore the low impedance of the cell was to expose the anode to flowing H_2 for at least 30 min. Holding the cell at OCV in flowing He overnight had no effect on the impedance. These results suggest that the increased impedance is due to the formation of a thin dense SnO_2 layer at the electrolyte interface. Once this layer is formed, oxidation of additional Sn is limited by transport of oxygen through the SnO_2 layer and the low solubility of oxygen in liquid Sn, which is only 0.10 mol % at 1073 K [2].

To confirm that cell deactivation was due to the formation of an oxide layer at the YSZ interface, a V-i cycle was performed like that shown in Fig. 2.1 at 1073 K. Then the cell was cooled to room temperature and the YSZ interface was examined using SEM and EDX. The total charge transferred in this experiment was 8.2 C/cm^2, which corresponds to the formation of a SnO_2 layer that is 4.6 μm thick. As shown in Fig. 2.3, this oxide layer is readily apparent in the cross-sectional SEM image. The SEM and EDX data indicate that there is indeed a SnO_2 layer, approximately 10 μm thick, at the YSZ interface. The somewhat larger SEM thickness is likely due to the SnO_2 layer being somewhat porous. Also, EDX results indicated that some SnO_2 on the spherical particles was farther from the electrolyte interface. It is unclear if this results from the process of fracturing the Sn-YSZ interface or if this is an indication that some SnO_2 may extend some distance from the YSZ electrolyte interface.

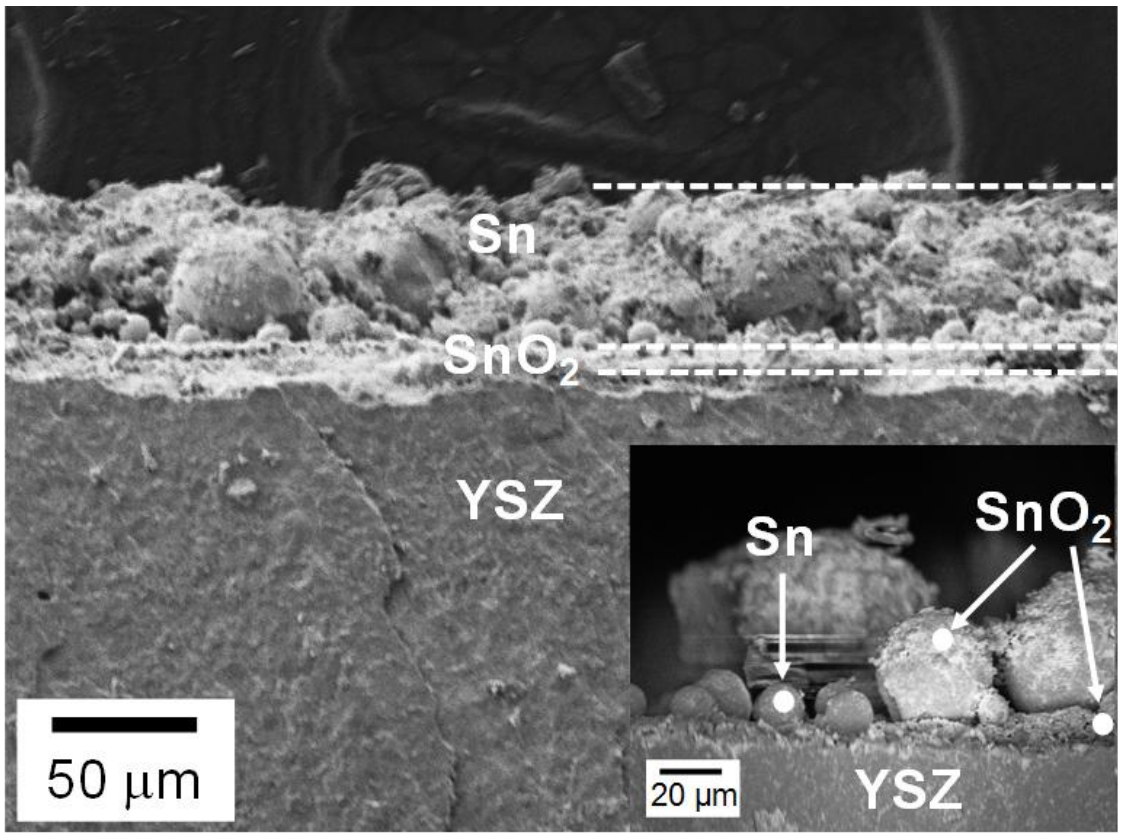

Figure 2.3: SEM and EDX results obtained at the molten Sn/YSZ electrolyte interface. The micrograph was obtained after passing 8.2 C/cm^2 of charge through the electrolyte at 1073 K, then quenching to room temperature, and shows the formation of a SnO_2 layer at the YSZ interface.

2.3.2 Molten Bi anodes

Bi has a similar melting temperature to that of Sn (545 K vs 505 K) so that it was of interest to examine the characteristics of a cell with a molten Bi anode. The cell was again operated in battery mode, with dry He flowing into the anode compartment after reducing the Bi, so that the electrochemical oxidation of the metal, given in Equation 2.3, could be studied.

$$Bi + 1.5O^{2-} \rightarrow BiO_{1.5} + 3e^{-} \qquad \text{Equation 2.3}$$

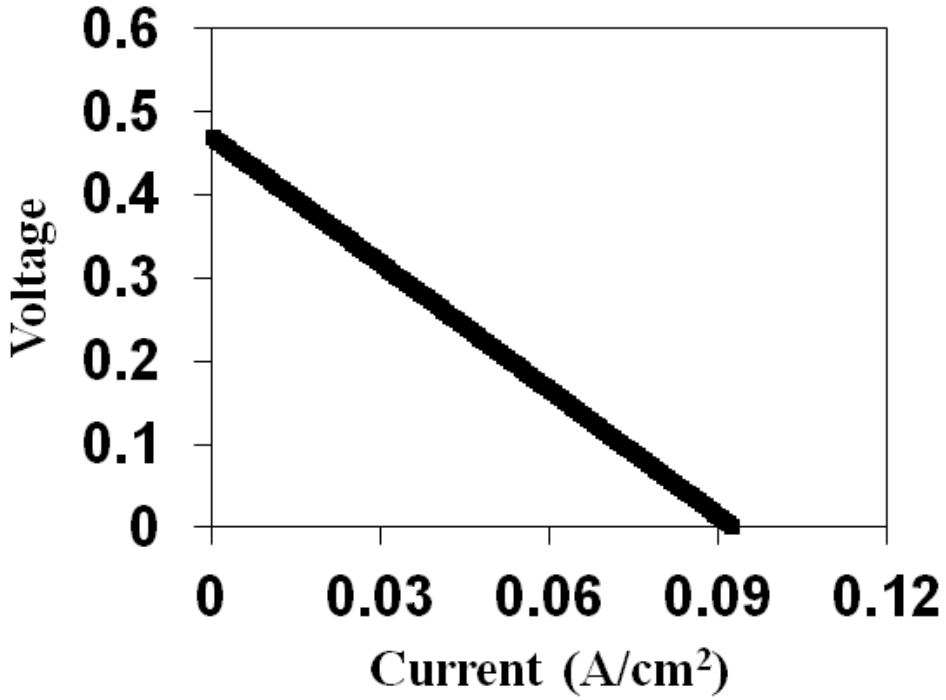

Figure 2.4: V-i polarization curve for the cell with the molten Bi anode at 973 K. After reduction of the Bi in humidified H_2, the anode compartment was exposed to dry, flowing He.

The mass of Bi used in the anode was also 800 mg, the same as that used for the Sn anode. The V-i plot at 973 K in Fig. 2.4 shows many important differences from that observed for the cell with the Sn anode. First, in agreement with expectations based on the thermodynamics of Equation 2.3, the OCV is only 0.48 V. Second, the V-i polarization plot is a straight line that exhibited complete reversibility when the potential was ramped up or down. The Cole–Cole plot for the Bi cell, shown in Fig. 2.5, demonstrates that the impedance of the Bi anode was very small. The ohmic impedance was again 4.8 Ω. cm^2, close to the value of 5.27 Ω. cm^2 expected for the 990 μm YSZ electrolyte. However, unlike the case for the cell with the Sn anode, the non-ohmic impedance for the cell with the Bi anode was very low, only 0.22 Ω. cm^2. Because this is

close to the impedance of the LSF-YSZ cathode [7, 8], the anode losses must be negligible. The fact that the V-i plot in Fig. 2.4 was linear implies that the impedance remains low under applied currents.

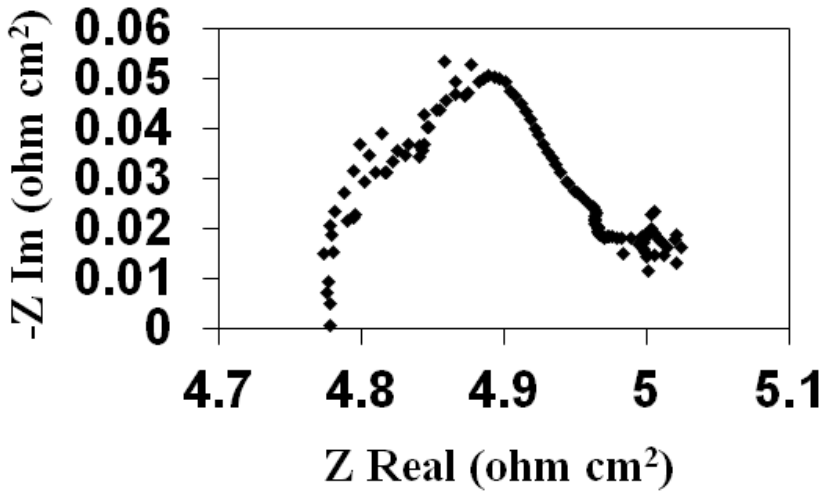

Figure 2.5: Impedance data for the cell with the molten Bi anode at 973 K, corresponding to the data in Figure 2.4.

To determine how much of the metallic Bi was accessible for oxidation in the cell, the cell potential was measured at a constant current density of 40 mA/cm^2 as a function of time at 973 K, with the results shown in Fig. 2.6. Literature data indicate that the solubility of oxygen in molten Bi at 973 K is very low, 0.38 mol % [9], so that deactivation processes similar to that observed with Sn are possible. However, Fig. 2.6 shows that the cell potential remained nearly constant for 13 h before dropping. Based on the charge that passed through the electrolyte during this time, approximately 85% of the metallic Bi reacted to Bi_2O_3 before significant changes were observed in the cell performance. Because the melting temperature of Bi_2O_3 is 1090 K, solid deposits must form at the YSZ interface with the Bi, just like those that formed with Sn. The large

difference between Bi and Sn is because Bi_2O_3 is a very good ionic conductor [3], allowing facile transfer of oxygen ions from the electrolyte to the metallic Bi.

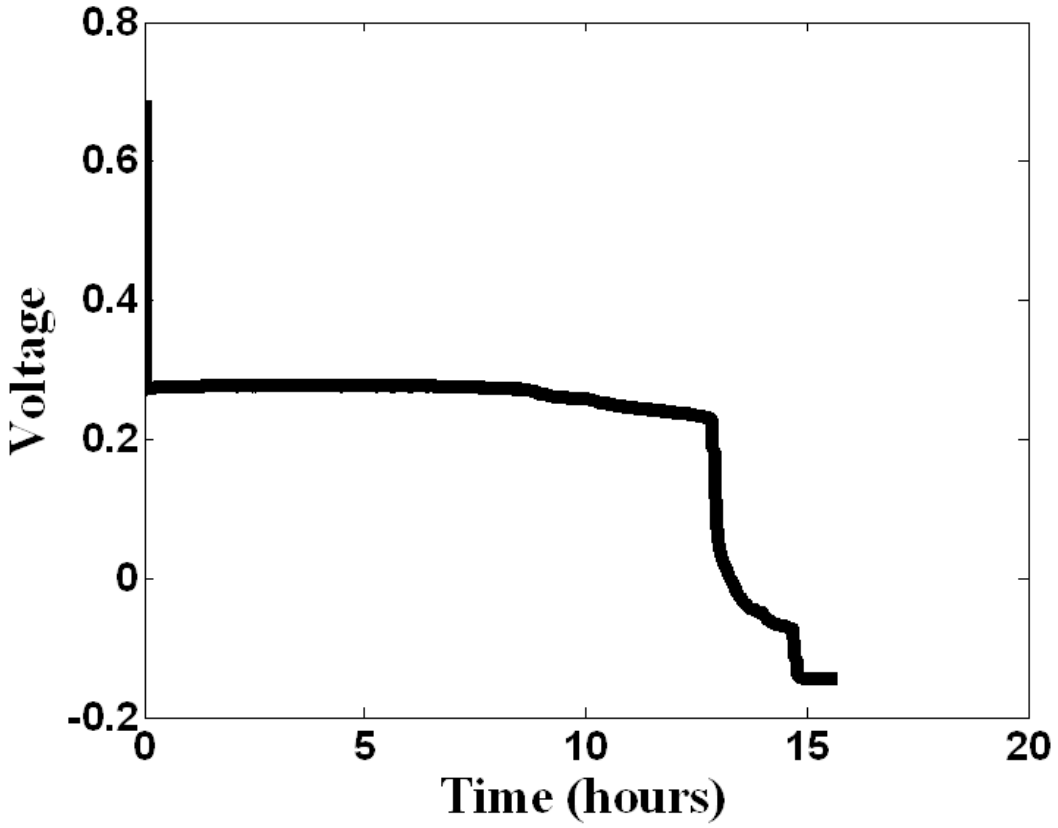

Figure 2.6: Cell voltage as a function of time for the cell with the molten Bi anode for a current of 40 mA/cm^2. The temperature was 973 K and a flow of dry He was maintained over the anode during the measurement.

2.4 Discussion

The comparison of Sn and Bi anodes for SOFCs highlights the major requirements of liquid-metal anodes. First, one would like to have oxidation thermodynamics that result in a high OCV, similar to what is observed with Sn [5]. Second, there must be facile transfer of oxygen ions from the electrolyte to the metal. There may be multiple ways to deal with each of these issues.

Regarding the cell operating potential, the OCV is obviously regulated by the thermodynamics of the metal oxidation reaction when the cell is operated in a battery mode; however, the chemical potential of oxygen could be much lower in the molten metal when fuel is present. In this case, the theoretical OCV would be determined by the thermodynamics of the fuel oxidation reaction. This is obviously the situation for normal SOFC operation. For the Ni-based anodes that are commonly used in SOFC, great care is taken to avoid reaching the point at which Ni is in equilibrium with NiO. With metals like Bi and Sn, the question is whether the metals and their oxides are sufficiently catalytic to allow rapid oxidation of fuels that are dissolved within the anode. If the rate of fuel oxidation is rapid compared to the rate of oxygen transfer through the electrolyte, the cell potential is established by the fuel. Indeed, published V-i polarization curves for cells with liquid Sn anodes in the presence of flowing H_2 show OCV above 1 V [4], implying that the OCV was established by H_2 oxidation, not by Equation 2.2. While Bi and Sn are not exceptional oxidation catalysts, their tendency to form molten alloys with well-known catalytic metals, such as Ni, may allow improvements in the catalytic activity.

While the facile oxygen transfer that was observed between YSZ and Bi is very encouraging, the deactivation observed following the formation of a dense SnO_2 layer at the YSZ interface needs to be avoided. Certainly, the effect of forming SnO_2 is much less at higher temperatures due to the higher solubility of oxygen in the molten Sn and due to higher ion diffusivity in the SnO_2, as demonstrated by the successful use of liquid Sn anodes in earlier work performed at 1273 K [1, 4]. However, because the rate of all processes increases at the higher temperatures, the rate-limiting step at 1273 K likely remains the diffusion of ions through SnO_2. The results of this study suggest two alternative paths for avoiding this problem. Using an M/MO_x system where the oxide has oxygen ion conductivity that is sufficiently high so that oxygen migration through the oxide does not limit performance, is one approach. This is likely to be the case for Bi/Bi_2O_3. The second approach to limit the effect of oxide barriers is to work above the melting temperature of the oxides that form at the electrolyte interface. This could be difficult for metals like Sn because SnO_2 has a melting temperature of 1903 K, but relatively easy for Bi, because Bi_2O_3 melts at 1090 K. With mixed metals, it may also be possible to form lower melting temperature eutectics.

In any case, the molten-metal anodes appear to show significant promise. This remains an area that has not yet been extensively explored.

2.5 Conclusions

Two important factors have been identified as affecting the performance of molten-metal anodes for SOFC: the thermodynamic oxidation potential of the metal and the tendency for the oxide to form a film at the electrolyte interface. For operation of

cells in the battery mode, where the metal is oxidized, the oxidation potential determines the OCV that can be achieved. Oxide films at the YSZ interface can effectively block charge transfer at the electrolyte interface if the oxide is a poor ionic conductor. However, both of these limitations have possible solutions, although further work is required to pursue these solutions.

2.6 References

1. Tao, T.; Slaney, M.; Bateman, L.; Bentley, J., Anode Polarization in Liquid Tin Anode Solid Oxide Fuel Cell. *ECS Trans.* **2007,** 7, (1), 1389-1397.
2. Ramanarayanan, T. A.; Rapp, R. A., The Diffusivity and Solubility of Oxygen in Liquid Tin and Solid Silver and the Diffusivity of Oxygen in Solid Nickel. *Metall. Mater. Trans B.* **1972,** 3, (12), 3239-3246.
3. Brett, D. J. L.; Atkinson, A.; Brandon, N. P.; Skinner, S. J., Intermediate temperature solid oxide fuel cells. *Chem. Soc. Rev.* **2008,** 37, (8), 1568-1578.
4. Tao, T.; Bateman, L.; Bentley, J.; Slaney, M., Liquid Tin Anode Solid Oxide Fuel Cell for Direct Carbonaceous Fuel Conversion. *ECS Trans.* **2007,** 5, (1), 463-472.
5. Tao, T., *Cells, Stacks, and Systems - Solid Oxide Fuel Cells IX (SOFC IX)*. Pennington, NJ 2005; Vol. 1.
6. Sasaki, K.; Maier, J., Re-analysis of defect equilibria and transport parameters in Y(2)O(3)-stabilized ZrO(2) using EPR and optical relaxation. *Solid State Ionics* **2000,** 134, (3-4), 303-321.
7. Huang, Y. Y.; Vohs, J. M.; Gorte, R. J., Fabrication of Sr-doped LaFeO3-YSZ composite cathodes. *J. Electrochem. Soc.* **2004,** 151, (4), A646-A651.

8. Wang, W. S.; Gross, M. D.; Vohs, J. M.; Gorte, R. J., The stability of LSF-YSZ electrodes prepared by infiltration. *J. Electrochem. Soc.* **2007,** 154, (5), B439-B445.
9. Risold, D.; Hallstedt, B.; Gauckler, L. J.; Lukas, H. L.; Fries, S. G., The bismuth-oxygen system. *J. Phase Equilib.* **1995,** 16, (3), 223-234.

Chapter 3: Molten-Metal Electrodes for Solid Oxide Fuel Cells

Summary

Molten In, Pb and Sb were examined as anodes in solid oxide fuel cells (SOFC) that operate between 973 and 1173 K. The results for these metals were compared with those reported previously (in chapter 2) for molten Sn electrodes. Cells were operated under "battery" conditions, with dry He or N_2 flow in the anode compartment, to characterize the electrochemical oxidation of the metals at the yttria-stabilized zirconia (YSZ)-electrolyte interface. In all cases, the open-circuit voltages (OCVs) were close to that based on equilibrium between the metals and their oxides. With Sn and In, the cell impedances increased dramatically at all temperatures after drawing current due to formation of insulating, oxide barriers at the electrolyte interface. Similar results were observed for Pb at 973 and 1073 K, but the impedance remained low after PbO formation at 1173 K because this is above the melting temperature of PbO. Similarly, the impedances of molten Sb electrodes at 973 K were low and unaffected by current flow because of the low melting temperature of Sb_2O_3. The potential of using molten-metal electrodes for direct-carbon fuel cells and for energy-storage systems is discussed.

3.1 Introduction

In chapter 2, fuel cells with molten Sn and molten Bi anodes were studied [1]. With Sn, the open-circuit voltage (OCV) was ~0.93 V at 973 K, close to the equilibrium Nernst potential for oxidation of Sn. This potential, which is roughly 0.1 V lower than the equilibrium value for carbon oxidation to CO_2, is nearly ideal for a DCFC because it

implies reduction of the oxide by carbon should be thermodynamically spontaneous while still allowing the fuel cell to produce electrons at a high enough potential for a high system efficiency. The problem with Sn is that oxygen solubility in the metal is very low. Therefore, oxidation at the electrolyte surface causes the formation of a high-melting, insulating SnO_2 layer at the electrolyte interface, leading to large increases in the cell impedance after transfer of just a few Coulombs per square centimeter of charge. With molten Bi, the oxygen solubility is similarly low, but the oxide is a good ion conductor, so that there is no increase in impedance, even after transfer of many Coulombs per square centimeter. The problem with Bi is that its OCV is only 0.48 V. It is not yet clear whether the presence of fuel in the molten Bi could reduce the oxide at a sufficient rate to prevent Equation 2.1 from reaching equilibrium so that a cell with a molten-Bi anode could operate at a higher potential; however, this would certainly not allow the oxidized Bi to be reduced in a reactor separated from the anode compartment of the fuel cell.

This chapter presents and discusses results from the study of fuel cells based on several additional molten-metal anode candidates: In, Pb, and Sb. The melting temperatures of these metals are 430, 601, and 904 K, respectively. Molten In is similar to Sn in that its oxide has a low solubility in the metal and a very high melting temperature, making it useful for determining whether the effects observed with molten Sn anodes are generally applicable to metals and oxides with these properties. Pb and Sb are of interest because their oxides have relatively low melting temperatures, 1161 K for PbO and 929 K for Sb_2O_3. This would allow the oxides to be removed from anode compartment as well as provide a mechanism for removing the oxide layer from the electrolyte interface.

It is shown here that the melting temperature of the oxide is, indeed, important in determining the performance of the electrodes. The results for the $Sb-Sb_2O_3$ system are particularly interesting, especially for energy-storage applications.

3.2 Experimental

The fabrication method of the electrolyte-cathode bilayer wafers used in these experiments is described in section 1.7. For the present study, the dense electrolyte layers were ~600 μm thick, whereas the porous layers used in making the cathode composites were 50 μm thick containing 40 wt.% of LSF.

The experimental setup of the cell is discussed in section 1.8. Current collection at the anode was accomplished using a circular ceramic pellet of $La_{0.3}Sr_{0.7}TiO_3$ (LST), pressing the molten metal onto the electrolyte. For the present study, 1200 mg of either In (Alfa-Aesar), Pb (Alfa-Aesar), or Sb (Sigma Aldrich) was added to the anode compartment. On the basis of the density of the metals and the inner diameter of the tube used for the anode compartment, this resulted in metal layers that were ~2.0−2.5 mm thick.

Electrochemical characterization was carried in the same manner as in chapter 2. The metal anodes were reduced by being held in humidified (3% H_2O) H_2 for at least 30 min. The H_2 was then flushed out using dry N_2 or He. The anode chamber was then maintained in the inert atmosphere to characterize the oxidation of the metal at the electrolyte interface using V-i curves and impedance spectra.

3.3 Results

Although results for molten-Sn anodes have been discussed in chapter 2 [1], a brief summary is presented here to point out the issues that arise with this material. Figure 3.1 shows the V-i polarization curves for a cell with a Sn anode at 973 and 1073 K obtained by ramping the voltage from its open-circuit value, to 0 V, and back to the open-circuit potential at 10 mV/s, while measuring the current produced by the cell. The V−i curves show that the OCV for Sn is 0.93 V at 973 K and slightly lower at 1073 K, close to the theoretical Nernst potentials for Equation 3.1 at these temperatures.

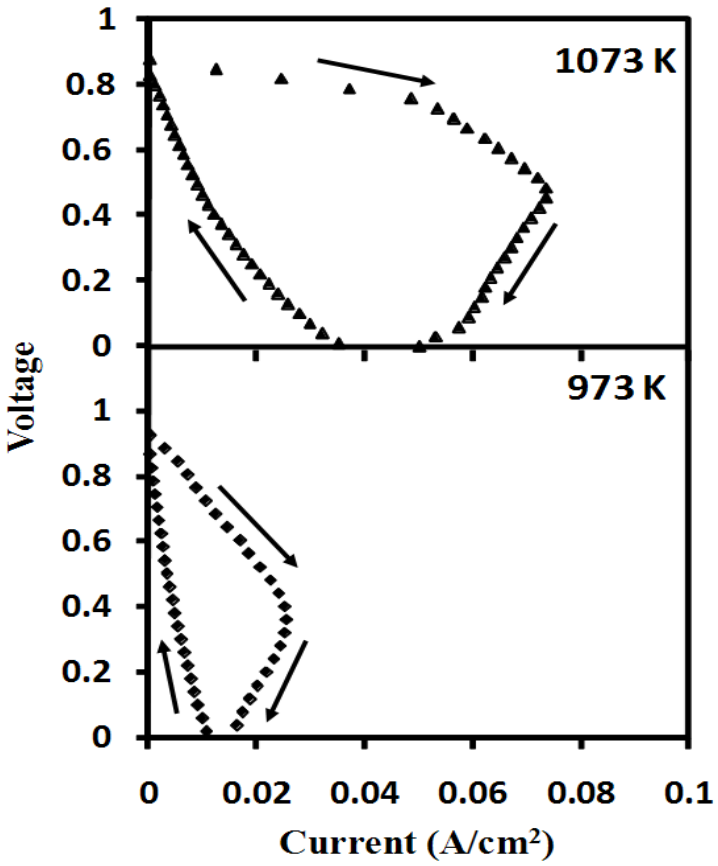

Figure 3.1: V-i polarization curves for a cell with molten Sn as the anode at 973 and 1073 K. After reduction of the Sn in humidified H_2, the anode compartment was exposed to dry, flowing He, while ramping the voltage from open circuit to 0V and back at 10 mV/s.

Although the current initially increases as the voltage decreases due to the increasing overpotentials at the electrodes and electrolyte, the current goes through a maximum and then decreases due to formation of the SnO_2 layer at the electrolyte interface. When the cell potential is allowed to again increase, the current density remains low due to the insulating oxide barrier [1]. The original cell performance could only be restored by again flowing H_2 into the anode compartment resulting in reduction of the SnO_2 layer. Impedance data presented in chapter 2 demonstrated that the ohmic resistance of the cell remained unchanged after completing the voltage-current cycle but that the non-ohmic impedance increased dramatically because of the barrier to diffusion of the oxide ions from the electrolyte. The thickness of the oxide layer can be calculated from the coulombs of charge that were transferred at the time of maximum current, using the bulk density of SnO_2. These values are 0.47 μm at 973 K and 0.80 μm at 1073 K. These values are somewhat lower than that measured by scanning electron microscopy, suggesting that the oxide films are not completely dense.

A similar set of data was obtained for the cell with the molten-In anode, with the V−i polarization curves reported in Figure 3.2. After reducing the anodes in flowing H_2, the initial OCV was 1.01 V at 973 K, but decreased slightly with temperature, in agreement with the theoretical Nernst potentials. As with the molten-Sn anodes, the current went through a maximum when the voltage was ramped down from OCV to zero and back at 10 mV/s. With In at 1173 K, the OCV also did not quite return to the Nernst potential after the voltage-current cycle, possibly because of current leakage and the large internal losses associated with the oxide layer. Using the same calculation as that used with Sn to estimate the characteristic oxide film thicknesses, the layers were estimated to

be 0.41, 0.89, and 2.0 μm at 973, 1073, and 1173 K, respectively. It is interesting that the oxide layer can be significantly thicker at the higher temperatures before the cell impedance increases dramatically. Certainly, part of the reason for this is the increased diffusivity of oxygen with increasing temperature. However, the result may also indicate changes in the way the film grows. For example, there may be more extensive dendrites of the oxide extending into the molten In at the higher temperatures.

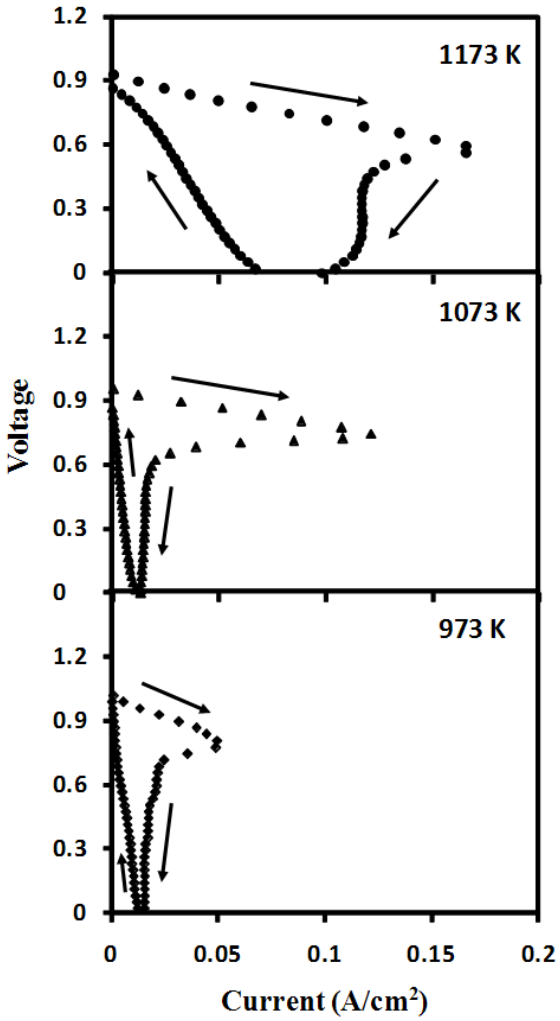

Figure 3.2: V-i polarization curves for a cell with molten In as the anode at 973, 1073, and 1173 K. After reduction of the In in humidified H_2, the anode compartment was exposed to dry, flowing N_2, while ramping the voltage from open circuit to 0 V and back at 10 mV/s.

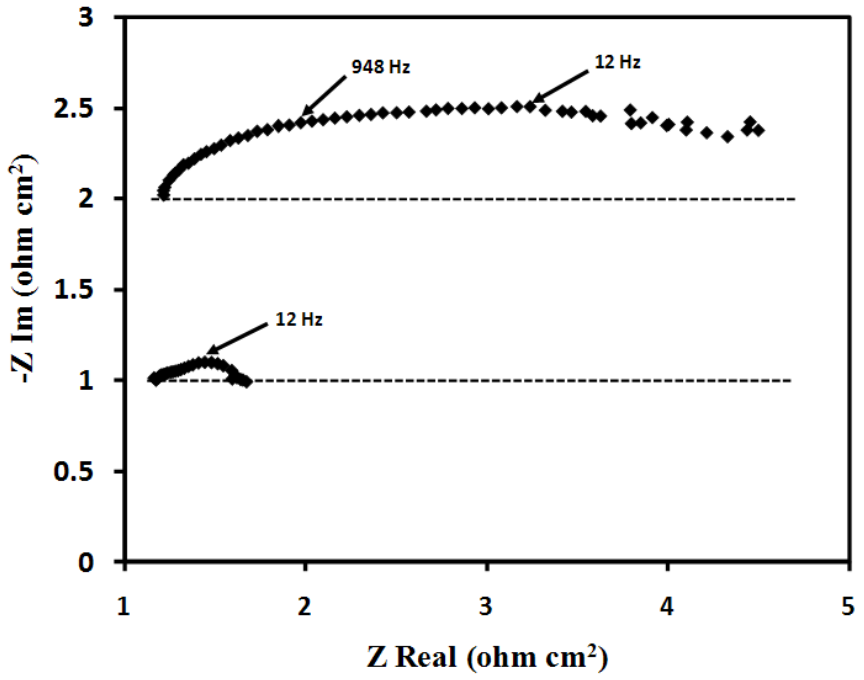

Figure 3.3: Impedance data for the cell with the molten In anode at 1073 K, corresponding to the V-i polarization data in Figure 3.2. The bottom curve is the Cole-Cole plot obtained near open circuit immediately after reduction of the In, while the top curve was obtained after completing the ramp from open circuit to 0 V and back.

The Cole−Cole plots of the cell impedances for the cell with molten In, measured at OCV and 1073 K before and after completing the voltage scan, are shown in Figure 3.3. These impedance data show that the ohmic contribution to the impedance, ~1.2 Ω cm^2, is unchanged after passing current and is close to the expected value of 1.4 Ω cm^2 based on the reported conductivity of YSZ at 1073 K, 0.0428 S/cm [2], and the thickness of the electrolyte, 600 μm. The change that occurs after passing current through the cell is mainly in the non-ohmic losses, determined from the length of the arc under the Cole−Cole plot, which increases from ~0.4 Ω cm^2 to greater than 3 Ω cm^2. At 1073 K, the impedance of the LSF-YSZ cathode is less than 0.1 Ω cm^2 [3, 4], so that most of the non-ohmic losses arise from the anode, even before passing current through the cell.

After the voltage cycle, most of the losses are clearly associated with an In_2O_3 barrier at the electrolyte interface. The peak frequency of approximately 12 Hz in the deactivated cell is also characteristic of a diffusion process. Experiments performed at 973 and 1173 K gave results that were qualitatively similar.

It seems apparent that performance improvements with molten-metal anodes require minimizing the losses associated with the oxide barrier formed at the anode−electrolyte interface. In chapter 2, it is demonstrated that the effects of the oxide barrier were minimal with Bi due to the fact that its oxide is a good ion conductor. An alternate approach to avoiding losses associated with oxide formation at the electrolyte is to use metals that have oxides with low melting temperatures, such as Pb and Sb, whose oxides melt at the more practically applicable temperatures of 1161 and 929 K respectively. The V-i polarization curves for Pb, obtained using the same voltage-current ramps as that used with In, are shown in Figure 3.4 at 973, 1073, and 1173 K. The initial OCV of the freshly reduced cell were slightly higher than the expected Nernst potentials of 0.60, 0.55, and 0.5 V at the three operating temperatures respectively. This suggests that some H_2 remained in the anode compartment after flushing with inert gases, perhaps dissolved in the molten Pb. For operation at temperatures below the melting point of PbO, the voltage-current characteristics are similar to that observed with In and Sn. The V-i curves change after current has been passed through the cell. At 1173 K, however, the only effect on the V-i polarization curve due to passing current is that it becomes a straight line passing through the Nernst potential.

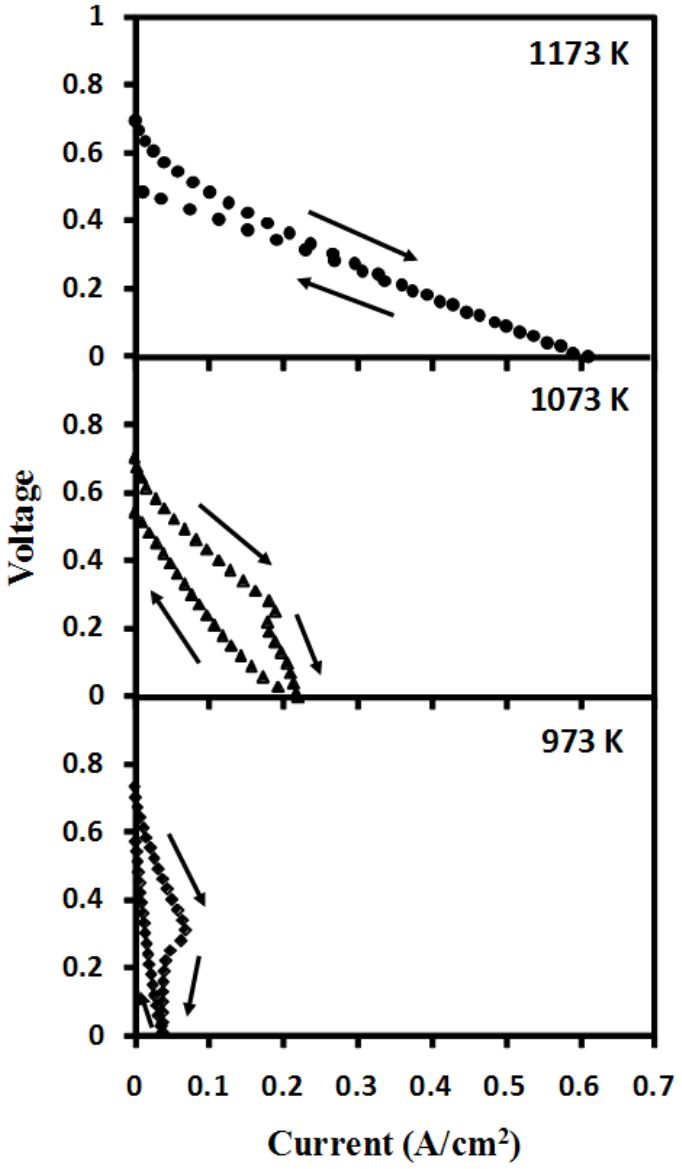

Figure 3.4: V-i polarization curves for a cell with molten Pb as the anode at 973, 1073, and 1173 K. After reduction of the Pb in humidified H_2, the anode compartment was exposed to dry, flowing N_2, while ramping the voltage from open circuit to 0 V and back at 10 mV/s.

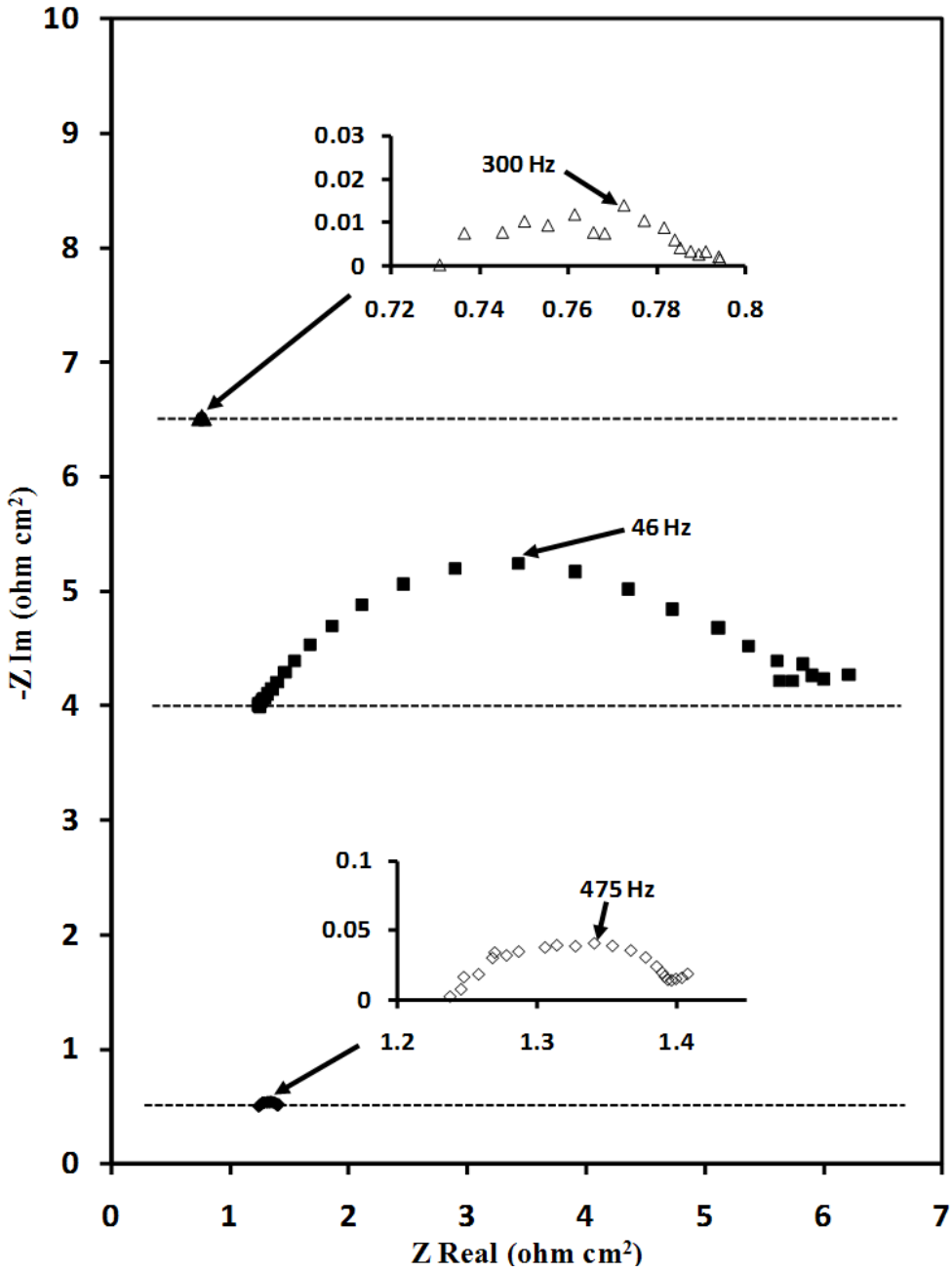

Figure 3.5: Impedance data for the cell with molten Pb anode, corresponding to the V-i data in Figure 3.4. The curve (a) is the Cole-Cole plot obtained near open circuit at 1073 K immediately after reduction of the Pb, while the curve (b) above it was obtained after completing the ramp from open circuit to 0 V and back. The curve (c) was obtained on the same cell at 1173 K, near open circuit, after completing the voltage ramp.

The impedance data in Figure 3.5 more clearly demonstrate the effect that operation above the melting temperature of PbO has on cell performance. At 1073 K, the initial impedance at open circuit shows the ohmic losses are 1.23 Ω cm^2 and the non-ohmic losses are 0.17 Ω cm^2. As discussed in the results for In, the ohmic losses are close to that expected for the YSZ electrolyte, and the non-ohmic losses are very low. After completing the voltage−current cycle, the OCV impedance data show that the ohmic losses are unaffected but the non-ohmic losses are now unacceptably high, 5 Ω cm^2. By contrast, the impedance obtained at 1173 K was independent of current density or voltage−current cycling. The ohmic and non-ohmic losses at this temperature were 0.73 and 0.06 Ω cm^2, respectively. Obviously, the OCV for Pb at 1173 K is still undesirably low, but the losses associated with electrode performance are impressively small and remained unchanged under current.

To confirm that performance can be very good when using a molten-metal anode for which the oxide has a low melting temperature, similar experiments were performed with Sb. Because the seals in the experimental apparatus were inadequate for preventing Sb_2O_3 from leaking through and breaking the electrical connections (The Ceramabond appears to be porous to Sb_2O_3.), only a limited set of data was obtained at 973 K with the apparatus; however, these initial results were promising. At 973 K, the V-i polarization data in Figure 3.6 are linear, with an OCV of 0.75 V, equal to the Nernst potential for Sb oxidation. There were no changes after allowing current to flow for several hours at short circuit. The impedance results in Figure 3.7 are consistent with this. The ohmic losses in this cell, 4.6 Ω cm^2, were higher than the expected value for the 600 μm electrolyte, 3.2

Ω cm^2, possibly due to leaks and poor electrical connections; but non-ohmic losses, ~0.6 Ω cm^2, were reasonably low.

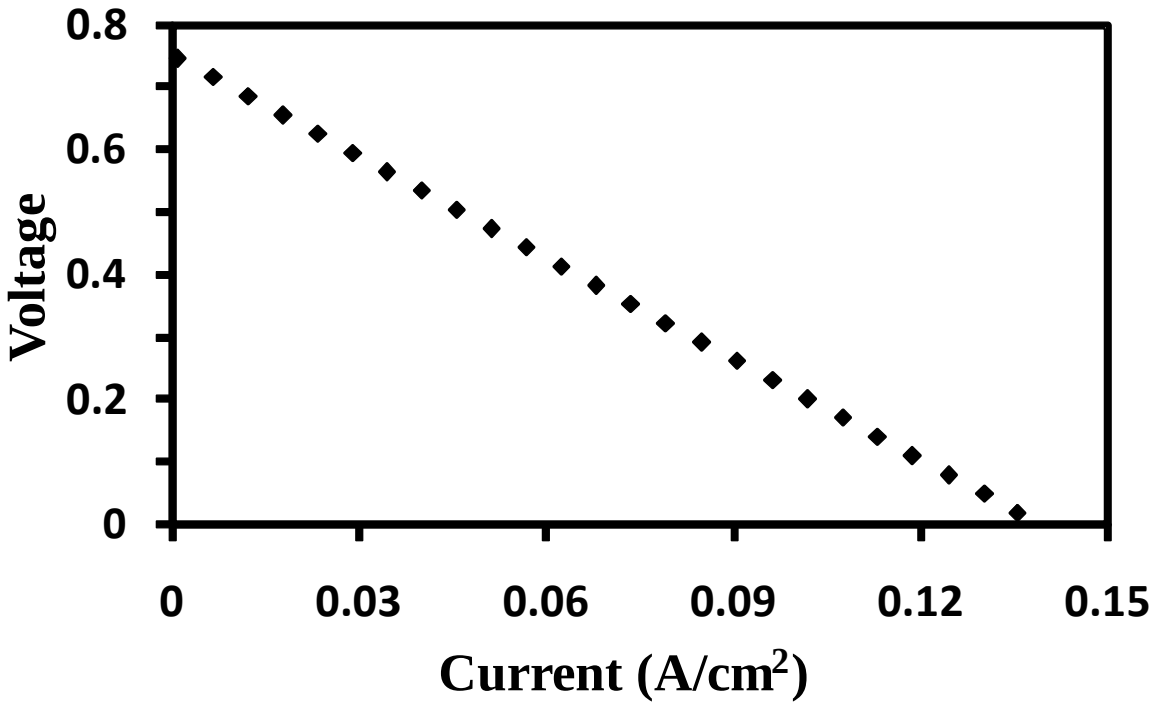

Figure 3.6: V-i polarization curve for the cell with the molten Sb anode at 973 K. After reduction of the Sb in humidified H_2, the anode compartment was exposed to dry, flowing N_2.

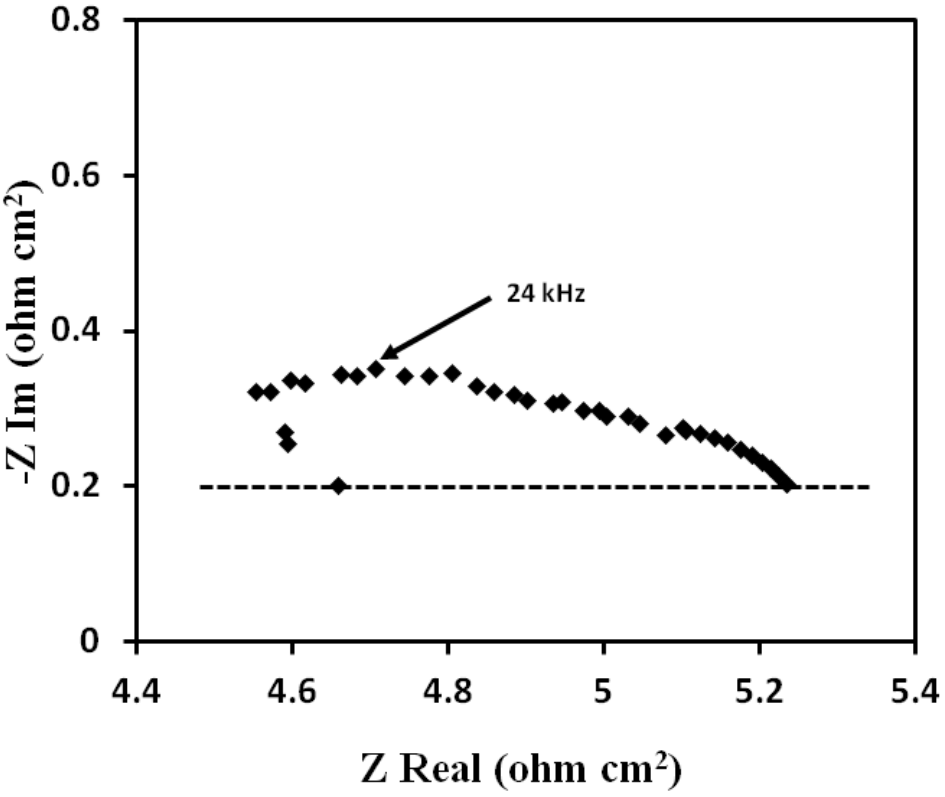

Figure 3.7: Impedance data for the cell with the molten Sb anode at 973 K, corresponding to the data in Figure 3.6.

3.4 Discussion

The performance data for anodes based on molten Pb and molten Sb for operation above the melting temperature of their oxides are most promising and demonstrate that the impedance for this type of electrode can be very good. So long as one can avoid the formation of oxide barriers, the impedance associated with oxygen transfer at the metal−electrolyte interface is very low so that high cell efficiencies could be expected. When both the metal and the oxide exist in the molten state, it is also easy to transport oxygen into a separate reactor for reduction by carbon.

Furthermore, the relatively low Nernst potential associated with oxidation of molten Sb would not be a problem for energy-storage systems, for which the oxide would be reduced to the metal by electrolysis during times of excess energy and the metal would be used to generate power during times when energy was needed. Indeed, the $Sb-Sb_2O_3$ system appears to have many attractive features for this application, given that the volumetric energy density of the metal would be relatively high as compared with that of H_2, which would be produced by normal steam electrolysis. In reversible H_2-H_2O fuel cells, there would also likely be an energy cost associated with pumping the H_2 to higher pressures.

Since there have been few studies of molten-metal electrodes, there is still much that is not known about these systems. In addition to the performance issues investigated here, relatively little is known about the reactivity of these materials with YSZ after long times at elevated temperatures. As was clear from our results with Sb, seals may well be a serious problem. Finally, the molten metals may produce an extremely corrosive environment. Still, the molten-metal electrodes are very interesting, and these systems could have applications in direct-carbon fuel cells and in energy-storage systems.

3.5 Conclusions

The impedance of molten-metal electrodes appears to be limited by formation of an oxide barrier at the electrode−electrolyte interface. By working at temperatures above the melting temperatures of both the metal and its oxide, it is possible to minimize the effect of oxide formation and achieve excellent electrode performance. These systems may have application in direct-carbon fuel cells and energy-storage systems.

3.6 References

1. Jayakumar, A.; Lee, S.; Hornes, A.; Vohs, J. M.; Gorte, R. J., A Comparison of Molten Sn and Bi for Solid Oxide Fuel Cell Anodes. *J. Electrochem. Soc.* **2010,** 157, (3), B365-B369.
2. Sasaki, K.; Maier, J., Re-analysis of defect equilibria and transport parameters in Y(2)O(3)-stabilized ZrO(2) using EPR and optical relaxation. *Solid State Ionics* **2000,** 134, (3-4), 303-321.
3. Huang, Y. Y.; Vohs, J. M.; Gorte, R. J., Fabrication of Sr-doped LaFeO3-YSZ composite cathodes. *J. Electrochem. Soc.* **2004,** 151, (4), A646-A651.
4. Wang, W. S.; Gross, M. D.; Vohs, J. M.; Gorte, R. J., The stability of LSF-YSZ electrodes prepared by infiltration. *J. Electrochem. Soc.* **2007,** 154, (5), B439-B445.

Chapter 4: A Direct Carbon Fuel Cell with a Molten Antimony Anode

Summary

The direct utilization of carbonaceous fuels is examined in a solid oxide fuel cell (SOFC) with a molten Sb anode at 973 K. It is demonstrated that the anode operates by oxidation of metallic Sb at the electrolyte interface, with the resulting Sb_2O_3 being reduced by the fuel in a separate step. Although the Nernst Potential for the Sb-Sb_2O_3 mixture is only 0.75 V, the electrode resistance associated with molten Sb is very low, approximately 0.06 Ωcm^2, so that power densities greater than 350 mW cm^{-2} were achieved with an electrolyte-supported cell made from Sc-stabilized zirconia (ScSZ). Temperature programmed reaction measurements of Sb_2O_3 with sugar char, rice starch, carbon black, and graphite showed that the Sb_2O_3 is readily reduced by a range of carbonaceous solids at typical SOFC operating conditions. Finally, stable operation with a power density of 300 mW cm^{-2} at a potential of 0.5 V is demonstrated for operation on sugar char.

4.1 Introduction

Oxygen transport in the molten metal anodes studied so far primarily occurs in the form their oxides. The performance limitations in the cases of Sn and In, caused by the formation of solid oxide barrier layers at the electrolyte interface, were avoided by using molten metals which form oxides that are also molten under the operating conditions. Such facile oxygen transfer resulting in very low anode polarization losses was observed in the cases of Pb and Sb [1].

In a DCFC, direct electrochemical oxidation of carbon will generate electrons at the Nernst potential of ~1 V. However, in the molten metal anode-SOFC based DCFC discussed here, the metal oxidation reaction is the electrochemical step producing electrons, while fuel oxidation follows as a separate step. Of the two anode choices available, Pb required a high operating temperature of 1173 K for PbO to be molten and generated electrons at the low OCV of 0.5 V. The Sb-Sb_2O_3 system, on the other hand, could operate at the desired intermediate SOFC operating temperature of 973 K since both Sb and Sb_2O_3 have low melting points (903 and 929 K respectively) and are molten at this temperature. Moreover, the OCV of Sb oxidation (Equation 4.1) is 0.75 V at 973 K. This will enable reasonable levels of energy efficiency to be achieved in these fuel cells that utilize carbon.

The anode reactions for a DCFC based on molten Sb are as follows:

$$2Sb + 3O^{2-} \rightarrow Sb_2O_3 + 6e^- \qquad \text{Equation 4.1}$$

$$Sb_2O_3 + 3/2\ C \rightarrow 2Sb + 3/2\ CO_2 \qquad \text{Equation 4.2}$$

In Equation 4.1, Sb plays the role of both the electronic conductor and fuel, and the entire interface between the electrolyte and the molten Sb is active for the transfer of ions from the electrolyte to form Sb_2O_3. Sb_2O_3 reduction (Equation 4.2) is thermodynamically favored at 973 K and occurs in a separate step. The high reactivity of most types of carbonaceous fuel with Sb_2O_3 is verified by temperature programmed reaction studies conducted in this chapter. In fact, reduction of Sb from its oxide is presently carried out on a commercial scale using carbon as the reductant [2].

In this chapter, it is demonstrated that a fuel cell based on the Sb-Sb_2O_3 redox couple can provide good performance while operating on carbonaceous fuels, even at 973

K. This chapter will also discuss how this might be used in a larger-scale system and how potential problems associated with the use of "dirty" fuels might be addressed.

4.2 Experimental

To obtain a qualitative measure of the reactivity of Sb_2O_3 (99.6%, Alfa Aesar) with various carbonaceous fuels, Temperature-programmed reaction (TPR) experiments were carried out. The experiments were conducted by mixing 0.1 g of fuel with a slight excess of Sb_2O_3 in an alumina boat and then placing this boat in a tubular flow reactor as shown in Fig. 4.1. The CO_2 production rate was determined in flowing N_2 (20 ml min^{-1}), while ramping the temperature at 3.75 K min^{-1} and monitoring the reactor outlet with a mass spectrometer. The experiments were carried out for four solid fuels, including a sugar char (sugar heated to 873 K in a covered crucible), rice starch (Sigma Aldrich), acetylene carbon black (99.99%, Strem Chemicals), and graphite (−325 mesh, >99.99% Sigma Aldrich).

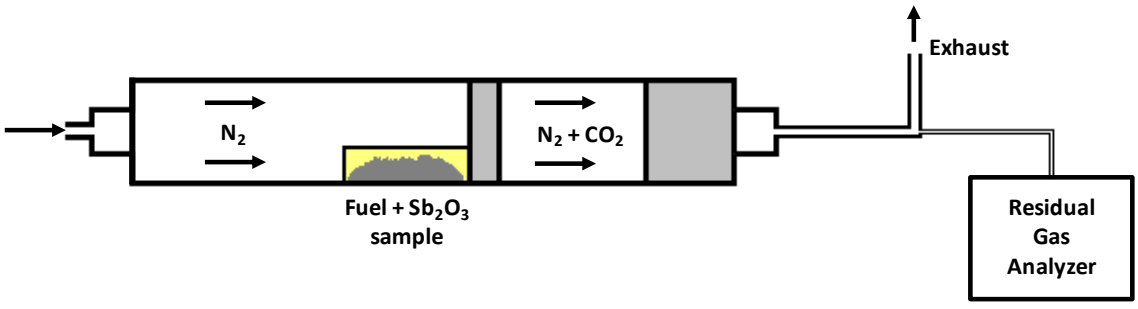

Figure 4.1: Temperature programmed reaction (TPR) apparatus.

For the fuel-cell measurements, the electrolyte-cathode bilayer wafer was fabricated as discussed in section 1.7 using 10% Sc_2O_3-stabilized ZrO_2 (ScSZ) powder. It consisted of a 100 μm dense ScSZ electrolyte layer and a porous LSF-ScSZ composite

cathode layer which was 50 µm thick. The cell was then setup as described in section 1.8 with 2 g of Sb powder (−100 mesh, 99.5%, Sigma-Aldrich) added to form the anode. Rhenium wires, held in place with the help of a rubber stopper plugged into the other end of the alumina tube, were inserted into the Sb layer and used for current collection on the anode side. Unlike the case for molten Sn [3], which must be compressed onto the electrolyte because of its tendency to "ball up" due to its high surface tension, Sb easily "wet" the electrolyte surface. Schematic diagrams of the experimental setup and anode reaction mechanism are shown in Fig. 4.2a and Fig. 4.2b.

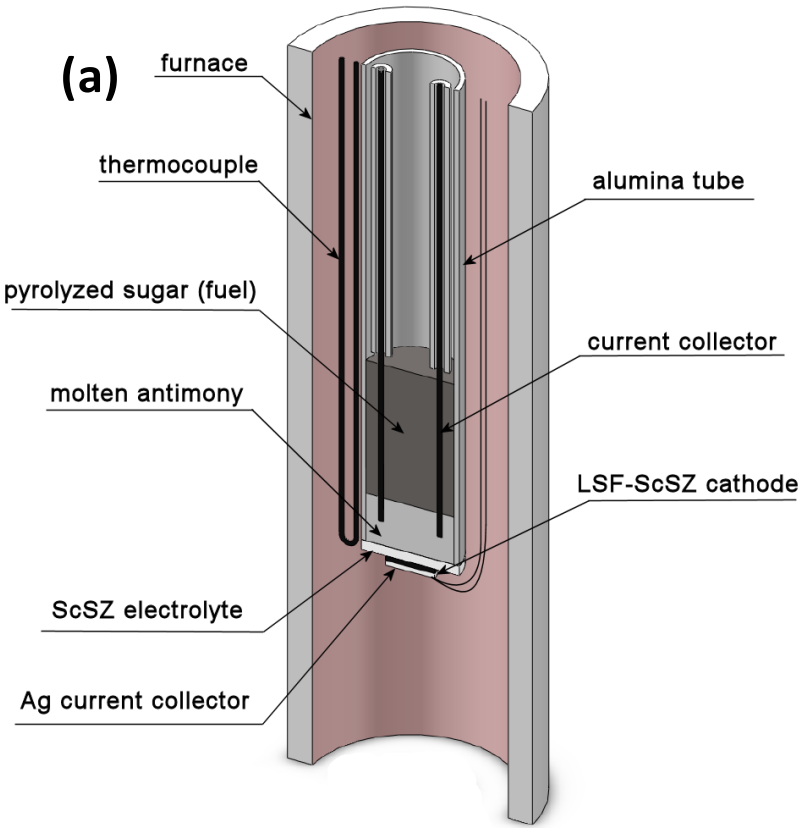

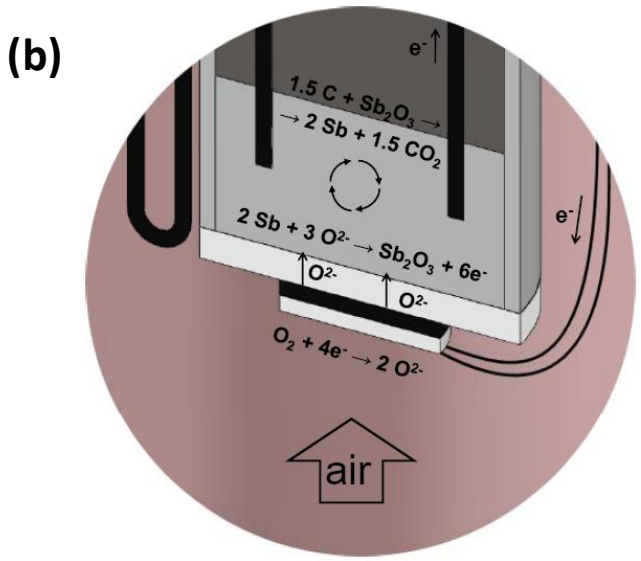

Figure 4.2 a-b: (a) Schematic of the experimental setup. (b) Working of the SOFC with molten Sb anode and solid carbonaceous fuel (sugar char).

Electrochemical characterization of the fuel cells was performed using V-i polarization curves and impedance spectra obtained using a Gamry Instruments Potentiostat. V-i polarization curves were obtained by ramping through the applied voltages from the OCV to 0 V (short circuit) at 10 mV/s and recording the corresponding currents. The impedance spectra were performed galvanostatically in the frequency range from 300 kHz to 0.1Hz with an a.c. perturbation of 1 mA. Current and power densities were normalized to the area of the cathode.

Direct carbon fuel cell experiments were performed by placing 0.5 g of sugar char directly above the Sb layer prior to heating the fuel cell. Since the system was sealed shut by the rubber stopper holding the Re current collectors in place, it was difficult to add more fuel to the system for this experimental configuration. Unfortunately, the other carbon-containing fuels were not suitable for the fuel cell measurements with this system. The rice starch contained a significant amount of ash, as observed from the gray residue

that remained after heating a sample in a muffle furnace. The carbon black had a very low density, so that very little of the sample could be added to the system. Furthermore, in attempts to use the carbon black in the fuel cell, most of the bed remained suspended above the Sb, so that there was no physical contact between the fuel and the molten anode. As demonstrated in the reaction measurements, the use of graphite as the fuel would require higher temperatures than intended for this study.

4.3 Results and Discussion

Fig. 4.3(a) shows the V-i polarization and power-density curves for the fuel cell operating at 973 K on pure Sb, without the carbon fuel. The open-circuit voltage (OCV) was 0.75 V, very close to the theoretical Nernst potential for equilibrium between Sb and Sb_2O_3. Furthermore, the V-i polarization curve was linear, with a slope of 0.37 Ωcm^2, demonstrating that the ASR of the cell was independent of current density. A maximum power density of 360 mW cm^{-2} was observed at a current density of 0.9 A cm^{-2}. Even at a cell potential of 0.6 V, a reasonable power density of >200 mW cm^{-2} was still achieved.

Impedance spectra were measured to determine the nature of the energy losses in the cell . As shown by the Nyquist plot in Fig. 4.3(b), most of the losses are due to the ohmic resistance of the electrolyte, 0.25 Ωcm^2. This resistance is close to that expected for a 100 μm ScSZ layer at 973 K, based on the reported conductivity of ScSZ, 0.045 S cm^{-1} [4]. The non-ohmic portion of the cell impedance was 0.12 $\Omega.cm^2$. Given that the losses associated with an identical LSF-ScSZ cathode have been reported to be 0.06 Ωcm^2 under these conditions [4], the resistance of the molten-Sb anode must also be ~0.06 Ωcm^2. It is noteworthy that the performance in Fig. 4.3(a) was achieved with an

electrolyte-supported cell . If the electrolyte losses were negligible, as they could be with a thin electrolyte in a cathode-supported cell, a fuel cell with an ASR equal to that of the electrode losses in Fig. 4.3(b) would achieve a power density of ~1 W cm^{-2} at 0.5 V. Improved power densities could also be achieved at higher temperatures, since the conductivity of the electrolyte increases significantly with temperature.

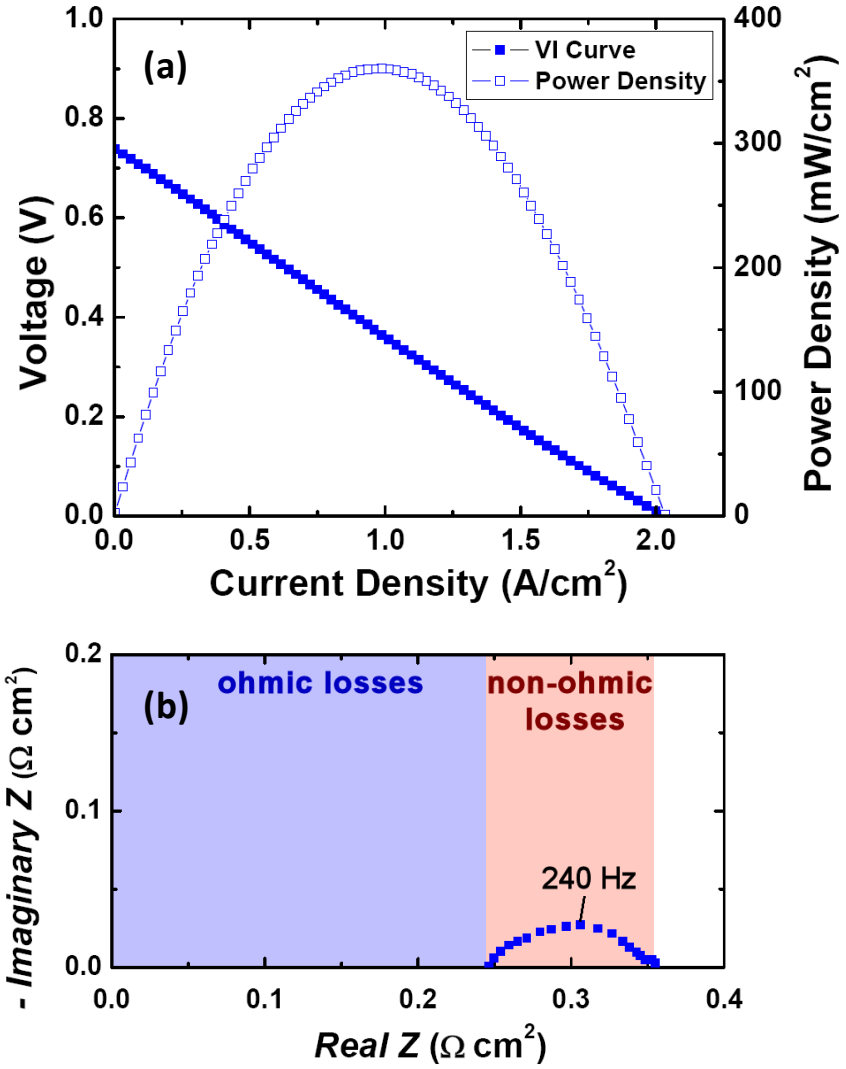

Figure 4.3 a-b: (a) Voltage vs current density (V-*i*) polarization and power density curves for the fuel cell at 973 K. (b) Nyquist plot of the impedance spectrum for the fuel cell at 973 K.

TPR measurements were carried out with various solid fuels in Sb_2O_3 in order to determine the ease with which Sb_2O_3 could be reduced, with results shown in Fig. 4.4 for the four solid fuels that were studied. These data indicate that the sugar and rice starch begin to reduce the Sb_2O_3 at approximately 850 K. (The CO_2 peak at 575 K for rice starch is due to decomposition of the starch.) Reaction is complete by 950 K for these fuels, demonstrating that their reaction with Sb_2O_3 will be rapid at 973 K. Carbon black requires slightly higher temperatures but reduction is still nearly complete by 973 K. Finally, the reaction rates with graphite are lower but all of the graphite could still be converted by heating to 1073 K. Physical observation revealed that all of the fuels were completely consumed at the end of each TPR experiment.

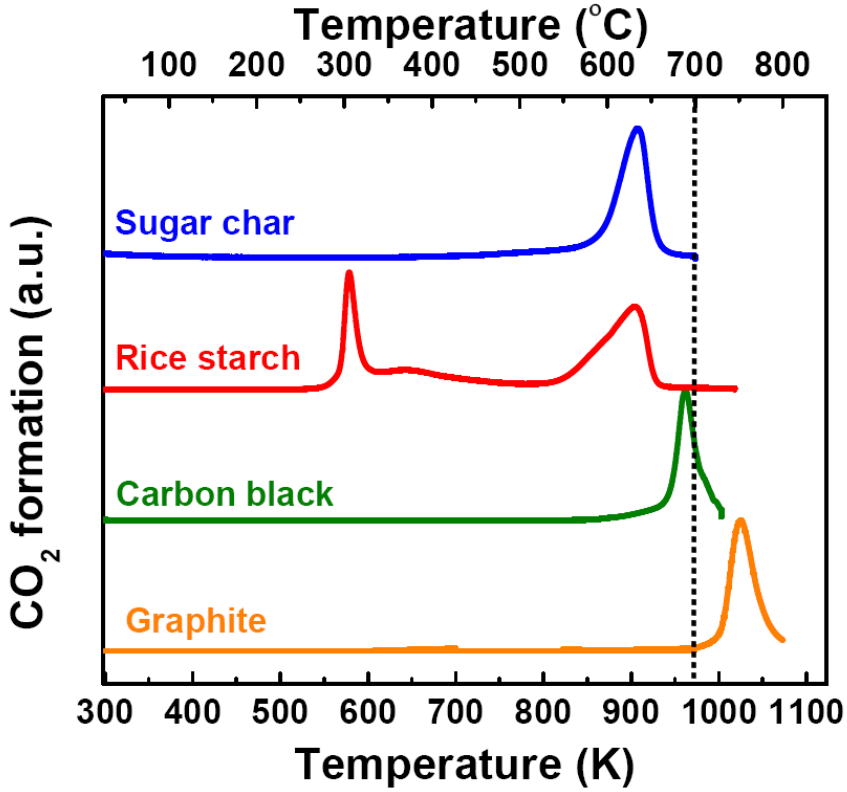

Figure 4.4: Temperature programmed reaction plots for various forms of carbonaceous fuel mixed with Sb_2O_3.

The addition of 0.5 g of sugar char above the molten Sb anode had no effect on the initial V-i polarization curves, which were identical to that in Fig. 4.3a, or on the impedance measurements Fig. 4.3b. As in the data in Fig. 4.3a, the OCV was again 0.75 V, demonstrating that the potential for the electrode was established by the Sb-Sb_2O_3 redox reaction. If the reduction by carbon were sufficiently rapid so as to avoid actual formation of Sb_2O_3, it is possible that a higher OCV could be obtained; but that was not observed with this experimental configuration.

The effect of having the carbonaceous fuel was observed in time-dependent performance. To determine this stability, the cell voltage was monitored as a function of time while drawing a constant current of 0.6 A cm^{-2}, corresponding to a cell potential of 0.5 V and a power density of 300 mW cm^{-2}. The results in Fig. 4.5 are shown for a cell with 2 g of Sb and no added carbon and for an identical cell with 0.5 g of sugar char placed above the Sb. For the pure Sb case, the cell potential began to drop after less than 1 h, corresponding to conversion of only about 10% of the Sb to Sb_2O_3. Beyond this conversion, the accumulation of Sb_2O_3 increased the cell resistance and the power density decreased. In experiments using 4 g of Sb, the power density could be maintained constant until 45% of the Sb had been converted, suggesting that slow mixing of the Sb and Sb_2O_3 due to natural convection is likely limiting the performance of the cell in Fig. 4.5. At the electrolyte interface, displacement of Sb_2O_3 with Sb will result from density differences between Sb (6.4 g cm^{-3}) and Sb_2O_3 (5.2 g cm^{-3}) but the displacement flows will depend on the thickness of the Sb-Sb_2O_3 film. The sharp features in the data of Fig. 4.5 are likely due to convection currents of the metal and insulating fluids.

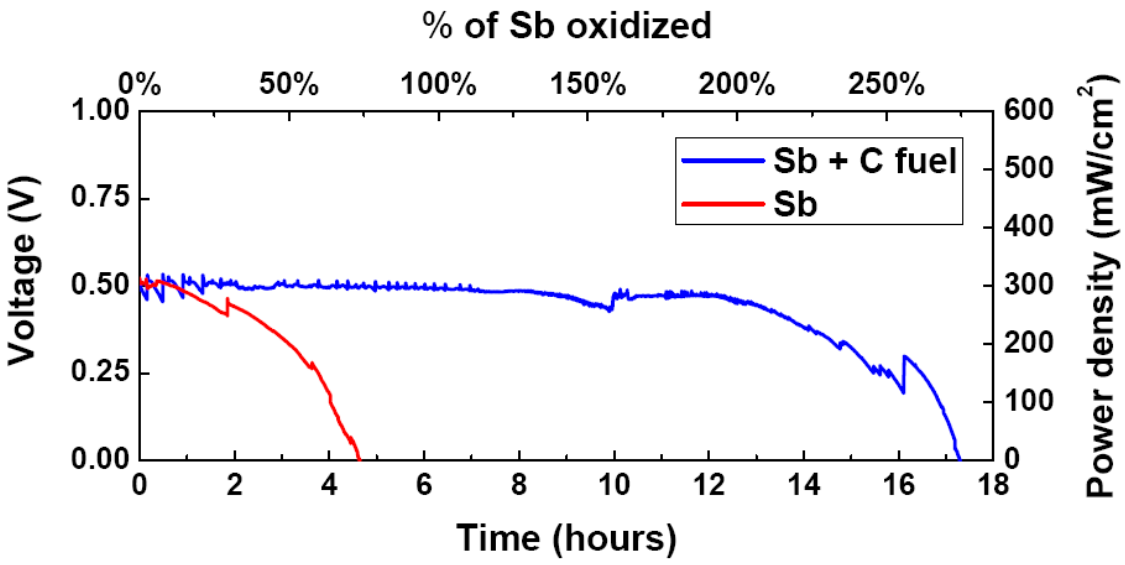

Figure 4.5: Long term performance plots for the cases of Sb anode with and without sugar char fuel.

Fig. 4.5 also shows data for the cell with 0.5 g of sugar char placed above the 2 g of Sb. With the added fuel, the cell performance was constant for more than 12 h, a time sufficiently long to have oxidized all the Sb twice, proving that the Sb_2O_3 formed at the electrolyte interface was being reduced by the carbon. Apparently, the Sb_2O_3 is being reduced as it is formed, maintaining the performance of the cell. Once the sugar char was consumed, the cell performance began to drop. Coulometrically, the additional 11 h of run time in the presence of the sugar char over that observed in its absence would correspond to oxidation of 0.3 g of carbon to CO_2, somewhat less than the 0.5 g of fuel that was added. Since physical examination of the cell after cooling showed that all of the fuel had been consumed, it suggests that the sugar char likely lost some of its contents by volatilization due to the increase from its initial pyrolysis temperature of 873 K to the operating temperature of 973 K and that the remaining char contained significant amounts of oxygen, as is typical of pyrolyzed biomass [5].

Attempts were also made to operate the cell with rice starch and carbon black. Again, the addition of these fuels had no effect on the initial cell performance; however, unlike with sugar char, the consumption of these fuels was incomplete due to poor contacting between the fuels and molten Sb. With carbon black, the density was so low that fuel remained suspended above the anode. With rice starch, the ash buildup between the starch and the molten anode prevented reaction. Since the TPR data demonstrates that both of these fuels are easily able to reduce molten Sb_2O_3 to Sb at 973 K, both of these fuels could be used to power the fuel cell based on molten Sb if it were possible to make better contact between the molten anode and the carbon source.

If the use of Sb anodes were commercialized, these contacting issues would not be problematic. Rather, a system can be envisioned such as that shown in Fig. 4.6, where the Sb_2O_3 reduction is carried out in a separate chamber from the fuel cell. This configuration is similar to that of a redox flow battery, except the oxidized electroactive species, Sb_2O_3, is regenerated via reduction with carbon in the holding tank. Indeed, the reduction of Sb_2O_3 to produce Sb has been carried out on a commercial scale for more than 100 years, using carbon as the reductant [2]. The removal of ash by settling and the reduction of Sb vapor pressure through the formation of a $NaSbO_x$ surface crust are established technologies [2]. Given the high energy density of molten Sb, the flow rates of molten metal to the fuel cell in a system like that shown in Fig. 4.6 would be relatively low. For a 10-kW system, the flow rate of Sb would need to be only 15 g s^{-1}, assuming 50% conversion of the Sb per pass and using the current and power densities of Fig. 4.5, 600 mA cm^{-2} and 0.3 W cm^{-2}, respectively. For these low flow rates, it may be possible

to use natural convection due to the density difference between Sb and Sb_2O_3, to produce the necessary flow.

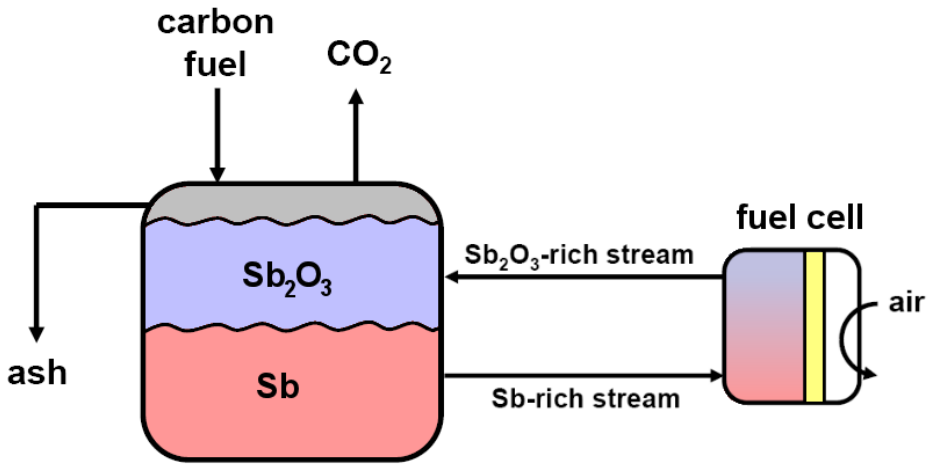

Figure 4.6: Schematic for the large-scale system with flowing Sb anode. Oxidation and reduction of the Sb occurs in two separate chambers.

Obviously, DCFC based on molten Sb have an intrinsic loss in energy associated with the low Nernst potential for the Sb-Sb_2O_3 equilibrium, 0.75 V at 973 K, when carbon oxidation could theoretically produce electrons at 1 V. As noted earlier, this loss of efficiency is partially compensated by the low electrode impedance, so that Sb-based fuel cells could be operated at reasonable voltages. Furthermore, unlike traditional fuel cells with gaseous reactants where the Nernst potential decreases significantly with fuel conversion, the Nernst potential for molten Sb oxidation will be independent of the extent of conversion in the fuel cell. In any case, most other types of DCFC are likely to involve carbon reforming to CO and H_2, with greatly added complexity and resultant energy losses that are higher than those anticipated for the Sb system. Finally, the efficiency losses associated with carbon oxidation will be available as thermal energy that could be used elsewhere.

4.4 Conclusion

We have shown that direct utilization of carbonaceous fuels, including biomass, can be accomplished in a SOFC with a molten Sb anode. These cells are capable of obtaining relatively high power densities while operating at 973 K. A fuel cell system based on this type of DCFC would be highly fuel flexible, tolerant of typical fuel impurities and could provide a high efficiency means of electricity generation from both coal and biomass while simultaneously allowing for easy CO_2 capture.

4.5 References

1. Jayakumar, A.; Vohs, J. M.; Gorte, R. J., Molten-Metal Electrodes for Solid Oxide Fuel Cells. *Ind. Eng. Chem. Res.* **2010,** 49, (21), 10237-10241.
2. DeCew, J. A., Some Studies on the Methods of Recovering Antimony from its Ores by Volatilization Processes. *Metall. Chem. Eng.* **1917,** 16, (8), 444-449.
3. Jayakumar, A.; Lee, S.; Hornes, A.; Vohs, J. M.; Gorte, R. J., A Comparison of Molten Sn and Bi for Solid Oxide Fuel Cell Anodes. *J. Electrochem. Soc.* **2010,** 157, (3), B365-B369.
4. Kungas, R.; Vohs, J. M.; Gorte, R. J., Effect of the Ionic Conductivity of the Electrolyte in Composite SOFC Cathodes. *J. Electrochem. Soc.* **2011,** 158, (6), B743-B748.
5. Ning, W.; Low, M. J. D., Spectroscopic Studies of Carbons .19. The Charring of Sucrose. *Mater. Chem. Phys.* **1990,** 26, (5), 465-481.

Chapter 5: The Stability of Direct Carbon Fuel Cells with Molten Sb and Sb-Bi Alloy Anodes

Summary

The long-term stability of direct carbon fuel cells (DCFC), based on solid oxide fuel cells (SOFC) with molten Sb and Sb-Bi anodes, was examined for operation with activated charcoal, rice starch, and bio-oil fuels at 973 K. With intermittent stirring of the fuel-metal interface, the anode performance was stable and reasonable power densities (~250 mW/cm^2) were achieved for periods up to 250 h. With Sc-stabilized zirconia (ScSZ), severe thinning of the electrolyte occurred in regions of high current flow. No electrolyte thinning was observed with a yttria-stabilized zirconia (YSZ) electrolyte operating at the same current densities.

5.1 Introduction

Based on the work discussed in chapter 4, the impedance of molten Sb electrodes was found to be very low, less than 0.1 Ωcm^2 at 973 K. In that study, stable generation of electrical power was demonstrated for a period of approximately 13 h using ash-free sugar char as the fuel in a SOFC with molten Sb as the anode [1]. Unfortunately, longer tests were not possible in that study since the experimental configuration did not allow additional solid fuel to be added after the initial charge of sugar char had been consumed. Also, because the solid fuels were placed directly on top of the Sb within the anode compartment, without any stirring, fuels that formed an ash layer were prevented from reducing Sb_2O_3 after only a fraction of the fuel had been oxidized. This was due to poor

contacting between the fuel and the Sb_2O_3 that formed by oxidation of the Sb at the electrolyte interface.

In this chapter, the results of a study of the long-term (>200 h) stability of SOFCs with anodes based on molten Sb and a Sb-Bi alloy are described. These SOFCs were operated on a variety of ash-containing carbonaceous fuels, including activated charcoal, a bio-oil, and rice starch. This was accomplished by modifying the experimental setup to allow the periodic addition of fuel with intermittent stirring of the molten anode to break up any barrier due to ash formation. Relatively small variations in performance are observed with time which may be due to incomplete mixing in the compartment. Cells with both yttria-stabilized zirconia (YSZ) and scandia- stabilized zirconia (ScSZ) electrolytes were evaluated. ScSZ electrolytes were found to undergo thinning in regions where the electrochemical reaction occurs. Fortunately, no such thinning was observed with YSZ, so that long-term operation of such DCFCs with Sb-based anodes should be possible.

5.2 Experimental

The fabrication of the electrolyte-cathode bilayer wafers is discussed in section 1.7. The two electrolyte materials tested in this study were 10% Sc_2O_3-stabilized ZrO_2 (ScSZ) and 8% Y_2O_3-stabilized ZrO_2 (YSZ). Although ScSZ is significantly more expensive than YSZ, it is mechanically stronger and has a higher ionic conductivity [2]. The cells made with ScSZ had 100-µm thick electrolytes, while the YSZ cells had electrolytes that were 160 µm thick, made by laminating two 80-µm tapes. In both ScSZ and YSZ cells, the porous composite cathode containing 40 wt% LSF was 50 µm thick.

The experimental apparatus is shown in Figure 5.1 and was similar to that used in an earlier study of electrochemical energy storage, where mixing of the molten Sb/Sb_2O_3 mixture was critical [3]. The basic cell setup remains the same as that discussed in section 1.8. Experiments with pure Sb used 10 g of Sb powder (-100 mesh, 99.5%, Alfa Aesar), while experiments with the Sb-Bi alloy employed a mixture 8 g of Sb and 3.45 g of Bi (-100 mesh, 99%, Sigma-Aldrich) to produce an alloy that was 20-mol% Bi. Rhenium wires were inserted into the anode for current collection. After inserting an alumina stirring rod to the anode-fuel interface, the top end of the alumina tube was plugged with glass wool. Finally, the fuel cell was placed in a tube furnace and heated to 973 K.

The powdered carbonaceous fuels were added directly onto the anode. The biomass fuels were added as a 40% by weight mixture with charcoal (Supelco). Fuel cell tests were conducted using an initial charge of 1.5 g of fuel, with further 0.5-g fuel additions made every 6 to 10 hours of cell operation. Stirring of the anode-fuel interface was carried out for 2 to 5 min before and after every fuel addition.

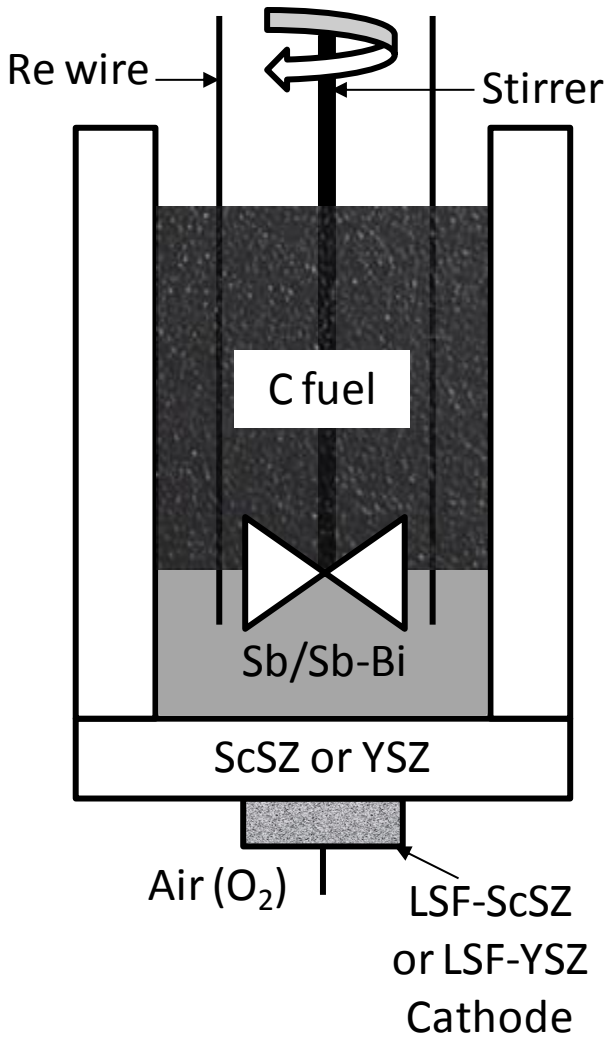

Figure 5.1: Schematic of the experimental setup of a DCFC with a molten Sb or Sb-Bi alloy anode.

To obtain a better measure of the amount of fuel that was added to the anode compartment, each of the fuels was briefly heated to 873 K in an inert gas in order to drive off volatile gases, prior to measuring the fuel weight added to the cell. In a typical 200-h experiment, the total amount of fuel added to the anode was approximately 13 g, of which approximately 5 g was recovered at the end of the experiment. As a point of reference, 4.0 g of pure C would be required to produce a current of 500 mA/cm^2 for 200 h, with the current density referenced to the active area of the cathodes, 0.353 cm^2. The

difference between the amounts of fuel that were consumed (~8 g) and the electron balance (4 g) is partially associated with oxygen in the fuel and partially due to remaining volatility in the fuel between 873 and 973 K [4]. Also, excess fuel was always maintained in the cell to compensate for unpredictable losses and to provide a barrier for Sb, and mainly, Sb_2O_3 vaporization.

The biomass fuels were rice starch (Sigma-Aldrich) and a bio-oil. This pyrolysis oil was obtained from sugar maple in an auger/transport bed reactor designed by Renewable Oil International LLC (ROI), as described elsewhere [5]. The reactor system is built around an adiabatic reactor zone which had three inlets: (1) the solid heat carrier (2) dried and ground biomass and (3) a N_2 sweep gas. The heat carrier is a stainless steel shot with a size of about 2 mm. During production, the heat carrier and char were carried away from the reactor zone to the char separation system using another auger. The pyrolysis vapors from the reactor zone were sent to a vapor recovery system which consisted of a tar trap, eight condensers and an electrostatic precipitator (ESP) in series. The pyrolysis oils were then filtered with a 1.4 μm filter to remove char impurities [6]. The yield of bio-oil produced in this reactor was 53 wt%. A range of techniques were used to characterize the bio-oil as shown in Table 5.1 [5]. The detected bio-oil composition included 39.5 wt% pyrolytic lignin, 30.3 wt% water, 9.4 wt% acetic acid, and 11.8 wt% other measured oxygenated organic molecules.

Table 5.1: Concentration of Products in the Pyrolysis Oil (wt%).

GC detected compounds	
Hydroxyacetaldehyde	1.46
Acetic Acid	9.02
Hydroxyacetone	1.25
1-Hydroxy-2-Butanone	0.34
1,2-butanediol	0.30
Gamma Butyrolactone	0.55
Phenol	0.12
3-Methyl-1,2-cyclopentanedione	0.68
Guaiacol	0.56
HPLC detected compounds	
C6 sugars	0.20
Levoglucosan	3.98
Formic Acid	1.52
Hydroxymethyl Fufural	0.93
Furfural	0.28
GC and HPLC identifiable carbon compounds	21.19
Water Content	30.27
Pyrolytic Lignin	39.49
Total Identified Products	90.95

The V-i curves and impedance measurements in this study were performed using a Gamry Instruments Potentiostat. Unless otherwise stated, the current densities reported in this chapter were normalized to the external area of the cathode. The V-i curves were obtained by ramping through the applied voltages from OCV to 0 V at 10 mV/s and measuring the corresponding currents. The impedance spectra were performed galvanostatically in the frequency range from 300 kHz to 0.1Hz with an a.c. perturbation

of 1 mA. Scanning electron microscopy (SEM) was performed using a JEOL 7500F HRSEM.

5.3 Results

5.3.1 Cells with ScSZ electrolytes

In Chapter 4, it was shown that relatively high power densities are possible using a molten Sb anode in an SOFC and that carbonaceous fuels preloaded into the anode compartment can be used to generate electricity [1]. However, the testing rig used in that study did not have the capability of adding fuel during the course of the measurements and therefore could not be used for long-term testing. Figure 5.2 shows results from a 200-h experiment in which the current density, normalized to the external area of the cathode, was monitored while holding the cell potential at 0.5 V, with intermittent addition of various fuels. The arrows indicate the times at which 0.5 g increments of fuel (60-wt% charcoal and 40-wt% of either rice starch or bio-oil) were added. The normalized power densities are reported on the right side. The cell used in this experiment had a 100-μm ScSZ electrolyte, with an LSF-ScSZ composite cathode and 10 g of Sb as the anode. The current and power densities initially drifted downward during the first 70 h, from a current density of 580 mA/cm^2 and power density of 290 mW/cm^2, to a current density of 460 mA/cm^2 and power density of 230 mW/cm^2, after which the performance started to increase.

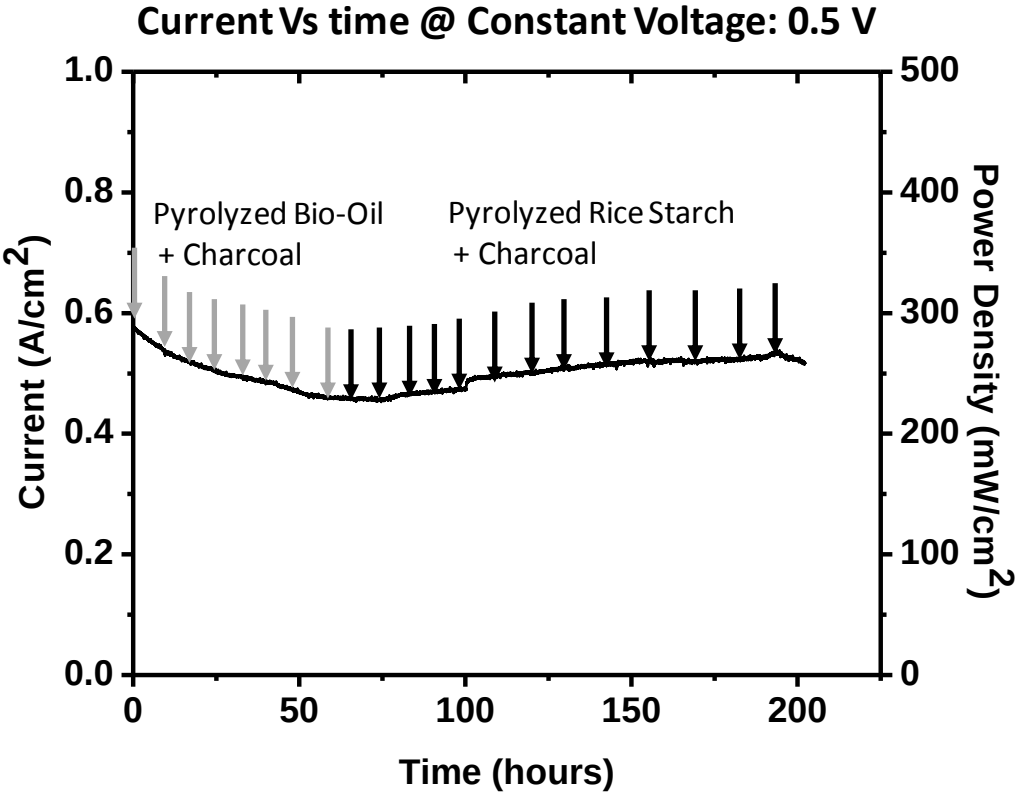

Figure 5.2: Long term performance plot for the DCFC with a pure Sb anode and a ScSZ electrolyte. The DCFC is run on 3 different solid fuels, pyrolyzed bio-oil, pyrolyzed rice starch and activated charcoal. Current is being generated at a constant voltage of 0.5 V.

To gain insight into the reasons behind the drifting current densities in Figure 5.2, V-i polarization curves and impedance spectra were collected at 0 h, 100 h, and 200 h, with the data shown in Figures 5.3 and 5.4. As shown in Figure 5.3, the open-circuit voltage (OCV) was 0.75 V at all times, in agreement with the expected Nernst potential for Sb oxidation to Sb_2O_3. The V-i relationships were nearly linear and the slope of the V-i relationship, which is the total area specific resistance (ASR) of the cell, increased from an average initial value of 0.38 Ωcm^2 to 0.50 Ωcm^2 after 100 h. The V-i relationships at 100 and 200 h were virtually unchanged.

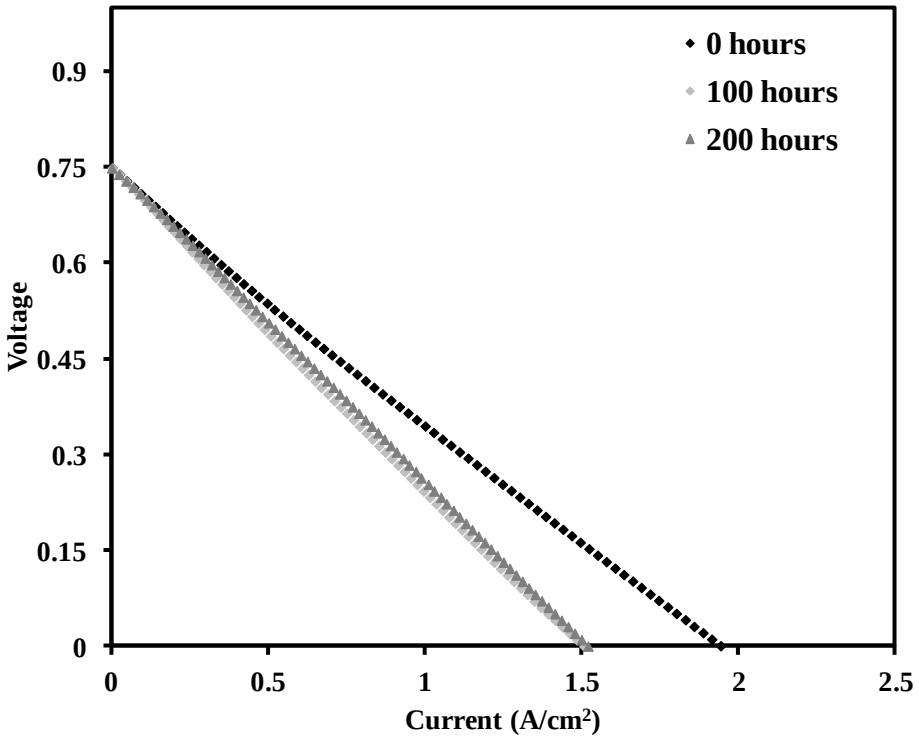

Figure 5.3: V-i polarization curves for the DCFC with a pure Sb anode and a ScSZ electrolyte.

The corresponding open-circuit impedance data at these three times are shown in Figure 5.4. At 0 h, the Nyquist plot of the impedance spectrum has a zero-frequency intercept with the abscissa at 0.38 Ωcm^2, identical to the slope of the V-i plot, as expected. The ohmic resistance of the cell, given by the high-frequency intercept with the abscissa, is 0.22 Ωcm^2, a value equal to the calculated resistance of a 100-μm ScSZ electrolyte [2]. The difference between these resistances, 0.16 Ωcm^2, corresponds to the losses associated with the two electrodes. Separate measurements of identical LSF-ScSZ cathodes indicate that the resistance of this electrode should be 0.06 Ωcm^2 at 973 K [2], implying that the anode losses are on the order of 0.1 Ωcm^2. After 100 and 200 h, the impedance spectra show that the total electrode losses increased from 0.16 Ωcm^2 to approximately 0.25 Ωcm^2. This increase is almost certainly associated with the molten

Sb-Sb_2O_3 anode, possibly due to a buildup of oxide at the electrolyte interface. Although, in a previous study it was shown that the impedance of a molten Sb electrode does not change significantly with the Sb:Sb_2O_3 ratio over a fairly wide range of compositions [3], that study was carried out with continuous vigorous stirring of the molten electrode. In this chapter, except for the intermittent mechanical mixing when fuel was added, natural convection was used for mixing, and it is likely that there was a buildup of the oxide at the electrolyte interface.

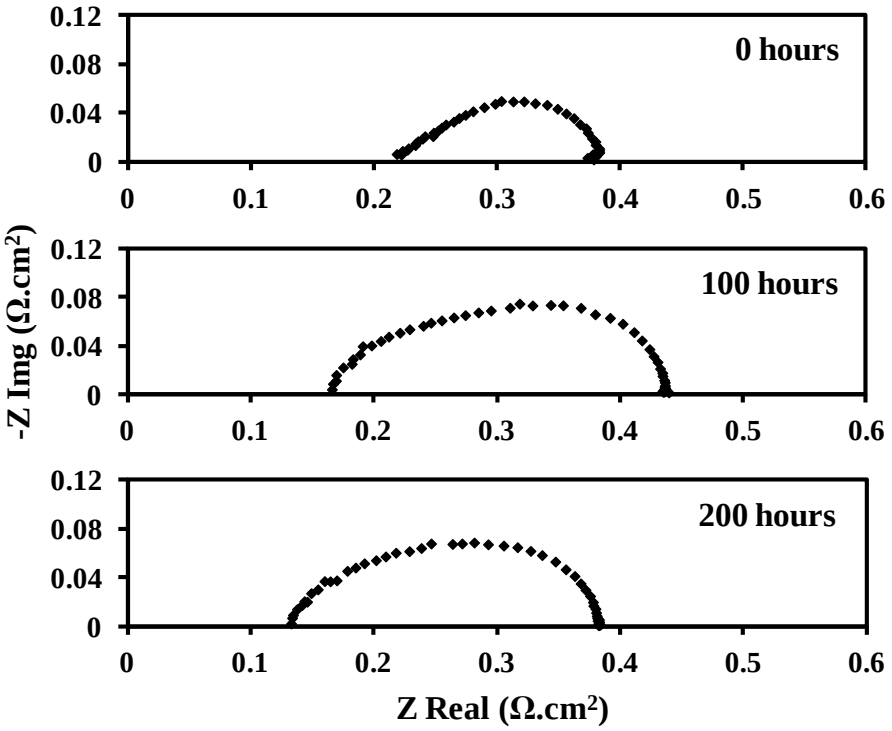

Figure 5.4: Nyquist impedance spectra for the DCFC with a pure Sb anode and a ScSZ electrolyte.

Of greater concern in Figure 5.4 is the decreasing ohmic resistance which declined to 0.17 Ωcm^2 after 100 h and to 0.13 Ωcm^2 after 200 h. Since the ohmic losses are associated with the electrolyte and must be at least as high as the resistance of the electrolyte, a decrease in this value suggests that the electrolyte has become significantly

thinner during the measurements. This was later confirmed by SEM, which showed that the dense ScSZ electrolyte had gone from an initial thickness of 100 μm to 73 μm over the 200-h experiment. As will be discussed later in this chapter, this thinning of the electrolyte only occurred in the active region between the cathode and the molten anode, implying that it is due to an electrochemical process and not simply corrosion of ScSZ in the molten Sb-Sb_2O_3 mixture.

In a previous study of mixed-metal anodes [7], the electrode performance characteristics followed that of the most easily oxidized metal. In the case of Sb-Bi mixtures, the OCV was close to that for the oxidation of Sb, ~0.738 V; when the Bi-Sb cell was operated in a "battery" mode, the Bi remained metallic and in contact with the electrolyte until all of the Sb was oxidized and floated to the top. The Bi-Sb system is of interest for the present study in that the buildup of oxide near the electrolyte interface might be avoided with a denser mixed-metal electrode. Long-term results for a cell with an anode containing a 20 mol%-80 mol% mixture of Bi and Sb are shown in Figure 5.5. While the initial current and power densities at 0.5 V were somewhat lower in this cell, in part due to the slightly lower OCV of the alloy, the performance was more stable, showing only a gradual increase in current density with time, from 400 mA/cm^2 to greater than 500 mA/cm^2 after 225 h. This observation lends support to the hypothesis that the initial downward drift of the current density in Figure 5.2 is due to a buildup of oxide at the electrolyte interface.

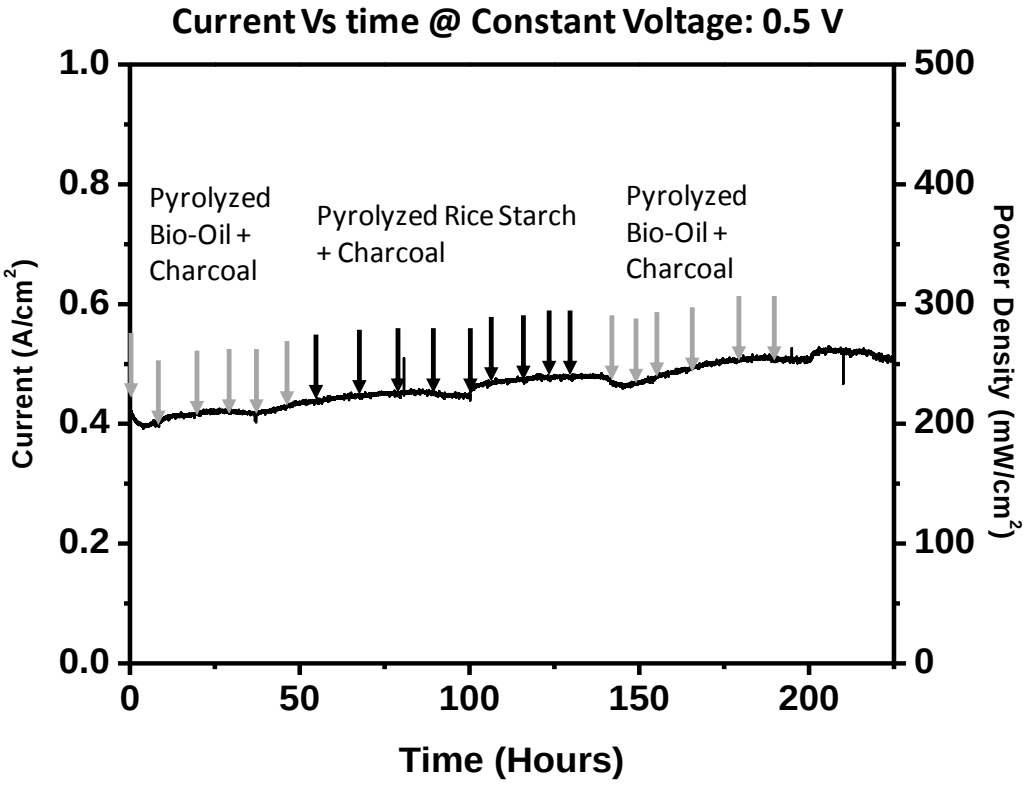

Figure 5.5: Long term performance plot for the DCFC with a Sb-Bi alloy anode and a ScSZ electrolyte. The DCFC is run on 3 different solid fuels, pyrolyzed bio-oil, pyrolyzed rice starch and activated charcoal. Current is being generated at a constant voltage of 0.5 V.

As in the case for the cell with the pure Sb anode, the primary reason for the increased current densities over time was a decreasing ohmic resistance. Indeed, the loss of ScSZ electrolyte was even more severe with the Bi-Sb mixture than it was with the pure Sb electrode. Figure 5.6 shows an SEM image of a cross section of the electrolyte, near the cathode boundary. Because some Ag paste spilled over from the cathode onto the dense electrolyte, lines have been drawn on the image to help the reader see the locations of the various boundaries. The image in Figure 5.6 shows that the ScSZ electrolyte away from the cathode remains 100 μm thick, indicating that the ScSZ is not

etched by the molten metal in the absence of current. However, beneath the cathode, the electrolyte had thinned dramatically, to a value of only 24 µm. It is interesting to notice that the shape of the molten-metal/ScSZ interface is similar to the expected field lines at an electrode-electrolyte interface with asymmetric placement of electrodes [8, 9]. Therefore, the thinning process must be electrochemical in nature and related to the amount of charge passed through the electrolyte.

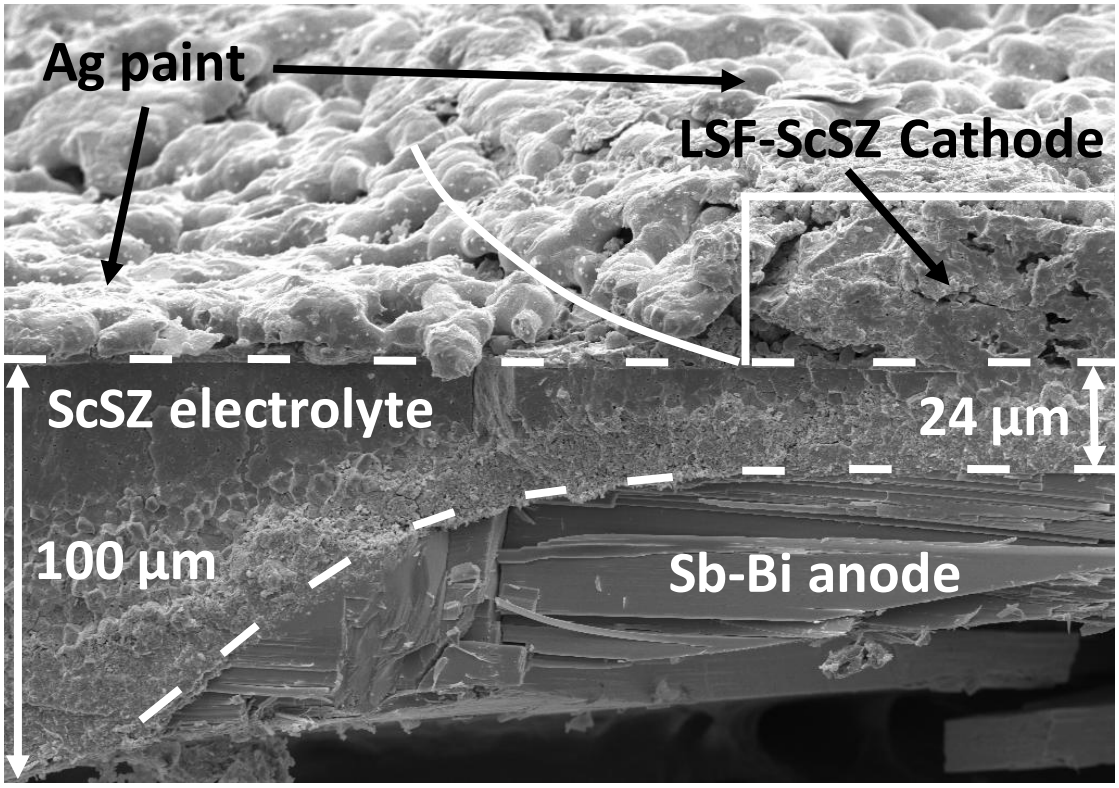

Figure 5.6: SEM image of the cell cross-section after the long term test of the DCFC with a Sb-Bi alloy anode and a ScSZ electrolyte.

5.3.2 Cells with YSZ electrolytes

The severe loss of electrolyte material found with the ScSZ would prevent any practical application of this technology. To determine whether damage to the electrolyte depends on the particular electrolyte that is used, another long-term test was performed

on a cell with a YSZ electrolyte and 10 g of Sb as the anode. Again, the test was performed with intermittent addition of fuel, briefly stirring before and after addition of the solids. Because the ionic conductivity of YSZ is lower than that of ScSZ and the YSZ cells had a thicker electrolyte, the cell performance was modest compared to that for the ScSZ cells. In order to mimic the conditions experienced by the ScSZ electrolyte, the long-term experiment with YSZ was carried out at a constant current density of 500 mA/cm^2, rather than at constant cell potential. Furthermore, because the aim of this experiment was to pass a similar amount of charge through the YSZ electrolyte, only a single Re wire was used for anode current collection, adding an additional ohmic contribution to the V-i relationship in the cell. With these conditions, the cell potential over the course of 270 h of operation was 0 V, fluctuating between ±0.05 V.

An SEM image of the YSZ electrolyte cross section after the 270-h test, near the cathode boundary, is shown in Figure 5.7. Unlike the case with the ScSZ electrolyte, there is no evidence for thinning of the YSZ electrolyte and its appearance between the cathode and the molten metal is identical to that of the YSZ that is away from the cathode. These data demonstrate that electrolyte etching with ScSZ is related to the Sc in some manner and does not appear to occur with Y doping.

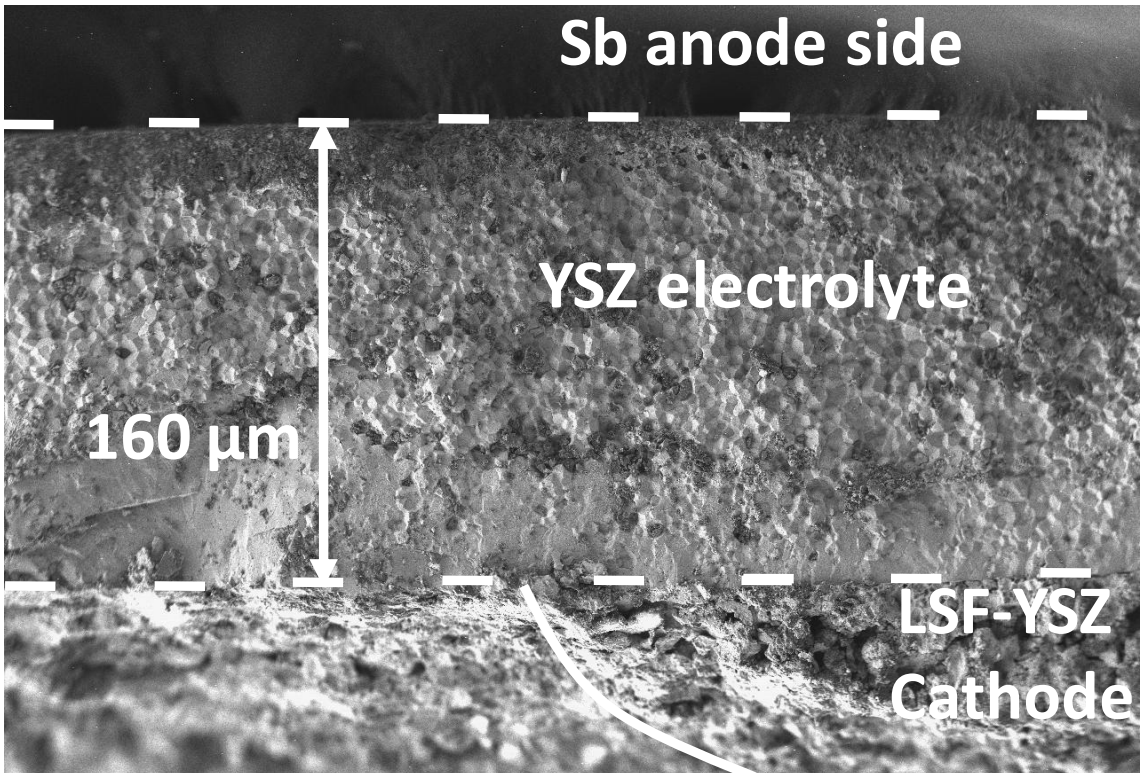

Figure 5.7: SEM image of the cell cross-section after the long term test of the DCFC with a pure Sb anode and a YSZ electrolyte.

5.4 Discussion

The results obtained in this study demonstrate that the direct utilization of biomass and other solid fuels in an SOFC is possible using a molten-Sb electrode. As discussed in more detail elsewhere [3], the theoretical electrical efficiency of a cell based on Sb, equal to $\Delta G/\Delta H$, is only 0.65; however, the remaining energy associated with fuel oxidation could be captured as heat and utilized in other ways. Because Sb_2O_3 is effective in assisting the conversion of the fuels, oxidizing even graphite at temperatures below 1073 K [1], NO_x emissions will be minimal. Impurities carried in with the fuel are a concern; however, with the exception of metals that could form alloys with Sb, most oxides can be separated by gravity. Sb does form a sulfide, but Sb_2S_3 has a melting point of 823 K and can be easily converted back to the metal. Obviously, stack design with

molten Sb will be a challenge but the actual cells could be simpler in that there is effectively no separate anode layer to design.

Because the impedance of the molten-Sb electrode is low, ~0.1 Ωcm^2 at 973 K, cell performance will be determined by the cathode and electrolyte losses. While the degradation of the ScSZ electrolyte suggests that the choice of electrolyte material will be dictated by stability, electrolyte losses can still be minimized through the use of thin YSZ electrolytes. Indeed, in conventional SOFC, 10-μm electrolytes are common and would add negligible resistance to cells operating at 973 K or higher temperatures.

The large difference in the stabilities of ScSZ and YSZ against etching by the molten Sb is noteworthy. Sc^{3+} cations are much smaller than Y^{+3} cations and are known to have a high mobility in the lattice of cubic ZrO_2 [10]. Therefore, it can be hypothesized that this mobility leads to the migration of Sc^{+3} cations out of the electrolyte and into the molten metal. A similar net migration of Sc^{+3} out of the electrolyte has been reported for ScSZ in contact with B_2O_3 [11]. Loss of Sc from the ZrO_2 lattice could in turn destabilize the cubic structure, causing mechanical stresses that could cause flaking of the zirconia from the surface of the electrolyte. The reason behind etching being so much larger with Bi-Sb mixtures is unknown but may simply be the result of minimizing the amount of oxide that is in the vicinity of the electrolyte interface.

It is interesting to compare the etching phenomenon of the present study with recent reports of large morphological changes in YSZ that occur at higher temperatures and current densities [12]. That work attributed the effect to a supersaturation of oxygen vacancies within the electrolyte. Whether these phenomena are related is unknown at this time.

Clearly, more work needs to be done in order to demonstrate the practicality of direct-carbon fuel cells based on molten-Sb anodes. However, the results of this study further demonstrate the potential of this technology for achieving breakthrough efficiencies and improved environmental impact with complex fuels, making this a promising area for future development.

5.5 Conclusion

The generation of electricity through the direct oxidation of various solid fuels, including rice starch, charcoal, and bio-oil, has been demonstrated using an SOFC with a molten-Sb anode. These cells are able to generate high power densities with stable anode performance. Although YSZ electrolytes exhibit good stability, an electrochemical etching phenomenon was observed with ScSZ that would prevent the use of ScSZ in this application.

5.6 References

1. Jayakumar, A.; Kungas, R.; Roy, S.; Javadekar, A.; Buttrey, D. J.; Vohs, J. M.; Gorte, R. J., A direct carbon fuel cell with a molten antimony anode. *Energy Environ. Sci.* **2011,** 4, (10), 4133-4137.
2. Kungas, R.; Vohs, J. M.; Gorte, R. J., Effect of the Ionic Conductivity of the Electrolyte in Composite SOFC Cathodes. *J. Electrochem. Soc.* **2011,** 158, (6), B743-B748.

3. Javadekar, A.; Jayakumar, A.; Gorte, R. J.; Vohs, J. M.; Buttrey, D. J., Energy Storage in Electrochemical Cells with Molten Sb Electrodes. *J. Electrochem. Soc.* **2012,** 159, (4), A386-A389.
4. Ning, W.; Low, M. J. D., Spectroscopic Studies of Carbons .19. The Charring of Sucrose. *Mater. Chem. Phys.* **1990,** 26, (5), 465-481.
5. Upadhye, A. A.; Polin, J. P.; Spooner, T. E.; Badger, P. C.; McGill, J. H.; Huber, G. W., Fast Pyrolysis of Lignocellulosic Biomass in an Auger/Transported Bed Reactor Technology with a Multiple Condenser System. *Energy Fuels* **2012**, under review.
6. Javaid, A.; Ryan, T.; Berg, G.; Pan, X. M.; Vispute, T.; Bhatia, S. R.; Huber, G. W.; Ford, D. M., Removal of char particles from fast pyrolysis bio-oil by microfiltration. *J. Memb. Sci.* **2010,** 363, (1-2), 120-127.
7. Javadekar, A.; Jayakumar, A.; Gorte, R. J.; Vohs, J. M.; Buttrey, D. J., Characteristics of Molten Alloys as Anodes in Solid Oxide Fuel Cells. *J. Electrochem. Soc.* **2011,** 158, (12), B1472-B1478.
8. Adler, S. B., Reference electrode placement in thin solid electrolytes. *J. Electrochem. Soc.* **2002,** 149, (5), E166-E172.
9. Adler, S. B.; Henderson, B. T.; Wilson, M. A.; Taylor, D. M.; Richards, R. E., Reference electrode placement and seals in electrochemical oxygen generators. *Solid State Ionics* **2000,** 134, (1-2), 35-42.
10. Idris, M. A.; Bak, T.; Li, S.; Nowotny, J., Effect of Segregation on Surface and Near-Surface Chemistry of Yttria-Stabilized Zirconia. *J. Phys. Chem. C* **2012,** 116, (20), 10950-10958.

11. Kishimoto, H.; Sakai, N.; Yamaji, K.; Horita, T.; Xiong, Y. P.; Brito, M. E.; Yokokawa, H., Destabilization of cubic-stabilized zirconia electrolyte induced by boron oxide under reducing atmosphere. *J. Mater. Sci.* **2009,** 44, (2), 639-646.
12. Kim, S. W.; Kim, S. G.; Jung, J. I.; Kang, S. J. L.; Chen, I. W., Enhanced Grain Boundary Mobility in Yttria-Stabilized Cubic Zirconia under an Electric Current. *J. Am. Ceram. Soc.* **2011,** 94, (12), 4231-4238.

Chapter 6: Conclusion

In this thesis, various molten metal-metal oxide systems were systematically evaluated for their viability as anodes for DCFCs based on SOFC electrolytes. These studies were conducted using dense-porous bilayer wafers of the SOFC electrolyte material fabricated by the technique of tape-casting. The dense layer served as the ionically conductive electrolyte, while the porous layer was infiltrated with an active perovskite phase to form the conductive composite cathode. The molten metal to be evaluated was then placed in direct contact with the blank face of the dense electrolyte layer.

Using this analytical platform, the oxygen transport characteristics at the electrolyte interface and in the bulk of different molten metal anodes were studied in the typical SOFC operating temperature range of 973 K – 1173 K.

At the beginning of this thesis research, the liquid tin anode solid oxide fuel cell (LTA-SOFC) being developed by CellTech Power Inc. was the only work going on with SOFCs involving the use of molten metal anodes. However, the power levels reported by them, even at the high operating temperature of 1273 K, were relatively low. Since typical cathode and electrolyte related impedance losses at this temperature are negligibly low, the majority of the cell impedance loss could only be attributed to the performance of the Sn anode.

In chapter 2, the study of the oxygen transport properties of the molten Sn anode system was the starting point of this thesis. This study revealed that, despite the desirably high open circuit voltage (OCV) of 0.93 V at 973 K, the poor performance of the Sn anode was due to the formation of an insulating layer of high melting solid SnO_2 on the

surface of the electrolyte, which effectively blocked the transfer of O^{2-} ions to the anode. It was apparent from this finding that the CellTech Power group was basically operating their fuel cells on the slightly increased diffusivity of oxygen in Sn and SnO_2 under the extreme operating temperature of 1273 K, which was a very inefficient anode mechanism for oxygen transport. For the purpose of comparison with the Sn case, the molten Bi system was then studied because it forms a highly ionically conductive oxide (Bi_2O_3). This anode system was able to maintain its performance stability, with a low impedance contribution, because the formation of Bi_2O_3 on the surface of the electrolyte did not hinder ion transfer from the electrolyte due its high ionic conductivity. However, as a practical solution Bi would be a poor anode choice because it has a very low OCV of 0.48 V at 973 K (as compared to the C oxidation potential of ~1 V) resulting in reduced performance efficiencies.

In chapter 3, the oxygen transport properties of the molten metal anode candidates of In, Pb and Sb were evaluated. In the case of In, it was seen that, despite a high OCV of 1.01 V at 973 K, the In anode exhibited a similar drop in performance as in the case of Sn, due to the formation of an insulating layer of high melting In_2O_3 at the electrolyte interface blocking further ion transfer to anode. This observation made it very clear that a metal that forms an insulating solid oxide cannot be used as an anode. To further demonstrate this and understand how having a molten oxide impacts system performance the molten Pb system was studied next, since it forms PbO (m. p. 1161 K) which is a lower melting oxide. It was seen that the Pb anode showed poor performance at the operating temperatures of 973 and 1073 K, similar to the Sn and In cases, but at 1173 K, above the melting point of PbO, the anode performance level was sustainably high, with a

constantly low impedance contribution. This was because the molten PbO formed at 1173 K, was a mobile phase that could readily move away from the electrolyte interface by natural convection allowing for further oxidation of the anode to occur. However, since the Pb anode system could only be used at the high operating temperature of 1173 K, and its OCV at this temperature was only 0.5 V, it was an unattractive option. The molten Sb system was then tested because it formed very low melting Sb_2O_3 (m. p. 929 K). This meant that a system using molten Sb as the anode could be operated at the intermediate SOFC operating temperature of 973 K. Surely enough, the test results with molten Sb were the most interesting. The OCV of the system was reasonably good (0.75 V at 973 K) and it could operate at a sustainable high power level at 973 K because it formed molten Sb_2O_3. This mobile Sb_2O_3 phase could also be effectively contacted with the solid fuel to regenerate Sb in the anode chamber itself or even in a separate chamber. These properties made the molten Sb anode system the most attractive option for DCFC applications. In Table 6.1, the oxygen transport characteristics of the tested molten metal anode candidates are summarized.

In chapter 4, reactivity studies showed that Sb_2O_3 could easily be reduced by most types of carbonaceous fuels at the operating temperature of 973 K, making a DCFC with a molten Sb anode possible at this temperature. The goal of the experiments in this chapter was then to demonstrate a working DCFC based on a molten Sb anode. And, using the model ash-free fuel of sugar char and a 100 μm Scandia-stabilized Zirconia (ScSZ) electrolyte, a high performance DCFC was demonstrated at a stable operating power density of 300 mW/cm^2 (with a maximum possible power density of 360

mW/cm^2), which is comparable to the power levels observed in state-of-the-art H_2-fuelled SOFCs (a mature technology).

Table 6.1: Oxygen transport properties of the tested molten metal candidates as anodes.

Metal Anode	OCV at 973 K	Performance characteristics	Viability
Sn	0.93 V	High melting SnO_2 insulating layer formed at electrolyte interface.	No
Bi	0.48 V	Ionically conductive Bi_2O_3 forms allowing continuous operation. OCV too low.	No
In	1.01 V	High melting In_2O_3 insulating layer formed at electrolyte interface.	No
Pb	0.60 V	Molten PbO forms at 1173 K allowing continuous operation, OCV of 0.5 V at 1173 K too low.	No
Sb	0.75 V	Low melting Sb_2O_3 forms allowing continuous operation at 973 K. Reasonable OCV.	Yes

In chapter 5, stirring of the anode-fuel interface was introduced to make the operation of the fuel cell on more traditional ash-containing carbonaceous fuels (like activated charcoal, rice starch and bio-oil) possible. The formation of an ash layer on the surface of the partially oxidized fuel prevented further reduction of the Sb_2O_3 and stirring is required to break up the ash layer and make the fuel available for oxide reduction. With the help of periodic stirring, the long-term stability of these DCFCs based on molten Sb anodes was then studied. After running cell tests for as long as 270 h at high currents, it was observed that the power levels of these DCFCs remained more or less stable apart from certain drifts in the observed performance. However, long-term thinning of the electrolyte was observed in the case of ScSZ. On replacing this electrolyte with a yttria-stabilized zirconia (YSZ) no such thinning was observed under similar operating conditions and time frames. This goes to show that the thinning of the electrolyte caused or aided by the molten Sb anode can be avoided and that this type of DCFC can be long-term stable with the correct choice of electrolyte material.

In conclusion, the results of this thesis research indicate that DCFCs based on a molten Sb anode and an SOFC electrolyte can generate electricity at high power levels and efficiencies with great fuel flexibility at the intermediate SOFC operating temperature of 973 K.